[redacted] DATA
[redacted] ENERGY ACT OF 1954

[redacted]

TECHNICAL MEMORANDUM

UB
NASA TM X-1420

CLASSIFICATION CHANGED
UNCLASSIFIED
TO [redacted]
By Authority of T.D. 7318 Date 9/13/72

FF No. 602(D)

X 68 10430 (ACCESSION NUMBER) | (THRU) 1
103 (PAGES) | 20 (CODE)
(NASA CR OR TMX OR AD NUMBER) | 23 (CATEGORY)

AVAILABLE TO U.S. GOVERNMENT AGENCIES AND CONTRACTORS

N72-74697

(NASA-TM-X-1420) 01FEASIBILITY STUDY OF A TUNGSTEN WATER-MODERATED NUCLEAR ROCKET. 1: SUMMARY REPORT S.J. Kaufman (NASA) Mar. 1968 103 p

Unclas
00/99 40221

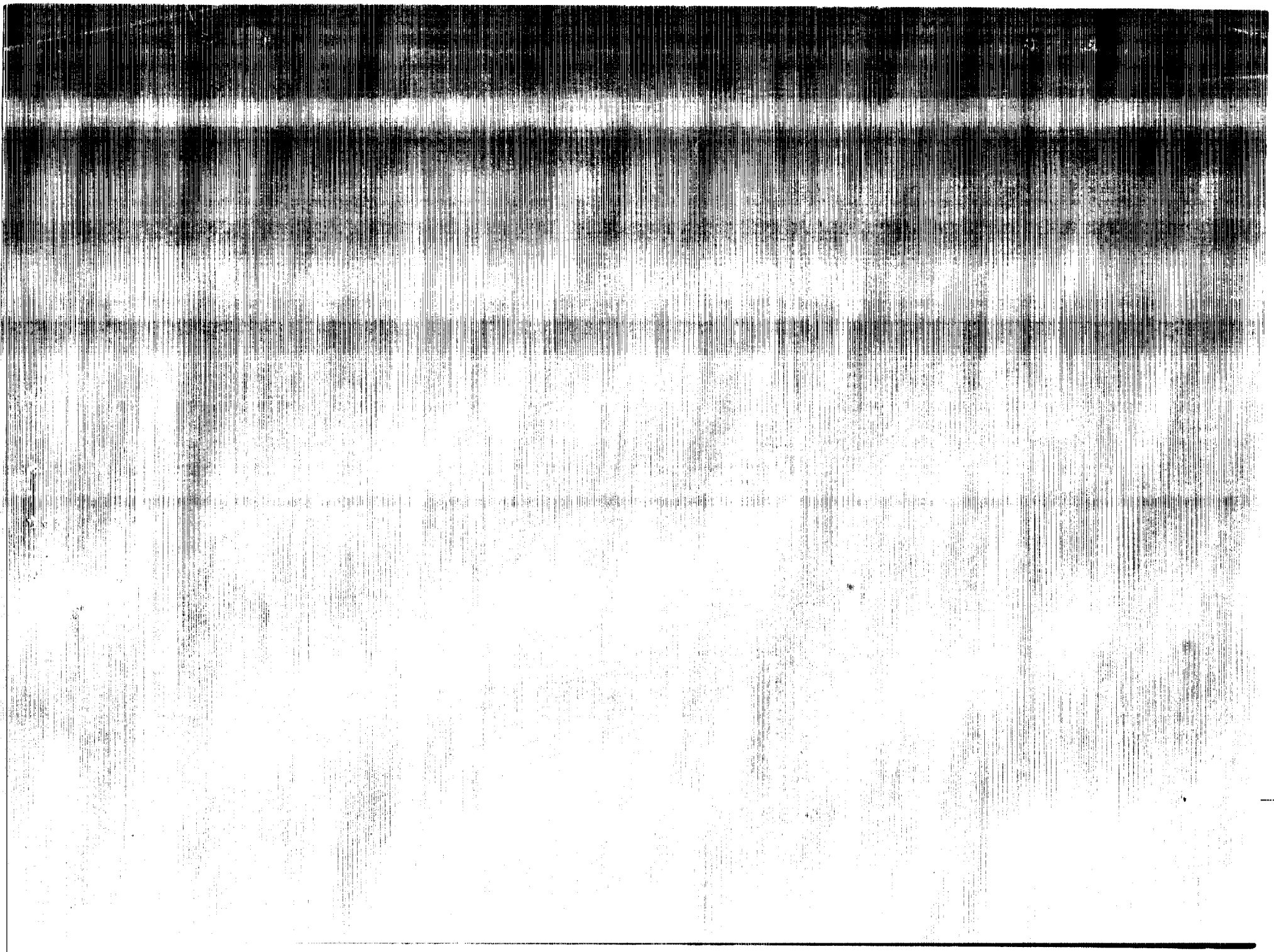

[redacted]

NASA TM X-1420

FEASIBILITY STUDY OF A TUNGSTEN WATER-MODERATED NUCLEAR ROCKET

I. SUMMARY REPORT

By Samuel J. Kaufman

Lewis Research Center
Cleveland, Ohio

[redacted]

ATOMIC ENERGY ACT OF 1954

[redacted]

[redacted]

NATIONAL AERONAUTICS AND SPACE ADMINISTRATION

[redacted]

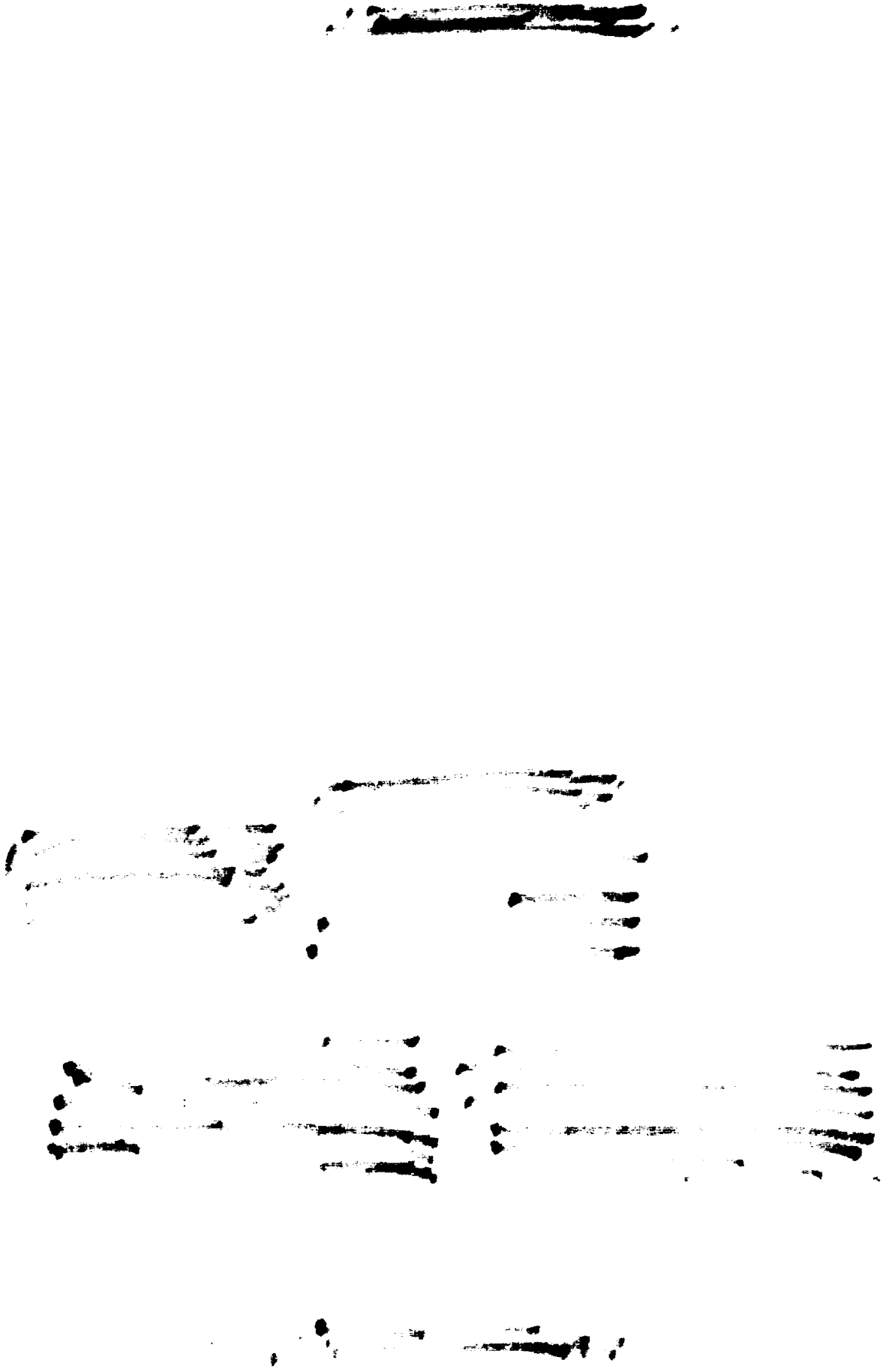

[redacted]

CONTENTS

	Page
SUMMARY	1
INTRODUCTION	2
REACTOR CONCEPT	3
Reference-Design Criteria	3
Core Fluid Flow Systems	4
Reactivity Control System	6
Core Structure Considerations	7
Engine Flow Systems	8
System Startup	9
Design for Other Power Levels	10
NEUTRONICS	10
Cross Sections	12
Reactor Analysis Methods	13
Reactor Design and Critical Experiments	14
Reference reactor-design considerations	14
Critical experiments	15
Power distributions	18
Reactivity and reactivity control	21
Larger and smaller cores	24
FUEL ELEMENTS	26
Fabrication of Fueled Composites	27
Fuel Retention Studies	29
Fuel loss through vaporization	29
Fuel loss induced by thermal cycling	29
Effect of operating variables on fuel loss	30
Radiation effects	30
Mechanical Properties	31
Tensile properties	31
Creep-rupture properties	31
Modulus of elasticity	32
Design Parameters	32
Fuel-Element Configurations	33
Concentric cylinder elements	33
Honeycomb elements	34

[redacted]

Fuel-Element Support 36
Axial support 36
Lateral support 36
Vibration 37

FLUID SYSTEMS 38
Hydrogen Feed System 38
Water-Moderator System 39
Water-hydrogen heat exchanger 40

HEAT TRANSFER 42
Fuel-Element Heat-Transfer Analysis 42
Temperature Distribution 44
Calculational Uncertainties 44

ENGINE DYNAMICS AND CONTROL STUDIES 45

SYSTEM SIZE AND WEIGHT 48

CONCLUDING REMARKS 49

REFERENCES 51

FEASIBILITY STUDY OF A TUNGSTEN WATER-MODERATED NUCLEAR ROCKET

I. SUMMARY REPORT (U)

by Samuel J. Kaufman

Lewis Research Center

SUMMARY

A study was conducted to establish the feasibility and performance capability of a tungsten water-moderated nuclear rocket reactor concept. The reactor is a thermal spectrum reactor that uses light water as a moderator and coolant, uranium dioxide as fuel, and tungsten enriched in the 184 isotope as the fuel-element structural material. It is intended to provide a high specific impulse, high thrust, and low weight system with hydrogen as the propellant.

Extensive analytical and experimental programs were conducted in the areas of reactor neutronics, fuel elements, and engine systems. Based on the neutronic studies, it has been determined that the nuclear aspects of the reactor are well understood, adequate margins of reactivity can be obtained, the negative temperature coefficient required for self-stabilized reactor operation can be achieved, and radial and axial power distributions can be adjusted for good heat transfer to the propellant. The fuel-element studies led to the development of tungsten - uranium-dioxide composites capable of operating for 10 hours to 4960° R (2755° K) with multirestart capability. These composites have sufficient high-temperature strength to be used as self-supporting components in fuel-element structures. Fabrication of suitable fuel-element structures has also been demonstrated. As a result of the engine system studies, it has been shown that the reactor along with the nonnuclear components, such as the nozzle, turbomachinery, etc., can be started, operated at the design point, and shut down in a stable manner.

The tungsten water-moderated reactor (TWMR) concept is applicable to power levels from about 400 to over 10 000 megawatts by increasing the number of fuel assemblies of the same size and design into a similar structure and increasing the size of auxiliary components. There is now reasonable confidence that the TWMR concept is feasible, that it has high performance capability, and that it could be developed.

INTRODUCTION

The historical role of the Lewis Research Center has been to conduct research and development programs on propulsion systems for future flight applications by careful analytical and experimental investigations of key problem areas in new propulsion concepts and advanced designs. In carrying out this mission with respect to the nuclear rocket, the tungsten water-moderated concept (TWMR) was evolved. A series of reports (refs. 1 to 6) presents the detailed results of an engineering study to establish the feasibility and performance of the TWMR concept. This report is a condensed version of the contents of the references cited.

The TWMR concept is shown schematically in figure 1. It is a thermal reactor that uses water as the moderator, uranium dioxide as the fuel, and tungsten enriched in the 184 isotope as the fuel-element structural material. As is common to all nuclear rocket systems, hydrogen is used as the propellant to maximize specific impulse. The reactor consists of a tank containing a number of pressure tubes that are attached to tube sheets at the inlet and outlet ends of the reactor. The space inside the tank between the tubes is filled with water that serves both as the neutron moderator and as a coolant for the structure. Heat is generated in the water by neutrons and gamma rays and is also transferred to the water by heat leakage from the hot fuel elements, each of which is located in a pressure tube. The removal of heat is provided by pumping the water through the core and a heat exchanger in a closed loop. The water is regeneratively cooled in the heat exchanger by the hydrogen propellant that flows from a supply tank through the nozzle and heat exchanger into the core. As the hydrogen flows through the fuel elements within the core pressure tubes, it is heated to a high temperature and is then expanded out the nozzle to produce thrust.

The potential advantages of the concept lie in the following areas: The use of tungsten provides a high-temperature material with good thermal shock resistance, tensile and compressive strength, thermal conductivity, and resistance to corrosion by the hydrogen propellant. The properties of tungsten permit the fabrication of fuel elements with very thin web cross sections that reduce thermal stress. The use of water as the moderator provides a good coolant for the pressure vessel and structural members and reduces core size and weight over that obtained for most moderator materials. In this concept, the fuel-element assemblies are structurally independent of each other. This arrangement permits individual development of these assemblies.

In order to utilize these advantages, the following conditions must be met: (1) the uranium must be contained in tungsten-matrix fuel elements, (2) the fuel elements must be constructed in the shapes required for optimum strength and heat transfer, (3) the neutronics must be acceptable in terms of temperature and power distributions through the reactor, (4) a reliable control system must be included, and (5) the water moderator

must be cooled by the hydrogen propellant without freezing. Performance, lifetime, and restart capability must also be evaluated.

These and other desirable characteristics of a nuclear rocket system, such as reliability, high specific impulse, low weight, small size, growth potential, ease of development, long running time, and restart capability, are discussed in references 1 to 6 as follows:

(1) Materials and Fuel Elements (refs. 1 and 2). The properties of the tungsten - uranium dioxide fuel-element material, selection of fuel-element configuration, and methods of fabrication are discussed. Methods of stabilizing the fuel-element material under conditions of thermal cycling to ensure fuel retention at operating temperatures are discussed, and the limiting conditions of operation presented.

(2) Neutronics (ref. 3). The neutronics of water-moderated heterogeneous reactors that use tungsten enriched in the 184 isotope is discussed. Analytical methods have determined and critical experiments have confirmed the margins of reactivity required for design. Separated and natural mixtures of tungsten isotopes are used to adjust overall radial and axial power distributions for best heat transfer. The desirable features of finely distributed in-core control systems are discussed.

(3) Engine System (ref. 4). A description is given of the engine design used as a reference in planning and executing the engineering study. Arrangement and types of components, normal operating conditions, and materials of construction are discussed. Heat transfer, fluid flow, and structural calculations are also included.

(4) Feed System and Rotating Machinery (ref. 5). The problem areas for major components in the hydrogen propellant system and in the water-moderator loop are reviewed. A study is presented of various propellant feed system types suitable for use with the TWMR. Detailed descriptions are provided of piping and equipment arrangements as well as the rotating machinery.

(5) System Dynamics (ref. 6). With the use of analog and digital representation, the performance of the components as an overall system has been studied. Stability and control aspects are also presented.

REACTOR CONCEPT

Reference-Design Criteria

In order to explore the TWMR concept fully, it was necessary to have a reference engine system. Coordination of the program and the evaluation of the experimental and analytical results were centered on this reference engine system. However, alternative designs and problem solutions other than those incorporated in the reference design were investigated and are discussed later.

The TWMR is a heterogeneous thermal reactor in which the fissionable fuel is separated from the moderator and is contained in tungsten. The tungsten acts as a structural material and provides heat-transfer surfaces for the propellant. The separation of fuel and moderator permits independent cooling of the moderator, which in turn allows consideration of a wider range of moderating materials which permits minimizing the reactor size.

The TWMR concept includes the same general types of auxiliary components as those in other nuclear rocket systems. These components can be identified as the reactor, the reactor control system, and the hydrogen flow system. In addition, this system requires a water flow loop and a heat exchanger for cooling the water. The reference design not only incorporates these components but also introduces certain innovations into the propellant flow and reactor control systems.

The performance characteristics of the reference system are as follows:

Reactor power, MW	1500
Average outlet gas temperature, ^{o}R; ^{o}K	4460; 2480
Hydrogen flow rate, lb/sec; kg/sec	93; 42.2
Number of fuel elements	121
Maximum fuel-element surface temperature, ^{o}R; ^{o}K	4960; 2755
Fuel-element outlet dynamic head, psi; N/cm^2	12.6; 8.7
Nozzle chamber pressure, psia; N/cm^2 abs	600; 414
Specific impulse (based on nozzle area ratio of 40 and efficiency of 98 percent), sec	830
Maximum heat flux in fuel elements, Btu/(sec)(in.^{2}); J/(sec)(cm^2)	7.2; 1180
Hydrogen flow area, ft^2; m^2	2.1; 0.195
Core power density (includes the metal reflector volumes), MW/ft^3; MW/m^3	40; 1410

The power level and outlet gas temperature, which together define flow rate, were design objectives based on earlier nuclear rocket studies. Design flow mass velocity was evaluated from propellant dynamic pressure and nozzle chamber pressure values, which were based on demonstrated or reasonable values. The mass velocity and flow rate define reactor flow area which, along with nuclear considerations, established the number of fuel elements. Heat-transfer calculations determined the surface temperature distribution and, in turn, the desired power distributions.

Core Fluid Flow Systems

The reactor arrangement is somewhat complicated because all the systems converge

in the core region. The general core arrangement and the fluid flow paths in the TWMR design are shown in figure 2.

The pressure vessel is 52 inches (132 cm) in diameter, and the core region is about 55 inches (140 cm) long. The fuel assemblies are contained in 2.5-inch-diameter (6.35 cm) aluminum pressure tubes in which hydrogen flow is from left to right. These tubes are fastened to two tube sheets and arranged as shown in the cross section in figure 2(a). Neutrons from the fissioning of the fuel in the assemblies are thermalized in the water surrounding the pressure tubes. The tube sheets and the cylindrical pressure vessel, also made of aluminum, form a container for the water moderator. A beryllium side reflector and inlet end reflector are also included in the core. This side reflector, with an outer surface diameter of 43 inches (109 cm), reduces neutron leakage and helps distribute the power radially in the core. The inlet end reflector is used to help shape the axial power distribution in the fuel assemblies. The goal in power shaping is to match the local heat generation with the changing heat-transfer characteristics of the hydrogen.

The water-to-hydrogen heat exchanger required in the concept to remove radiation-induced heat from the water is included inside the pressure vessel to couple this component closely with the active core both in time and space flow paths. The heat exchanger is divided into six shell-and-tube sections and placed in an annular space just outside the beryllium side reflector (fig. 2(a)). The rest of this annulus forms a water flow path and acts as a reflector. Because of gamma radiation, all materials in the vicinity of the reactor core require cooling. The flowing moderator is in contact with most of the pressure vessel walls and performs this cooling function.

The water enters the pressure vessel (fig. 2(b)) near the inlet end of the core and is distributed by a header formed by the inlet tube sheet and the inlet end reflector. The water then flows outside the pressure tubes and through the side and top reflectors. It is then returned through the shell portion of the heat exchangers toward the core inlet. The water leaves the pressure vessel by again reversing direction and flowing toward the outlet end core. Water circulation is accomplished by a pump located outside the pressure vessel.

Hydrogen flows from the nozzle cooling passages (fig. 2(c)) at a temperature of 170° R (94.5° K) directly into the tubes of the water heat exchangers. After flowing through the six heat-exchanger units in parallel, the gas is collected in a header and piped out of the pressure vessel to a turbine. The energy deposited in the gas as it passes through the nozzle and heat exchangers is used to supply part of the power required to force the propellant through the system. The gas leaving the turbine reenters the pressure vessel head, which forms a plenum for distributing the propellant.

A shadow shield can be located inside the head to be conveniently cooled by the gas flowing over and through it on the way to the fuel assemblies. Of the 121 fuel assemblies

included in the core, 117 are used to heat about 97 percent of the propellant to 4460° R (2480° K) before it is discharged into the nozzle chamber. Insulation protects the outlet tube sheet from the hot gas. The remainder of the hydrogen is heated to 1860° R (1030° K) in four special fuel assemblies located in the central part of the core, as shown in figure 2(a). This reduced temperature bleed gas is used to supply the additional pumping requirements. The fact that the fuel assemblies are individual units makes this possible. The four bleed gas units (fig. 2(c)) discharge at the inlet end of the core into separate ducts, which carry the flow to the turbopumps.

Reactivity Control System

Another major component required for the reactor in addition to the fuel assemblies, moderator, and coolant, is a control system. To maintain a good power distribution within the core, an aqueous solution of cadmium sulfate contained in fixed tubes was used for the control system. These Zircalloy tubes extend down into the water moderator and are uniformly interspersed among the fuel assemblies shown in figure 2(e). The result is a core containing about 200 stationary small control rods. The amount of neutron absorbing cadmium in the solution must be varied to control the reactor. The control tubes are connected to a flow loop in which the solution concentration can be adjusted. A schematic drawing of the control-solution loop is shown in figure 3; one control tube is used in this schematic to represent all the tubes. It contains an inner tube for bringing solution into the core; flow out of the core is through the annular space between the tubes. The large number of tubes requires careful manifolding to ensure good poison distribution. The rest of the control-solution flow system is outside the pressure vessel. A heat exchanger that uses cold hydrogen gas as a coolant removes the heat deposited in the poison solution by radiation, and a pump circulates the fluid at a constant rate around the loop. To decrease the poison concentration, a portion of the poison solution flow is bypassed through a mixed-bed ion exchanger. The bypass flow reenters the main flow and dilutes the solution concentration before the flow reaches the core. Cadmium concentration in the poison solution is increased by injecting cadmium sulfate concentrate into the main flow from a pressurized storage container. A combination pressurizer-accumulator is installed on the main flow line to accommodate volume changes and to maintain 600 pounds per square inch absolute (414 N/cm^2 abs) in the system. Solution temperatures are maintained from 585° to 675° R (325° to 375° K).

Core Structure Considerations

As shown in figure 2(d), the pressure vessel consists essentially of two containers. One contains hydrogen and is formed by the head, the inside surfaces of the pressure tubes, and the tube sheets. The other contains water and is formed by the pressure vessel cylinder, the outer surfaces of the pressure tubes, and the tube sheets. To reduce the loads across the common walls of these two containers, the water system pressure is regulated to match the hydrogen pressure. This pressure is regulated specifically in the region of the outlet tube sheet since cooling is most difficult in the vicinity of the hot gas. With little or no pressure drop across the tube sheet, its thickness can be minimized and the cooling problem reduced.

The principal load on the inlet tube sheet results from aerodynamic forces on the fuel assemblies. In the arrangement shown in figure 2(b), the tube sheet is supported by the inlet end reflector, so that the 3-inch-thick (7.62 cm) beryllium member serves a dual purpose. The load is transferred by a collar attached to each pressure tube, which bears on the reflector. A forged beryllium disk would be used in its fabrication since forged beryllium has reasonable room-temperature ductility and high strength. Forgings of this general size were produced for early project Mercury capsules.

Cooling of the beryllium reflector is very important. Water is not only in contact with both flat surfaces, but also flows through the thickness in the annular space around the holes provided for the pressure tubes. This distribution of coolant assures very low temperature gradients resulting from gamma heating, and thus thermal stress problems common to heavy support grid plates are avoided.

The pressure tubes, the inlet and outlet tube sheet, and the inlet end reflector form an independent structural network; its integrity does not depend on fuel assemblies inserted into the pressure tubes.

The principal functions of the fuel assemblies are to hold the fuel material in position and to provide flow passages for the propellant, but they must also reduce heat leakage from the hot fuel elements to the aluminum pressure tubes. To maintain the thermal stresses at acceptable levels, all these functions must be accomplished with minimum restraint of the relative thermal expansions of fuel-assembly components and the aluminum structure.

Figure 4 is a section through one of the propulsion-type fuel assemblies in which the inlet and outlet tube sheets, the pressure tube, the load transfer collar, and the inlet end reflector are shown. The fuel element (which is defined as the fueled material and its support tube) is broken into 26 fuel stages, 1.5 inches (3.81 cm) long, with 0.125-inch (3.18 mm) spaces between stages to allow for flow redistribution, which would not occur in long continuous flow paths. The stages are attached to an axially continuous support tube, which is made up primarily of tungsten and is attached to the inlet tube sheet for

axial support. To dampen excessive vibrations in the 55-inch-long (140 cm) support tube and attached stages, lateral supports are located along the tube length. The main lateral support, at the hot end of the core, consists of a spline and keyway arrangement, which allows relative axial and radial expansion between the pressure and supports tubes. The pressure tube is also supported laterally near its midlength by an orifice plate used for water distribution.

The cold end support tube attachment incorporates a seal that makes possible the stagnant hydrogen zone between the pressure and support tubes. The low conductivity of a gas, coupled with the presence of the support tube acting as a radiation shield, thermally insulates the pressure tube. This same technique of radiation shields and insulative gas spaces is used to protect the outlet tube sheet.

A beryllium reflector plug is located at the inlet end of each fuel assembly to make up for the holes provided for the pressure tubes in the inlet end reflector.

Engine Flow Systems

Figure 5 is a schematic drawing of the overall engine flow systems. The control-solution loop is omitted for simplicity. Figure 6 shows the water flow loop portion of figure 5 and design-point operating conditions. It consists of the heat exchanger and pump, with parallel flow through the beryllium side reflector and reactor core. Only the pump is outside the pressure vessel. System pressure is maintained at 600 pounds per square inch absolute (414 N/cm^2 abs) at the outlet tube sheet of the core. The total flow rate is 1040 pounds per second (472 kg/sec), and temperatures range from 700° R (389° K) at the core exit to 655° R (364° K) at the heat-exchanger exit. The flow rate through the active core region is 946 pounds per second (429 kg/sec).

The propellant (fig. 7) must be forced from the liquid storage tank at a pressure of 35 pounds per square inch absolute (24.2 N/cm^2 abs) through the reactor to pick up the energy of the power source, and through the nozzle to convert the energy to thrust. All the hydrogen pumping is done by two pumps in series, each with a different source of power. The pumps raise the pressure of the flowing hydrogen to 1179 pounds per square inch absolute (812 N/cm^2 abs). The hydrogen then cools the nozzle walls and the water moderator in the heat exchanger in succession. In the process the temperature is raised to 300° R (167° K). The controlled bypass line around the heat exchanger provides flexibility of operation at off-design conditions. The heat picked up by the hydrogen in the process of cooling the nozzle and water is extracted by the topping turbine to supply two-thirds, or 6000 horsepower (4.68 MW), of the required total pumping power. Turbine control is achieved with throttling and bypass valves. On leaving the topping turbine, the gas performs another secondary cooling function when part of the flow is

diverted through a heat exchanger to cool the poison control solution. The entire flow reenters the pressure vessel at a pressure of 712 pounds per square inch absolute (491 N/cm^2 abs) and 320° R (178° K). The hydrogen flows through the propulsion fuel assemblies at 90.5 pounds per second (41.1 kg/sec), is heated to 4460° R (2480° K) and discharges into the nozzle chamber at 600 pounds per square inch absolute (414 N/cm^2 abs) and expands to create thrust.

The remaining 2.5 pounds per second (1.13 kg/sec) of the hydrogen flow is heated to 1860° R (1030° K) in four special tube assemblies to supply the remainder of the system pumping power. Figure 8 shows the path of this bleed flow. The gas that is bled off in the reactor head region at a pressure of 600 pounds per square inch absolute (414 N/cm^2 abs) flows through three turbines in series before being discharged. These turbines drive the control-solution circulating pump, the water-moderator circulating pump, and the first-stage propellant feed pump. Each turbine is controlled by a bypass line and a throttling valve.

System Startup

The conditions given in the three preceding figures (figs. 6 to 8) are for operation at design power. Since the TWMR design incorporates innovations in the propellant feed and reactor control system, the startup phase was also considered in the program. Although there is more detailed discussion in references 3 and 6, the effect of the water moderator on raising the system to operating power is discussed here. For this discussion, one possible startup sequence is described.

Small startup pumps, requiring about 1 horsepower (746 W), are used to circulate the control solution and water moderator slowly. With no hydrogen flow, the reactor is brought critical and to some low power level by reducing the poison concentration in the control solution. Still with no hydrogen flow, the fuel elements increase in temperature, and heat is transferred to the circulating water moderator. Thus, low-power condition is maintained until the water heats to about normal operating temperature. The liquid hydrogen tank shutoff valve is then opened and hydrogen flow starts, being forced through the system under tank pressure to initiate a bootstrap procedure in the pumping system. The mass of warm water in the reactor system has two effects on this operation. First, it is a source of stored energy that can be transferred to the propellant in the heat exchanger upstream of the topping turbine to help the bootstrap operation. Second, it not only tends to keep up the hydrogen flow, but also starts to increase reactor power by reducing the temperature and increasing the density of the water moderator (negative water temperature coefficient). Hydrogen flow and water flow are rapidly increased

as power increases until design conditions are established at rated power and full thrust is developed.

Design for Other Power Levels

The rated power for the reference design is 1500 megawatts. Certain variations would be required for a nuclear rocket with a different power level. Obviously, a different power level would require a different number of fuel assemblies, but any reasonable number of pressure tubes could be incorporated into a structure similar in nature to the one described. Fuel assemblies of exactly the same size and design could be used in this structure to provide the new power level. The heat exchangers would be sized to handle the energy deposited in the water moderator, and modification of the pressure vessel diameter would be required to house the required components. Since other system components depend primarily on fluid flow rates and pressure drops, these conditions would establish the size requirements for turbopumps, nozzles, valves, and piping for different power levels.

The structurally important inlet end reflector would be expected to vary in thickness as core diameter changed. However, since its worth as a neutron reflector depends on thickness, it may be desirable to maintain that dimension at a minimum of 3 inches (7.62 cm) even at lower power levels.

Reactor physics considerations also enter into this process of varying design power. As core sizes become larger, required excess reactivity becomes easier to achieve. Therefore, greater flexibility in the manipulation of nuclear parameters and the possibility of better performance are obtainable. Conversely, as core sizes decrease, neutron leakage from the core increases and required reactivity becomes a more difficult and finally a limiting problem. Design flexibility therefore decreases as power is reduced, and reactor control system possibilities may also change as power varies.

NEUTRONICS

The reactor physics work dealt with the neutronic behavior of the reactor concept within the mutual limitations imposed by the other phases of the study. Analytical methods have determined and critical experiments have confirmed the margins of reactivity required for the design that uses separated tungsten enriched in the 184 isotope. As a means for tailoring the overall radial and axial power distributions to maximize heat transfer, mixtures of natural tungsten and a single mixture of enriched tungsten have been considered and their use demonstrated. The experimental critical assembly

program completed to verify the conclusions of the analytical power tailoring study is only briefly reported herein. The results of the experiments with zoned critical assemblies are fully discussed in reference 3.

A cross section of the reference reactor is shown in figure 2(a). Most of the fissions in this reactor take place at essentially thermal energies because of the good neutron slowing-down properties of the water moderator. Core reflection is provided by the primary beryllium and the secondary water reflector. For fuel-element structural material, tungsten is used that is enriched in the 184 isotope which has one-tenth of the absorption cross section of natural tungsten.

The reference-design reactor employs a finely distributed in-core control system. The reentrant control tubes contain a flowing dilute solution of cadmium and water. They are distributed throughout the entire core, as shown in figure 9 by the small circles in the water spaces between the fuel assemblies. Because the control tubes affect only neighboring fuel assemblies, the amount of control that can be obtained becomes virtually independent of core size.

The radial beryllium reflector is an average of 2.5 inches (6.35 cm) in thickness and contains about 10 volume percent of cooling water. The beryllium is scalloped to displace water near the outer fuel assemblies in order to minimize circumferential power peaking.

In the reference-design reactor, the fuel-element spacing is kept constant at 3.1 inches (7.87 cm) so that the entire core is made up of repetitive hexagonal cells, as shown in figure 9. The initial objective of the neutronics work was to determine the multigroup parameters of these cells. These cell parameters were then used to arrive at a tailored reactor design. The incentive for flattening and shaping the power distribution is to produce maximum propellant temperature in each fuel assembly. These maximums must be consistent with the maximum allowable metallic fuel temperatures and the maximum allowable dynamic loads on the fuel-element stages.

There are many methods that may be exploited to shape the power distributions. For example, in one method the fissionable materials are nonuniformly distributed throughout the core and in another method the water spacing between fuel assemblies is varied.

In the reference design, a range of fuel loadings of uranium dioxide in the tungsten - uranium dioxide matrix has been employed to flatten the power radially in the individual fuel cells. The method for flattening power from cell to cell across the core in the radial direction employs natural tungsten as a distributed parasitic absorber. This is accomplished by making some of the tungsten support tubes for fuel-element stages of natural tungsten rather than of separated tungsten.

The method of adjusting axial power distribution to heat the propellant to the required temperature with the shortest length reactor requires a combination of heat-

transfer and neutronic calculations. Here too, natural tungsten is used as a distributed parasitic absorber. Axial power can be shaped by replacing part of the separated tungsten by natural tungsten in strategic fuel stages of the fuel assembly. Since the reference design uses separated tungsten in the fuel elements, judicious use of these special stages, in conjunction with the use of inlet reflectors, has made it possible to approach the desired axial power distribution quite closely.

The selection of the fuel-assembly center-to-center spacing is reserved to fulfill an important requirement of the reactor design: that the reactor be inherently self-stabilizing during power operation. This requirement is achieved by designing for a negative water temperature reactivity effect.

Cross Sections

The feasibility of the reactor concept required precise neutron cross sections for all the tungsten isotopes. Therefore, considerable emphasis was placed on cross-section measurements early in the program. Tungsten has many large resonances in the intermediate neutron energy range (fig. 10), and an accurate knowledge of the resonance parameters is required for precision neutronic calculations.

The major competitors for neutrons in the TWMR are tungsten and uranium 235. Uranium enriched to 93 percent in uranium 235 is employed to maximize absorptions in the fuel; absorptions in the tungsten should be minimized. Natural tungsten has a thermal cross section of 18.3 barns, which may be reduced by almost an order of magnitude by enrichment in the tungsten 184 isotope. Since tungsten 184 has no significant resonances below 185 electron volts (2.96×10^{-17} J), enrichment is even more attractive. Even with large enrichment, a significant fraction of the neutrons will be absorbed in separated tungsten. The resonances may be effectively bypassed, however, by slowing down the neutrons in the water outside the fuel elements, thereby keeping neutrons away from the tungsten.

Several integral experiments were undertaken to check the precision and completeness of available microscopic cross sections. The first of these was the measurement of effective resonance integrals for the isotopes of tungsten. Figure 11 shows the effective resonance integrals (I_{eff}, in b) for separated tungsten 184 mixtures. The data points are for tungsten samples made of isotopic mixtures that were highly enriched, to approximately 94 percent, in tungsten 184. In the reference reactor, the geometries of the tungsten 184 samples correspond to surface to mass values for $(S/M)^{1/2}$ of 0.50 to 1.00. The Nordheim calculations that use the known resonance parameter data for the tungsten isotopes predict the experimental data very well. Interestingly, the tungsten 184 contribution to I_{eff} is only about 25 percent of the total integral, even for these highly

separated tungsten 184 mixtures. The importance of the large resonances of the tungsten isotopes other than tungsten 184 is thus illustrated.

The second integral experiment was a tungsten-water Fermi-age experiment. The Fermi age for fission energy neutrons is proportional to the mean square distance a neutron will travel from the point of fission to where it becomes a low energy neutron. Comparison of the experimental and calculated values of the age is a check on how well high energy elastic and inelastic cross sections are known.

The age results are shown in figure 12 for plutonium-beryllium source neutrons. The Fermi age to 1.44 electron volts (2.3×10^{-19} J) in square centimeters is plotted as a function of percent tungsten in tungsten-water mixtures. Three tungsten-water mixtures were measured, and the Fermi ages for these mixtures proved less than the age for pure water. The tungsten slows down fast neutrons better than the displaced water, which indicates the importance of the tungsten inelastic cross sections. The calculated curves are from the GAM II cross section multigroup compilation that was used for reactor studies. The calculated results are shown by the solid line, which is about 10 percent lower than the Fermi ages measured for the tungsten-water mixtures. This difference is a result of the model used for calculations at high energies, which slightly exaggerates the inelastic scattering effects due to tungsten.

Reactor Analysis Methods

The development of reactor analysis methods ordinarily depends heavily on the results of critical experiments. Because of the unavailability of the required amounts of separated tungsten, semiempirical approaches that rely on critical experiments to a large extent were rejected. Reliance was placed on neutron transport calculations using the S_n (discrete angular segmentation) transport programs for the core cell calculations. The basic separability of the axial and radial neutron flux distributions and the relative uncoupling of the fuel-element cells permit the use of one-dimensional, multigroup programs for gross criticality calculations. The validity of this approach was checked by two-dimensional calculations: the analytical part of the reference reactor study program provided a vehicle for the understanding and interpretation of physical phenomena, for the design and specification of pertinent experiments, and for the extension of experimental data into areas not specifically covered by the experiments.

The basic calculation for the reference reactor is the solution of the fuel-cell problem. The GAM II and GATHER programs (refs. 7 and 8) were used to obtain multigroup spectrum averaged microscopic cross sections for the materials in the fuel element. The Nordheim resonance calculation was done within the GAM II program for the tungsten isotopic and uranium 238 resonances.

Spatial neutron flux solutions for fuel-element cells were obtained by using an S_n transport theory program. The self-shielding factors resulting from these cell calculations were used in the GAM II and GATHER programs to recompute the neutron spectrum and macroscopic average cross sections.

These cross sections were then used in full core spatial calculations to obtain the reactor multiplication factors and gross radial and axial power distributions. A radial-axial buckling synthesis technique was used with one-dimensional programs, although two-dimensional (r, z) calculations also have been performed.

Another analytical problem that is important to the TWMR is that of gamma heating. Since the water temperature is important in system operation, accurate calculations of the energy deposition in the water by gamma rays are required. To perform the basic tasks of determining the origins, capture locations, and energies of the gamma rays, the Monte Carlo program ATHENA (ref. 9) was developed. In this program, neutrons and gamma rays, both primary and secondary, are tracked by Monte Carlo methods in three-dimensional geometry to provide heating rates in any part of the reactor. Up to 81 energy groups may be used. Also, a statistical estimator is used to compute, in reasonable computing times, the heating rates and fluxes at point detectors inside or outside the core.

Reactor Design and Critical Experiments

Reference reactor-design considerations. - The basic calculation for the reference reactor is the estimation of the multiplication factor for the fuel cell. This cell consists of a fuel element, its pressure tube, and the proportional amount of surrounding water moderator.

The infinite multiplication factor as a function of water thickness for several concentrations of tungsten 184 is shown in figure 13. The water thickness parameter shown is the distance between adjacent pressure tubes. The multiplication factor, in the absence of any leakage of neutrons, is the number of neutrons produced per neutron absorbed in the cell. The bottom curve is for natural tungsten with 30.7 percent tungsten 184. Results for enriched tungsten containing 78.4, 87, and 94 percent of tungsten 184 are also shown.

The general similarity of the shape of the curves is noted. As the water thickness is increased from small values, the number of neutrons slowing down past the resonances increases and the multiplication increases. A point is reached, however, where additional water moderator acts as a parasitic absorber and the multiplication decreases. This decreasing multiplication corresponds to an overmoderated condition; the region to the left of the peak multiplication corresponds to the undermoderated region.

A substantial gain in multiplication is obtained with increased enrichment in tungsten 184. The gain is a result of the decreasing thermal absorption cross section which goes from 18.3 to 2.9 barns with enrichment, while the effective resonance integral goes from 38.6 to 10.7 barns. These factors account for a major part of the increase in multiplication. It is clear that some enrichment of tungsten 184 is required. The availability and cost of tungsten enriched in the tungsten 184 isotope are therefore of prime importance.

The aspects of separated tungsten 184 production have been studied in detail by the AEC at the Oak Ridge - K-25 gaseous diffusion plant, which is capable of separating tungsten isotopes. The results of this technical and economic study for producing tungsten 184 are shown in figure 14. The unit costs are also shown for various enrichments in tungsten 184. This unit cost curve rises very rapidly above 90-percent enrichment. The choice of the 87-percent enrichment for the reference isotopic mixture shown provides a reasonable unit cost, while the annual production for this enrichment, is indicated to be 10 000 pounds (4540 kg).

Figure 15 again shows neutron multiplication as a function of water thickness for the reference cell, using tungsten enriched to 87 percent in tungsten 184. The maximum multiplication of about 1.39 occurs at a water thickness of a little more than 0.5 inch (1.27 cm) and decreases for less water due to increased resonance absorption in the tungsten.

The lower curve shows the effective neutron multiplication for the reference core with 121 fuel elements inside the beryllium reflectors, as previously described. This curve takes into account the neutrons that leak out as well as those absorbed in the reactor. For a water thickness of 0.5 inch (1.27 cm), the multiplication is decreased to about 1.18. The undermoderated region to the left of the maximum is of special interest because this is the region where significant negative temperature water reactivity coefficients can be obtained. With a negative coefficient, as the core water temperature increases, the core loses reactivity so that the reactor power is self-stabilizing. Since temperature is the key parameter that must be controlled for reliable rocket reactor operation, this negative temperature coefficient of reactivity can be a very useful feature for taking the reactor up to power and for power regulation.

Calculation of the exact water temperature coefficient of reactivity is difficult because of the many variables that are temperature dependent. Also, the use of isotopically enriched tungsten in a thermal reactor was without precedent. Therefore, an experimental critical program was initiated to determine the precise amount of excess reactivity available and to determine if the water temperature reactivity coefficient was sufficiently negative.

Critical experiments. - The reference-design reactor was neutronically and physically simulated by a series of critical experiments to check the overall accuracy of the

calculations and to measure the negative temperature coefficient of reactivity. The first two experiments were made at two different fuel-element spacings to study the change of the core excess reactivity and temperature coefficient with fuel-element spacing. These experiments were made with the core reflected solely with water, because of the flexibility of water reflectors in permitting changes in fuel-element spacing. One of these fuel-element spacings was then selected for the beryllium-reflected experiment, which was a mockup of the reference design.

In the critical assembly used (fig. 16(a)), the core is contained in a 6.5-foot-diameter (1.98 m) water tank, and the 121 pressure tubes containing the fuel assemblies are inserted through the upper and lower grid plates, as shown in figure 16(b).

The beryllium reflector used consisted of a 4-inch (10.2 cm) inlet reflector (not shown) that was assembled in the area below the core and the 2.875-inch (7.3 cm) beryllium side reflector. This side reflector was backed by 0.25 inch (6.35 mm) of boral sheeting to reduce the reactivity effects of the exterior water. In the experimental configurations the reference core was upside down, that is, the inlet beryllium reflector is at the bottom. The beryllium side reflector was faced by a scalloped aluminum plate to simulate the true shape of the reflector. Before the reactor was made critical, water was pumped into the tank filling the spaces between the fuel elements and around the core. The dilute poison control tubes located at the midpoints of the triangular water gaps between the fuel elements contained cadmium solution to hold down the excess reactivity of the core.

Since large quantities of separated isotopes were not available for construction of fuel elements, the neutronic characteristics of the fuel element had to be simulated in the mockup core. Figure 17 presents a cutaway view of the fuel element to show how the simulation was accomplished mechanically. The fuel stages contained the correct amount of uranium 235 but required substitute materials for the tungsten 184 mixture. The two views at the right of the figure show schematically how the simulation materials are distributed. A uranium-aluminum alloy was used as the fuel, and the enriched tungsten was simulated by using natural tungsten in reduced amounts to match the correct thermal cross section. In order to match the correct resonance region capture, a single ring of depleted uranium 238 was employed.

The final sizes of the simulating materials were based on numerous calculations to assure an accurate neutronic simulation. Table I gives the calculated results showing the precision of the simulation in terms of absorptions per source neutron for the reference-design and simulated cores. The hydrogen, oxygen, and uranium 235 absorptions agree very well. Since the separated tungsten is simulated by a combination of natural tungsten and uranium 238, the sums in both cores must be compared; the sum is 0.150 for the reference core and 0.153 for the simulated core. The aluminum shows some mismatch, although the total absorptions per source neutron compare very well.

The total for the reference core is 0.851, and the total for the simulated core is 0.854. The difference of the absorption from 1 is the result of neutron leakage. The thermal utilization quantity shown is the ratio of thermal absorptions in fuel to total thermal absorptions, and the match in this parameter indicates the precision of the simulation at the thermal energies. The slowing-down ages may be compared as an indication of the match of the slowing-down properties of the two cores. The difference shown is the result of a small, high-energy, scattering mismatch.

These comparisons of reference and simulated cores are made on the basis of calculations. In order to obtain experimental confirmation of the simulation, several kilograms of calutron-separated tungsten isotopes were obtained from Oak Ridge. These isotopes were used to fabricate five concentric ring stages. These special stages were substituted for five stages in the center fuel assembly of the mockup core. The resulting change in reactivity was then measured.

The isotopic tungsten composition of the reference fuel cell, which was based on as yet unavailable diffusion-separated material, could not be matched exactly with these special stages made with the calutron-separated material. However, the expected reactivity worth was bracketed by varying the number of rings in the special stages. The number of grams of each isotope in a reference-design stage and in three configurations of special stages is shown in table II. The 5-ring stage closely matches the reference-design stage in every isotope except tungsten 184. Because of the deficiency in the 184 isotope, this 5-ring special stage is less absorptive than the reference stage. As more rings are added to increase the tungsten 184 content, the amounts of the other isotopes also increase. Consequently, when the amount of tungsten 184 is closely matched, as it is in the 11-ring case, there is a surplus of the other isotopes, making this configuration more absorptive than the reference-design stage. Therefore, the reactivity of these 5- and 11-ring special stages will bracket the reactivity of the reference-design stage.

The results of the experiment are shown in figure 18. The ordinate gives the reactivity that would result from a total replacement of all the mockup stages in the core by special stages, which have the number of rings listed in the abscissa. The reactivities measured with the special fuel-element stages were converted to their full core counterparts by an analytically derived constant. The reactivity of the mockup stages was experimentally determined to lie between that of the 5- and 11-ring special stages. Thus, from the extremes of this experiment it can be expected that the reactivity of the mockup is within ±2 percent of that of the reference-design core.

Actually, the agreement is considerably better than this. The comparative deviation between the mockup core and the core built of 8-ring special stages was calculated. The result of this calculation is shown by the triangle in figure 18, which agrees to within 0.5 percent in reactivity with the measured value. This close agreement lends strong

support to the method of treating the individual isotopes of tungsten in the calculation used in establishing the mockup core.

The purpose of the first two critical experiments, with the 2.9- and 3.0-inch (7.37 and 7.62 cm) water-reflected configurations, was to find the fuel-element spacing that had a suitably negative temperature coefficient with sufficient overall core reactivity. The multiplication values obtained for these spacings with water reflectors are shown in figure 19. The 3-inch (7.62 cm) spacing proved to be most satisfactory. The beryllium-reflected reference-design core was then built with the 3-inch (7.62 cm) spacing. When the beryllium reflectors were added, a 5-percent increase in multiplication was obtained for the 3-inch (7.62 cm) spacing.

The values calculated prior to the experiment are shown by the solid lines in figure 19. The lower curve is for water-reflected cores, while the upper one is for beryllium-reflected cores. The reactivity of all cores was consistently underestimated initially by about 2 percent.

More detailed calculations were subsequently performed for the water-reflected configuration with 3-inch (7.62 cm) spacing. These calculations included two-dimensional calculations of the fuel-element cell and the total core, and improved treatment of the resonance effects. These refined results are shown as the dashed line in figure 19 and agreed with experiment to within 0.5 percent in reactivity.

Power distributions. - The power distribution in the core is important in the reactor design, since the maximum exit gas temperature can only be obtained if each fuel ring is operating near the maximum allowable temperature. This section discusses the radial and circumferential power distribution within a fuel element and the overall radial and axial power distribution in the core.

An experiment conducted to measure the radial power distribution within a simulated fuel element is shown in figure 20. The relative power density is plotted as a function of the radius of the fueled region. The circles are the experimental data points, normalized to 1.0 at the outside radius of the fuel. The triangular points are values calculated by using multigroup transport theory, and the agreement is very good.

The radial power falloff is a result primarily of the attenuation of the thermal neutron flux. The power distribution shown is typical of an unzoned fuel element. This distribution would require orificing of each propellant channel within the fuel element for operation at maximum exit temperature. The more desirable alternative is to flatten the power in the fuel element by fuel zoning. The flux will still decrease toward the center of the element but the fuel is distributed so that the power is relatively flat. Since the calculation and experiment are in good agreement for the experiment shown in figure 20, this same calculation can be used to compute the loading schedule for uniform power.

Figure 21 shows the radial power in a zoned 10-ring fuel element. The power dis-

tribution relative to the average power in the cell is shown for each of the 10 fuel rings. The ring numbers correspond to the fuel rings indicated in the inset, and the fuel loading used for each is given. A loading of 32-volume-percent uranium dioxide in tungsten is assumed to be the metallurgical limit for these fuel elements, and this loading was used in the center ring. The loading decreases to 12.9 volume percent at the outside. This zoned distribution of fuel, compared with the unzoned fuel element, results in a reduction of about 1-percent reactivity. The variation of the power through the fuel ring is not serious because of good tungsten thermal conductivity.

The fuel-element circumferential power distribution is also important. A sector of the reference reactor is shown in the inset of figure 22, in which the variation of the amount of water around the perimeter of the fuel element can be seen. The greatest amount of water is in the triangular gaps where the control tubes are located. There are two competing effects that tend to cancel one another: an effect causing flux peaking where the most water exists and an effect causing flux depression due to the cadmium in the control tubes. These effects were checked experimentally, and circumferential peaking around the central fuel element was found to be negligible when reference cadmium concentration is in the poison tubes. Figure 22 shows the results of activation measurements made with foils placed circumferentially around two of the fuel elements in the critical assembly. The purpose of the measurements was to determine the effects of the poison control tubes and of the reflector on the circumferential power distributions. The ratio of the power at the angle φ to the average power around the fuel element is plotted as a function of φ. For the center fuel element, negligible circumferential power variation was observed with the dilute reference concentration in the control tubes.

The results of circumferential power measurements made on a fuel element located at the edge of the core indicate a power peaking of about 9 percent in the direction of the water gaps between the fuel elements at the reflector. The thickness of these water spaces between the fuel elements and the reflector can be reduced and still allow adequate cooling; this reduction should reduce the power peaking at the reflector. The power peaking is included as a local factor in heat-transfer calculations.

The overall radial and axial power distributions in the core were investigated. Figure 23(a) shows the radial density in the uniform or unzoned core. The measured local to average radial power for all the fuel elements in a one-twelfth sector of the core is plotted as a function of the radial position of the fuel element. The measurements were made by counting the fission product gamma activity of the middle axial fuel stage of each fuel assembly.

The values calculated by a one-dimensional cylindricized representation of the core are shown by the solid line. Good agreement is obtained except near the edge of the core. The deviations here are believed to be a result of the cylindrical approximation of the hexagonal boundary of the core employed in the calculation.

Flattening the radial power distribution in the unzoned core of the reference design, without changing the fuel loading or fuel-assembly spacing, was achieved by replacing the enriched tungsten support tubes in the central-fuel assemblies with natural tungsten. Figure 23(b) shows an example of radial zoning in which the relative power generated in the fuel assemblies is plotted as a function of radius in the core. The effect of replacing the tungsten 184 support tubes in the central 19 fuel assemblies with the more absorptive natural tungsten support tubes is shown by comparison of the curve for the uniform core with a calculation and with the measured values for the zoned core. The power generated in the outer fuel assemblies is significantly closer to that generated in the central assemblies in the zoned core. This zoned core has about 2 percent less reactivity than the uniform core.

The axial power distribution is concerned with the distribution of power between the axial stages. The composition of materials in some of these fuel stages can be adjusted to make the amount of power generated in the stage closer to that which is desired for efficient heat transfer. In addition, the axial power distribution is shifted by use of a neutron reflector at the inlet end of the core. This reflector consists of a beryllium plug (see fig. 4) with axial holes sized to set the hydrogen flow to the fuel assembly, a beryllium plate that supports the fuel assemblies, and the water in and around the inlet plenum.

Figure 24(a) shows the axial power density in a uniform core, including the power measured in each of the stages of three fuel elements, one located at the center of the core, one at an intermediate position, and one at the edge of the core. The measured power in each stage normalized to the average of all the stages in that assembly is shown plotted against the axial location of each stage. The inlet beryllium reflector is at the left, and the outlet water reflector is at the right. The normalized results for the three fuel elements are seen to coincide closely. Thus, the similarity of the axial power distributions for all the fuel elements is an indication that the axial and radial power distributions are separable.

The solid line shows a diffusion theory calculation for the axial power distribution. Good agreement is found everywhere except near the inlet beryllium reflector, where a 10-percent underestimation occurs. Better results might be obtained at the inlet beryllium reflector with transport theory calculations.

Figure 24(a) shows the power shifted toward the inlet end by the beryllium reflector. This shift toward the inlet is desirable because, for a given fuel surface temperature, more heat can be transferred to the cold hydrogen entering at the inlet than to the hot hydrogen farther along the core. Since separated tungsten is being used in this reactor, the use of some natural tungsten as a parasitic absorber provides a convenient means to shift the axial power distribution farther to the inlet to satisfy heat-transfer needs better.

The calculated axial power distribution in the core is shown in figure 24(b), with the power distribution for each stage of uniform composition again shown as the dashed line.

However, by using a mixture of 30-percent natural tungsten and 70-percent separated tungsten in the stages of the region shown in the figure, this more absorptive mixture shifts the axial power distribution to the solid line shown. The effects obtained are the results of zoning by epithermal absorption rather than by zoning with fuel. This eliminates thermal spiking at zone boundaries and gives a smooth power distribution. However, the introduction of some natural tungsten to accomplish this power shift reduces the available reactivity by about 4 percent relative to an unzoned core.

Reactivity and reactivity control. - From a control standpoint, the two important reactivity effects are those that result from changes in water and fuel temperatures. Figure 25(a) shows the change in reactivity from the room-temperature value as a function of the average water temperature in the core. In this early calculation, the radial power was flattened by varying the fuel-element spacing. The points plotted in this figure are experimentally measured values for the unzoned isothermal critical assembly with a beryllium reflector. The isothermal temperature coefficient was measured by heating the moderator water in a series of steps to 640° R (356° K) and measuring the reactivity change by using calibrated control rods.

From the estimated curve in figure 25(a), about 1 percent in reactivity is lost in taking the water from room temperature up to the nominal operating temperature. Although this loss in reactivity must initially be available from the control system, it can be used to control the reactor in the hot critical condition.

The reactivity change with fuel temperature is a result of the absorptive tungsten resonances undergoing Doppler broadening with increasing fuel temperature and thereby interacting with a larger part of the neutron slowing-down flux. The result is an instantaneous decrease in reactivity with an increase in fuel temperature. Figure 29(b) shows the decrease that promptly accompanies increasing fuel temperature. About -1.5 percent reactivity is introduced as the fuel heats to its average temperature of 3760° R (2090° K). Although the maximum fuel temperature is 4960° R (2755° K), the net Doppler effect is from the average over the entire core.

Another reactivity effect that must be accounted for is that due to transient fission products. The most troublesome of these for the high-thermal-flux reference reactor is xenon 135. During full-power operation, the core reactivity worth gradually decreases by about 0.4 percent reactivity at the end of 1 hour due to xenon poisoning. If the reactor is shut down after a period of operation, the decay of iodine to xenon results in a buildup of transient xenon that rises to a peak of -8.5 percent reactivity 12 hours after shutdown, while decaying with its own characteristic half life, as shown in figure 26.

The upper curve assumes 100 percent retention of the iodine and xenon in the fuel. There is evidence that fission product gases diffuse through the tungsten clad at high temperature. The lower curve shows that, for a 70-percent retention of the iodine and xenon, transient xenon reactivity has a peak value of 6 percent. This amount of excess

reactivity will be required to override peak xenon.

A summary of all reactivity effects, given in table III, totals 19 percent so that this amount, which was available in the unzoned critical assembly, is indeed necessary. The 7.4 percent for power tailoring is made up of a little over 1 percent for flattening the power distribution within the fuel element, about 2 percent for the gross radial power flattening, and about 4 percent for the axial power adjustment required for the reference core. The 2.5 percent for the change of reactivity with temperature is made up of 1 percent for the water temperature and 1.5 percent for the fuel temperature change.

The reactivity required for operating the reactor for 10 hours is about 1.7 percent: 0.4 percent for the xenon poisoning accrued in a 1-hour run, 0.8 percent for long-lived fission product poisoning including samarium, 0.3 percent for fuel transmutation, and 0.2 percent for an assumed fuel weight loss of 1 percent in 10 hours. The 6 percent required for complete transient xenon override assumed 30 percent loss of iodine and xenon through the clad. If this is a good assumption and this 6 percent were available, the reactor could be restarted any time after full power runs up to 1 hour in duration. The ±1.5 percent in table III is an allowance for design and manufacturing tolerances.

The propellant hydrogen reactivity is very small in this reactor. There is so much more hydrogen in the water than in the propellant that the hydrogen propellant has an insignificant effect on reactivity.

Not all these reactivities need to be controlled. The reactivities that do need to be controlled are shown in table IV along with the assumed reactivity control rates. In the table, 4.5 percent is required for taking the reactor from the cold shutdown to the hot critical condition; 2 percent of this 4.5 percent is the shutdown margin and the other 2.5 percent is the loss in reactivity with temperature. The 0.057-percent-per-second rate, a nominal reactivity control rate, is sufficient to allow getting to hot critical in about 80 seconds; however, in starting up a rocket reactor, considerable hydrogen can be wasted in 80 seconds. To shorten the time for reaching full power after the hydrogen flow has been started without increasing the 0.057-percent-per-second control rate, the reactor can be brought to hot critical at a very low power level with no propellant hydrogen flowing. The negative temperature reactivity coefficient can then be used to take the reactor from the low-power no-flow condition to 95 percent of full power in about 15 seconds by simply accelerating the hydrogen flow.

After the hydrogen flow reaches its nominal value, this temperature reactivity will maintain the core temperatures during hydrogen flow fluctuations by its self-stabilizing reactivity characteristic. Once reactor temperatures are set at their maximum operating values, it is desirable to keep them there throughout the power run. Thus, the only function of a reactivity control system during steady-state operation is to compensate for the 1.7 percent change in reactivity that occurs during 10 hours of operation. The required reactivity insertion rate is considerably less than the 0.0035 percent per second

allowed for fine control of temperature.

For the transient xenon, the 0.014-percent-per-second rate can insert the required 6 percent in about 7 minutes. This rate is also sufficient to provide negative reactivity when the transient xenon is burning out.

Thus, the total needed from a reactivity control system is about 12 percent. Also, the largest rate of increase of reactivity needed for this rocket reactor is no greater than rates presently used in operating power reactors.

Independent emergency shutdown methods such as injecting gadolinium nitrate directly into the water in the center of the core will probably be required to make the finely distributed in-core control systems that are under consideration completely safe. This method should be able to insert 15 percent at the fast rate of 5.7 percent per second. It can then be removed at the slower rate of 0.057 percent per second.

Investigations have shown that, if conventional rods are used to control the 12 percent in reactivity, the axial power distribution is completely distorted. Also, the control rods investigated caused considerable circumferential power peaking. As a result, the thrust to weight ratio and the specific impulse of a rocket reactor with control rods would be less than could be obtained with a finely distributed control system.

On the other hand, reflector control drums distort the radial power distribution, and large cores cannot be satisfactorily controlled by drums. Figure 27 shows various reactor reflector control effects. The reactivity of a thick beryllium reflector is plotted as a function of core diameter. The worth of the reflector is large for small diameter cores and is indicated to be worth about 35 percent in reactivity for a 20-inch-diameter (50.8 cm) core. As the diameter of the core increases, the percentage of neutrons that leak out decreases and, consequently, the reflector worth decreases. For a 50-inch-diameter (127 cm) core, the reflector is worth only about 6 percent in reactivity.

If the reflector control method is used, the percentage of neutrons that return to the core is varied by rotating control drums in the reflector. About 40 percent of the total reflector worth can be obtained by rotating control drums. The estimated control swing available from control drums as a function of core diameter is shown in the lower curve of figure 27. Rotating drum control in the thermal reactor can provide up to 20 percent reactivity control swing for a 15-inch-diameter (38.1 cm) core. For the 32-inch-diameter (81.2 cm) reference core only about a 5-percent swing can be attained. This value is much less than the desired 12 percent. Therefore, the liquid poison control system was chosen for the reference design.

The control worth of the finely distributed soluble poison system is shown in figure 28. The reactivity of the cadmium solution is shown plotted against the cadmium concentration in the control tubes. The required reference reactor poison concentrations for a 12-percent control swing can be attained by very dilute poison solutions without approaching the solubility limit. The concentrations measured in the clean critical

(unzoned) experiments are also shown. The control swing for zoned core poison concentrations have been calculated and are shown as the solid line.

A flow loop shown in figure 29 was built to verify the uniformity of the poison concentration throughout the 210 poison tubes in the core under actual flow conditions. The construction of the loop past the injection point is identical to that proposed in the reference reactor design.

The results of the experiments showed that the poison concentration in any tube varied from the average concentration by less than 5 percent at any time. Calculations showed that a 5-percent decrease in the cadmium concentration in two central poison tubes would result in only a 0.1-percent rise in the power of the center fuel element, and this change is negligible.

The flow loop was also used to check the speed of response of changing poison concentration throughout the control tubes in the core. It was determined from calibrated electrical conductivity cells that the poison entered the core within 0.2 second after opening the injection valve and the core poisoning transient lasted for 2 seconds, which is slightly less than one loop time. Therefore, the full effect of a given rate of change of poison insertion occurs in 2 seconds.

Since aerospace systems should take advantage of lightweight components whenever possible, a reactor control system that uses a strong neutron absorbing gas, such as helium 3, was also investigated. A detailed discussion of this control system is presented in reference 3.

Larger and smaller cores. - Much of the TWMR feasibility study effort has been devoted to the 121-element reference reactor design, which acts as the focal point for the many technical disciplines involved. However, as previously mentioned, other reactor sizes are possible using the same reference fuel-element design. Some analyses were therefore performed for larger and smaller core sizes to define the effects on major nuclear design variables.

The axial power distribution and local radial fuel stage power distribution are relatively independent of size and are well defined by the previous analysis for the reference core. The overall radial power distribution and neutron multiplication, which are the major design variables affected by size, are characteristics shown in figure 30. The inset illustrates the overall radial power flattening technique used for the reference reactor size. The heavy circles in the central part of the core indicate those fuel elements that utilize the neutronic poisoning of natural tungsten support tubes to improve the overall radial power distribution. For larger reactors, core size is increased simply by increasing the number of reference-design fuel elements and the number of natural tungsten support tubes. The criterion used to establish a power-flattened core is that the peak to average power density should be equal to or less than that of the reference core.

The neutron multiplication factor is given as a function of core diameter in figure 30

for both radially uniform and radially zoned cores. The peak to average radial power density as a function of core diameter is also shown in the figure. For every core size, the fuel-element spacing, fuel-element length, and beryllium-reflector thickness are the same as for the reference reactor.

For the uniform cores, the multiplication factor increases with core size as expected due to reduced neutron leakage. For the zoned cores, the radial peak to average power actually decreases somewhat, showing some improvement over the reference reactor power distribution. This zoning decreases the multiplication factor at every size, but nevertheless results in a net gain over the reference core value.

Large cores with low leakage will require the use of some or all this excess reactivity gain to obtain a negative temperature coefficient. One means to achieve this would be to reduce the amount of water in the core by reducing the fuel-element center-to-center spacing. The temperature coefficient and the stability of the power distributions in very large cores are areas that should be investigated.

The characteristics of two of the smallest possible separated tungsten cores are shown in table V. Both these cores are unzoned radially, since natural tungsten support tubes have not been used to improve the gross radial power distribution. The fuel-element spacing and length are the same as for the reference reactor. In each case, the beryllium radial reflector has been sized to minimize the value of maximum to average power density across the core. The radial reflectors on these small cores have sufficient reactivity for reflector drum control systems.

The smallest uranium 235 core, listed in table V would not have sufficient reactivity for overriding peak xenon. However, it would have a sufficient amount for axial power tailoring so that 39 inches (99 cm) of fuel will give the same 4460° R (2480° K) exhaust gas temperature as the reference core.

The second core listed in table V uses neutronically superior uranium 233 as fuel so that this core can be made smaller. This core almost has sufficient reactivity for both axial power tailoring and peak xenon override. Figure 31 shows a cross-sectional view of this core. Only 15 kilograms of uranium 233 fuel are required for the 19 fuel assemblies. A water-cooled beryllium reflector with 12 rotating control drums is indicated. This reactor is potentially capable of producing a power of 360 megawatts and a hydrogen propellant exit temperature of 4460° R (2480° K). The core diameter is 15 inches (38.1 cm), and the primary reflector diameter is 22 inches (56 cm). If it were desirable to incorporate the water-to-hydrogen heat exchanger, a secondary water reflector would be added and this would increase the pressure vessel diameter to about 30 inches (76.2 cm). The weight of this reactor, pressure vessel, pumps, nozzle, and piping is approximately 2500 pounds (1130 kg).

FUEL ELEMENTS

Fuel elements were fabricated and tested as part of the overall TWMR program. This work included

(1) A study of the ability of fuel elements to contain fissionable material and of the physical and mechanical properties of fuel elements under simulated operating conditions

(2) The design and selection of fuel-element configurations for nuclear rocket application and the development of techniques for fabricating and supporting these shapes

As a basis for the work on fuel retention and properties, certain operating goals were defined early in the program. High-temperature fuel-element operation would be necessary to realize the specific impulse potential of the nuclear rocket. The nominal operating temperature for the fuel elements was chosen to be 4960° R (2755° K). Although no specific space mission has been defined, the operating time was assumed to be short and consistent with high-thrust propulsion. To allow for development testing, the total operating time was fixed at 10 hours. The number of startups and shutdowns was unknown; therefore, to allow for development testing, the thermal cycling capability goal was set at 25 cycles. Some fuel losses could be tolerated, but to limit the excess reactivity necessary to compensate for fuel loss, the allowable fuel loss was specified to be less than 1 percent. In addition to these goals, good high-temperature strength would be necessary; that is, the presence of fuel should not overly compromise the strength of the fuel elements.

At the beginning of this program, it was decided that these goals could best be met with dispersion-type fuel composites with a continuous matrix of tungsten. Tungsten was selected because it has the highest melting point of all metals, has relatively good strength and excellent thermal conductivity over the operating temperature range, and does not react with the hydrogen propellant. Uranium dioxide was chosen as the fissionable fuel to be dispersed in the tungsten matrix because it is one of the most refractory fuels, has a fairly high uranium density, and, for the most part, is not reactive with either tungsten or hydrogen.

The work on development of a suitable fuel-element design for the TWMR included fabrication, support structure, and testing of potential fuel-element configurations. Methods were developed to fabricate two of the most promising configurations. These were examined as to their ability to withstand the aerodynamic forces of the high velocity hydrogen and the thermal stresses generated within the element. Support of the fuel elements under axial drag loads and vibratory lateral loads also was studied.

Fabrication of Fueled Composites

To evaluate the effects of fuel vaporization and decomposition and to develop methods for controlling fuel loss due to these factors, it was necessary to fabricate suitable test specimens. In addition, these specimens were used to determine the mechanical properties of the fueled composites. Also, methods for fabricating fuel elements of complex geometry such as might be required in an actual reactor were developed.

Several methods were investigated to produce fueled test specimens with uranium dioxide particles dispersed in a continuous tungsten matrix. These methods included consolidation of mixtures of tungsten and uranium dioxide particles as well as tungsten-coated uranium dioxide particles into dense bodies. Early in the program, it became obvious that uranium dioxide was being lost from the composites during continuous heating because, at the operating temperature of 4960° R (2755° K), uranium dioxide has a vapor pressure of about 3 millimeters of mercury (400 N/m^2). This high vapor pressure can cause large amounts of fuel loss from tungsten - uranium dioxide composites by vaporization of all surface-exposed uranium dioxide particles as well as of interconnected internal uranium dioxide particles. Methods were developed to prevent fuel vaporization. One method for reducing loss is the use of a thin (0.001 in. (0.0254 mm)) layer of tungsten on all outer surfaces of the composite. Tungsten coating of uranium dioxide particles also has been shown to reduce vaporization losses as well as to give a more uniform fuel dispersion in the composites.

The method developed at Lewis for fabricating flat plates from mixtures of tungsten and uranium dioxide powders is basically a powder-metallurgy and hot-rolling operation. A mixture of powders is cold compacted into flat plates and sintered at 3560° (1980° K) to yield a cermet plate with a density in excess of 90 percent of theoretical. Additional densification is achieved by rolling at approximately 3960° R (2200° K). The finished cermet plates are about 20 mils (0.508 mm) thick and have a density in excess of 99 percent of theoretical. This hot-rolling technique has been successful in the fabrication of plates that contain up to about 40-volume-percent uranium dioxide.

The plates can be clad on the major faces with a thin layer of unfueled tungsten (~0.001 in. (0.0254 mm)) during the rolling operation by roll bonding wrought tungsten foil to the cermet. The resultant cladding is fully dense, uniform in thickness, and metallurgically bonded to the core.

Several photomicrographs of rolled fuel plates are shown in figure 32. These fuel plates contained 10-, 20-, 30-, and 40-volume-percent uranium dioxide. The white areas in the photomicrographs are tungsten, and the darker areas are uranium dioxide particles. The high density of the tungsten matrix and the uniformity of the tungsten cladding applied by roll bonding are noteworthy. The fuel particles were initially spherical and about 50 microns in diameter before consolidation, but these were elongated

somewhat during rolling.

With the roll-bonding technique, however, the edges of the plates are still unclad. Various cladding methods, such as powder sintering and plasma spraying, have been used effectively to clad the edges of the fuel plates, but these methods are essentially limited to composites of simple geometry.

Other techniques were investigated, therefore, for cladding all exposed surfaces with one process; vapor-deposition techniques proved to be the most promising. Vapor deposition employs hydrogen reduction of a tungsten halide at elevated temperatures to deposit tungsten metal on heated surfaces. A typical photomicrograph of a composite clad by vapor deposition is shown in figure 33. The cladding is fully dense and metallurgically bonded to the fueled core.

The consolidation of tungsten-coated uranium dioxide particles is complicated by the fact that the large tungsten - uranium dioxide particles do not sinter well. However, two processes based on hot roll compaction and hot isostatic compaction have been developed for the consolidation of these particles. In both processes, the tungsten-coated uranium dioxide particles are loaded into flat molybdenum cans and vibratory compacted to a density of about 65 percent of theoretical. The canned particles are then heat treated in hydrogen at 2460° R (1370° K) to remove any surface oxide on the particles. In the roll-compaction process, densification of the particles is achieved by hot rolling the unsealed can at about 3560° R (1980° K). For isostatic compaction, the molybdenum cans must be evacuated and sealed prior to compaction. Compaction of the sealed cans is then achieved by a combination of temperature (3460° R (1920° K)) and pressure (30 000 psia (2.07×10^4 N/cm^2 abs)) in an autoclave. In both processes the molybdenum canning material is removed with a nitric acid solution, which dissolves the molybdenum but does not harm either the tungsten or the tungsten-encapsulated uranium dioxide particles.

Typical microstructures of plates produced by both methods are shown in figure 34. The fuel dispersion in the plate produced by roll compaction is quite uniform, but the uranium dioxide particles are rather elongated and this could result in anisotropic properties in the fuel element. The uranium dioxide particles in the isostatically compacted plate are no longer spherical, but the distortion is much less than that obtained with roll compaction.

For the fabrication of fuel elements of more complicated geometry than flat plates, several consolidation methods were investigated. Of these methods, hot isostatic compaction and hot pneumatic impaction (a process similar to hot isostatic compaction) were the most satisfactory. Both these methods involved filling a molybdenum die assembly with a powder mixture of tungsten and uranium dioxide or tungsten-coated uranium dioxide particles using dams or a special filling device to generate the desired radial fuel loading distribution. The loaded die assemblies then were sealed in molybdenum cans under vacuum and were hot isostatically compacted or hot pneumatically impacted at

temperatures of about 3460° R (1920° K). After consolidation, the molybdenum forms were dissolved in nitric acid. The microstructures of these assemblies looked similar to that of the isostatically compacted plate shown in figure 34.

Fuel Retention Studies

The purpose of these studies was to determine the effect of time, temperature, and thermal cycling in purified hydrogen on loss of fuel from cermets and to develop methods for restricting fuel loss to <1 weight percent of the uranium dioxide originally present. These fuel retention measurements were carried out on thin rectangular cermets prepared by consolidation of tungsten and 50-micron uranium dioxide particle mixtures or of 50-micron uranium dioxide particles coated with tungsten. The principal consolidation techniques used were hot roll compaction and isostatic compaction. Most of the specimens evaluated were clad on the external surfaces with a thin layer of tungsten.

Fuel loss through vaporization. - The effects of tungsten cladding on the surfaces of cermets and of the use of tungsten-coated particles on fuel loss due to vaporization of uranium dioxide during continuous heating for 2 hours at 4960° R (2755° K) in hydrogen are shown in figure 35. Surface cladding was particularly effective in restricting fuel loss. The use of tungsten-coated uranium dioxide particles also resulted in decreased fuel loss. Thus, the combined use of surface cladding and coated particles would be the best choice for restricting fuel loss through volatilization.

Fuel loss induced by thermal cycling. - Tungsten - uranium dioxide cermets, even though clad, lost fuel under thermal cycling conditions, as shown in figure 36. One curve shows the loss under continuous heating conditions, and the other curve shows the more severe loss where thermal cycles of 2 hours duration were used. Also, metallographic sections of specimens after cycling (fig. 37) showed a uranium-bearing phase in the grain boundaries of the tungsten matrix for the cycled specimens. The best method found for reducing fuel loss during thermal cycling consisted of the addition of small amounts of metal oxides like yttrium oxide or cerium oxide in solid solution with the uranium dioxide fuel. The effectiveness of this method is shown in figure 38, where the fuel loss is plotted as a function of the number of 10-minute cycles to 4960° R (2755° K) in flowing purified hydrogen at 1 atmosphere pressure for an ordinary clad cermet and for clad cermets stabilized with 5- and 10-mole-percent yttrium oxide (Y_2O_3) or cerium oxide (Ce_2O_3) in uranium dioxide.

In summary, the recommended method for restricting fuel loss from fuel elements includes a complete external cladding on the elements with a thin layer of tungsten, the use of tungsten-coated uranium dioxide particles, and the use of uranium dioxide with 10-mole-percent Y_2O_3 or Ce_2O_3 in solid solution.

Effect of operating variables on fuel loss. - Although the reduction of fuel loss was quite promising under the test conditions used, actual operating variables could extend beyond the range of the conditions tested. The fuel loss curves, for example, have been shown for a maximum cycling temperature of 4960° R (2755° K), but "hot spots" conceivably could cause higher temperatures in an actual operating reactor. Also, cycling conditions could involve longer or shorter holds than the 10 minutes at temperature that were used in the tests discussed. Furthermore, the tests were made at 1 atmosphere hydrogen pressure, whereas an element in a reactor would experience much higher pressures (e.g., about 600 psia (414 N/cm^2 abs)). Finally, the effects of fission heating must be considered.

The effect of maximum temperature during cycling is shown in figure 39. Comparison of these curves shows that fuel loss is increased by an increase in temperature from 4960° to 5160° R (2755° to 2860° K). The loss after 25 cycles to 5160° R (2860° K), however, is not more than 2 percent.

The effect of time at temperature during each cycle on fuel loss appears in figure 40. For long hold times (e.g., 120 min), the total operating time goal of 10 hours was met, but the number of cycles was small (6 cycles), and for short operating cycles (e.g., 2 min), the total time to reach 1 percent fuel loss was less than 10 hours, but 80 were completed. When 10-minute cycles were used, a 10-hour total operating time and 50 cycles were possible. Therefore, reactor operating cycles should be carefully selected, particularly during ground testing.

The effect of hydrogen pressure on fuel loss has been measured (fig. 41) on fully clad composites with 35-volume-percent uranium dioxide stabilized with 10-mole-percent cerium oxide. Data at a pressure of 600 pounds per square inch absolute (414 N/cm^2 abs) hydrogen have been obtained through 50 cycles. The loss up to 25 cycles is essentially the same at 600 pounds per square inch absolute (414 N/cm^2 abs) as it is at 15 pounds per square inch absolute (10.3 N/cm^2 abs) and well below the 1-percent level indicated by the horizontal dot-dash line. Tests conducted on specimens in 600 pounds per square inch absolute (414 N/cm^2 abs) hydrogen at 5160° R (2860° K), however, showed rapid fuel loss well before 25 cycles were reached.

Apparently, no serious fuel loss problem was introduced by changes in the cycling program or high-pressure hydrogen except that, in high-pressure hydrogen, temperature excursions above 4960° R (2755° K) should not be allowed or should be kept as brief as possible.

Radiation effects. - The nuclear rocket application requires relatively low values of total neutron exposure (nvt) and low value of burnup. The total burnup for a high-thrust mission is of the order of 0.2 percent. Therefore, any noticeable radiation damage or fission product pressure buildup for this application would not be expected. In-pile capsule tests, nevertheless, have been conducted on fuel-element material specimens to

check the validity of furnace tests. A typical capsule used in these tests is illustrated in figure 42.

The specimen was heated by fission of the fuel in the specimen, and the heat was removed by thermal radiation to the capsule walls, which were cooled by water flowing over the outside surface of the capsule. Fuel loss tests were conducted for 4 hours at temperatures from 3960° to 5460° R (2200° to 3030° K). Weight loss measurements and metallographic examination indicated no difference between fission heating and furnace heating. Although in-pile tests did not include thermal cycling in hydrogen, fission heating itself does not appear to pose any new problems.

Mechanical Properties

Knowledge of the mechanical properties of fuel-element materials is necessary for the design of the reactor. All the current mechanical property data were obtained on rolled plates prepared by the hot-rolling powder-metallurgy techniques. The use of tungsten-coated uranium dioxide particles (compacted by either hot rolling or isostatic pressing) rather than mixtures of tungsten and uranium dioxide powders could possibly result in changes in the data, and this possibility is discussed further in reference 1.

Tensile properties. - The results of tensile tests conducted at 4960° (2755° K) on fuel plates with 0- to 50-volume-percent uranium dioxide are shown in figure 43. The strength of unfueled tungsten (shown at the left, 100-percent W) is about 3700 pounds per square inch (2550 N/cm^2) and the ductility (not shown) is about 10 to 15 percent reduction in area. From these results, it appears that the loading of the fuel elements should be less than 35-volume-percent uranium dioxide in order to avoid the region of rapidly decreasing strength. If more strength is required, it might be possible to use a stronger tungsten alloy in place of the unalloyed tungsten used in these studies.

The effect of test temperature on the tensile strength of several different tungsten - uranium dioxide composites with 20-volume-percent uranium dioxide is shown in figure 44. Little change in strength was observed in these tests when a metal-oxide-stabilized fuel (calcium oxide stabilized) was used in place of the standard uranium dioxide. A significant increase in the strength of the composites containing 50-micron-diameter uranium dioxide was achieved by the addition of 2 volume percent of fine (1 μm) thorium oxide particles to the tungsten matrix. Thus, a thoriated matrix might be used in combination with a metal-oxide-stabilized fuel to increase the strength of the composites. If tungsten-coated uranium dioxide particles are to be used, however, methods would have to be developed for the introduction of fine thorium oxide particles into the tungsten.

Creep-rupture properties. - A series of creep-rupture tests was performed on the

tungsten-uranium oxide composites over a range of temperatures and fuel loadings corresponding to those intended for use in the TWMR. Some of the results of this study are shown in figure 45. As fuel is added to the composite, the maximum allowable stress that will give a 10-hour rupture life decreases.

Modulus of elasticity. - The deflection of a fuel element under a given load is another important design property, and the results of the study are shown in figure 46. The modulus of elasticity values shown here for tungsten are higher than other static test data reported in the literature. Test conditions in this study were controlled very carefully so that creep would not affect the test results.

Composite plates containing 10- to 40-volume-percent uranium dioxide were tested, and all the results fall in the shaded area of the figure with very little difference in the values for the different fuel loadings. The rapid decrease in the moduli of the composite materials between 3960° to 4460° R (2200° and 2480° K) is not fully understood, but one possible explanation is that, in this temperature range, the modulus of the uranium dioxide decreases rapidly and contributes progressively less to the overall moduli of the composites.

Design Parameters

The fuel elements of a rocket reactor contain the fissionable fuel and transfer the heat released by the fission process to the propellant. Some of the important fuel-element design parameters are discussed herein.

In order to achieve maximum propellant temperature, the fuel elements must operate at the maximum uniform temperature consistent with the materials of construction, and the heat-transfer flow passage must have a length to diameter ratio large enough so that the propellant temperature approaches the fuel-element surface temperature. The effect of passage length to diameter ratio on propellant to surface temperature is shown in figure 47 along with the effect of Reynolds number. At a Reynolds number of 10 000, a flow passage length to diameter ratio of 240 is required, for the propellant temperature to approach within 10 percent of the fuel-element surface temperature. Actually, a slightly larger ratio is needed because axial power distributions corresponding to constant surface temperature may not be practical from a reactor physics viewpoint. Thus, for a reactor 3 feet (91.5 cm) long, an equivalent passage diameter of 0.125 inch (3.18 mm) is about the size of interest.

The mass velocity is also significant because, with a fixed outlet temperature, it determines the power and thrust from a given reactor. Also, as the mass velocity is increased (fig. 48), the core pressure drop increases, the aerodynamic load on the fuel element increases, and the outlet Mach number of the propellant increases. Each of these factors at some point will limit the mass velocity through the reactor passages

because it requires (1) a fuel element capable of withstanding high aerodynamic loads, (2) a core structure capable of supporting high pressure and pressure drop, and (3) sufficient pumping power to deliver the propellant to the reactor at the required high pressures.

Fuel loading and fuel-plate thickness are also important design parameters. Selection of values for these parameters involves complex relations between nuclear, heat transfer, and material property considerations. Preliminary studies have shown that a reasonable compromise for this reactor concept is a thickness of 20 mils (0.508 mm), an average uranium loading of 20 volume percent, and, to allow for tailoring the power distribution, a maximum fuel loading of about 30 volume percent.

Fuel-Element Configurations

Various fuel-element configurations such as flat plates, concentric cylinders, tube bundles, and honeycombs were considered. Because of expected performance limitations or fabrication difficulties, only two configurations, the concentric cylinder and the honeycomb, were selected for further study.

Concentric cylinder elements. - One of the primary reasons for considering the concentric cylinder element was that it could be made by forming plate stock into cylinders of various diameters. The cylinder wall thickness was 20 mils (0.508 mm), and the annular gap between cylinders was 0.0625 inch (1.59 mm), corresponding to an equivalent of 0.125 inch (3.18 mm). In this type of fuel element, each cylinder can have a different uranium fuel loading to achieve uniform radial power within the element. The maximum number of cylinders that can be used without exceeding a loading of about 30-volume-percent uranium dioxide is approximately 11 cylinders, which corresponds to a fuel-element diameter of 2 inches (5.08 cm).

Fueled tungsten cylinders from 0.5 inch (1.27 cm) up to several inches (cm) in diameter were easily formed at 2160° R (1200° K) from tungsten - 20-volume-percent uranium dioxide plates. However, the joining of these tungsten - uranium dioxide composites was a difficult problem because dispersed uranium dioxide melts at a temperature of about 1200 R° (667 K°) less than the tungsten. Ordinary fusion-welding techniques, such as electron-beam or tungsten - inert-gas welding, could not be used without extensive gas bubbling and resultant porosity in the weld zone. Therefore, several other joining techniques were investigated under contracted programs, and the results indicate that the most promising technique is gas-pressure bonding. A sample joint that can be obtained with this method is shown in figure 49(b). In the photomicrograph grain growth has occurred across the interface and clad-to-clad bonding has been achieved. Tensile tests at 4960° R (2755° K) on joined plates have shown that gas-pressure bonding results in

joints that are as strong as the base metal.

High-temperature tests to measure the aerodynamic forces (dynamic head) that a concentric cylinder fuel-element stage can withstand are difficult to conduct. High-temperature material-property data for tungsten suggested that a lead-antimony alloy at room temperature would best simulate tungsten at high temperature. Therefore, preliminary flow tests were conducted on lead-antimony elements at room temperature.

Lead-antimony elements were placed in an airflow test facility, and the flow rate was increased until failure occurred. The three types of elements tested are shown in figure 50. The first fuel-element stage had two support combs at the leading edge of the cylinders (fig. 50(a)). Fuel-element stages of this type failed at an average dynamic head of 12.6 pounds per square inch (8.7 N/cm^2). Additional supports were added at the leading edge, as indicated in figures 50(b) and (c). These lead-alloy fuel-element stages failed at dynamic heads of 26 and 30 pounds per square inch (17.9 and 20.7 N/cm^2). A typical failure is shown in figure 51.

As a check on the material simulation, tungsten concentric cylinders were flow tested at reactor operating temperature using hot nitrogen from an arc-jet facility. Both the tungsten and the lead-antimony results are for fuel elements with leading edge supports at 90° intervals, as shown in figure 50(a). The highest dynamic head available from the arc-jet facility was 12 pounds per square inch (8.28 N/cm^2). A tungsten element of this type did not fail at this dynamic head. Failure occurred while increasing the temperature to 5560° R (3090° K). Lead-antimony, which failed at a dynamic head of 12.6 pounds per square inch (8.7 N/cm^2), therefore appears to simulate tungsten at a temperature somewhat higher than the nominal design temperature.

One other effect noted during the lead-antimony tests was that elements tested for long duration failed at lower dynamic heads than those under short-time tests indicating that creep contributes to failure. No long-duration high-temperature test data have been obtained for tungsten.

The test results indicate that the concentric cylinder configuration may be suitable for the reference-design conditions, but this configuration imposes a severe dynamic head limit unless many supports are added to the cylinders. Because of the many supports required, it is desirable that these supports also be fueled so that they can contribute most effectively to heat transfer. This obviously leads to a fine grid in which all the webs are fueled. Such a configuration is represented by the honeycomb element.

Honeycomb elements. - The very rigid structure of the honeycomb stages shown in figure 52 has two advantages. It permits the use of thin fueled sections and does not have dynamic head as a limiting parameter. The web thickness is 20 mils (0.508 mm), and the distance across flats of each hexagonal flow passage is 0.125 inch (3.18 mm). The outside diameter of the stage is about 2 inches (5.08 cm). For uniform heat generation, the fuel loading can be varied radially from about 30 volume percent in the center of the

honeycomb to about 10 percent at the edge. Present fabrication techniques, such as hot isostatic compaction and hot pneumatic impaction, have advanced to the point that fabrication of honeycomb configurations is feasible (see fig. 52). Some additional development of the fabrication processes is required before actual reactor fuel elements could be produced. In particular, improvements are needed to control dimensions and fuel distribution within these structures.

While the rigidity of the honeycomb essentially eliminates the dynamic head problem, the inherent stiffness could cause thermal stress problems. Even though the fuel elements are designed to achieve uniform temperature, some temperature gradients will always exist. Materials with different thermal expansion coefficients, such as fueled and unfueled tungsten or variably fueled tungsten in the honeycomb stage itself, also cause thermal stress.

Plastic flow and creep would essentially eliminate stresses at high temperatures. However, on cooling, low-temperature stresses would appear, as the honeycomb would try to return to its original unstrained condition. At room temperature, tungsten is strong but brittle, and the internal stresses might cause the honeycomb to crack. The situation is aggravated by thermal cycling where thermal fatigue enters in.

In order to evaluate the thermal stress problem, stresses were imposed on a uniformly loaded honeycomb stage by radial temperature gradients. Hot gas from a tungsten preheater was forced to flow through the 19-hole central region of the honeycomb. At the same time, the outer periphery of the honeycomb was cooled by the flow of cold gas. The temperature gradient was controlled by varying the amount of cold gas flowing around the outside of the honeycomb. This radial temperature gradient induced thermal stress in the radial, tangential, and axial directions.

A honeycomb was thermally cycled 25 times with a hot gas temperature of 4460° R (2480° K) in the central region and a thermal gradient of 1200 R° per radial inch (667 K° per radial cm; 150 R° (83 K°) per hexagonal passage). Inadvertently during one of the 25 cycles, a rapid shutdown occurred resulting in a cooling rate in excess of 1000 R° (556 K°) per second compared with the normal cooling rate of 20 to 30 R° (11 to 16 K°) per second. A second honeycomb was subjected to a hot gas temperature of 4960° R (2755° K) in the central 19-hole hexagonal region and a maximum thermal gradient of 3200 R° per radial inch (700 K° per radial cm; 400 R° (228 K°) per hexagonal passage) for three cycles.

Inspection of the honeycombs by nondestructive testing techniques and then by inspection of the microstructure showed that no cracks developed in the structures as a result of the testing. Test results indicate that the honeycomb can withstand both the high-temperature stresses imposed and the low-temperature stresses resulting from inelastic strain and that thermal fatigue due to cycling does not set in for at least 25 cycles.

There are other fine-geometry configurations that could also be considered. For

example, the element shown in figure 53 could, with some development, be fabricated by the same process used for the honeycomb. It may have some advantages from a thermal stress viewpoint and it conforms more readily to the cylindrical support tube without compromising the flow passages at the periphery of the element. Since the thermal stress tests on the honeycomb did not reveal a thermal stress problem, however, the configuration was not pursued.

Fuel-Element Support

Figure 54 shows the arrangement of the fuel-element components. The fuel-element assembly is housed inside the aluminum pressure tube and consists of a tungsten support tube and a series of fuel-element stages. The support tube fits inside the aluminum pressure tube and runs the full length of the core. Its functions are to keep the hot hydrogen flow away from the aluminum tube and to support the fuel-element stages. The proposed full-length fuel element is made up of 26 stages arranged in series with each stage individually attached to the support tube. The tungsten support tube is fixed to the cold end of the reactor. Additional lateral support is necessary along the length to center the fuel-element assembly inside the aluminum pressure tube.

Axial support. - Two methods for fastening the fuel-element stages to the support tube have been evaluated: mechanical joints that use tungsten pins and metallurgical bonds that use vapor-deposited tungsten.

These fastening methods were tested on assemblies at reference-design conditions of the last fuel-element stage. The tests consisted of cycling each assembly five times at a temperature of 3960° R (2200° K) with the maximum reference design axial load of 20 pounds (88.9 N), as shown in figure 55. The time at temperature was 2 hours per cycle for a total time at temperature of 10 hours.

The test results show that the mechanical joint is not suitable for use at the reactor exit without modification but could be used near the reactor inlet where temperature and drag loads are lower. The metallurgical joint successfully withstood the reference design exit conditions. It was then loaded to 2.5 times the reference-design exit load, and again cycled 5 times at 3960° R (2200° K). There was no indication of joint failure.

Lateral support. - A lateral support is required in the 0.125-inch (3.18 mm) annulus between the tungsten support tube and the aluminum pressure tube of the reference design to maintain concentricity. In addition, the lateral support must provide adequate stiffness at room temperature to reduce support tube bending stress induced by ground handling or chemical rocket boost.

In fulfilling the preceding requirements, the support itself must not introduce additional problems. For example, the support must be able to accommodate lateral differ-

ential thermal expansion between the tungsten support tube and the aluminum pressure tube. In addition, it must not provide a heat conduction path that would allow local overheating at the aluminum interface of the pressure tube.

Of the lateral supports considered, one made of 5-mil (0.1270 mm) corrugated tungsten sheet best satisfied the preceding requirements. Tungsten was chosen to withstand contact with the high-temperature support tube. The thin cross section of the corrugation plus its added circumferential length reduces heat conduction to the aluminum pressure tube. The amount of relative expansion between the aluminum pressure tube and the tungsten support tube is a function of its position along the axial length of the reactor. At the midcore position, where the support tube temperature is about 1960° R (1090° K), the relative expansion is only 2 mils (0.0508 mm) in the radial direction. The relative expansion increases to 8 mils (0.203 mm) at the reactor exit where the support tube temperature is 3960° R (2200° K).

The ability of the lateral support to accommodate this relative thermal expansion was determined experimentally. Test results indicate that a 5-mil (0.127 mm) 12-lobe tungsten corrugated spring, as shown in figure 54, will withstand reference-design midcore conditions with no measurable clearance resulting between the spring and the pressure and support tubes. However, near the reactor exit, where the tungsten support tube temperatures are considerably higher, permanent deformation of the spring may occur.

Vibration. - Experimental tests were also conducted to evaluate the vibrational behavior of these corrugated springs. A test model consisting of a spring mass system comprised of a 12-lobe spring and a simulated fuel-element stage mass of 1.1 pounds (0.5 kg) was used for this purpose.

The most significant result of these tests was that the spring provides a very stiff lateral support. The 5-mil-thick (0.127 mm) material previously discussed has a spring constant of 180 000 pounds per square inch (1.24×10^5 N/cm^2). The corrugated spring, with its high spring constant, is expected to provide a rigid coupling between the support tube and aluminum pressure tube and thus reduce the bending stresses in the support tube. The damping factor of the spring-mass system of this study is small, but served to dissipate the energy and eliminate potential damaging amplitudes at resonance.

Such a corrugated spring was used in a vibration test of a full-length support tube. Strain gages were located at various axial positions. The tube with simulated fuel-element masses was mounted on a shake table, and tests were run with and without the lateral support spring. Tube bending stresses resulting from 1-g lateral forced vibration loads are shown in figure 56. The maximum stress with no spring was approximately 27 000 pounds per square inch (18 600 N/cm^2) at the resonant frequency of 41 cps (Hz). With one spring between the aluminum pressure tube and tungsten support tube, the maximum stress was reduced to about 8000 pounds per square inch (5520 N/cm^2) at the resonant frequency of 53 cps (Hz). When water was added on the outside of the aluminum tube,

the resonant frequency decreased to 39 cps (Hz) because some of the water moving with the tube had increased the effective mass of the system. The maximum stress remained about the same.

Thus, the high spring constant of the corrugated tungsten support spring in effect provides one additional point of support to reduce the maximum stress from 27 000 to 8000 pounds per square inch (18 600 to 5520 N/cm^2).

FLUID SYSTEMS

The tungsten water-moderated reactor has two major fluid flow systems: the hydrogen feed system and the water-moderator system. These two flow systems, their components, characteristics, and interrelations with the core temperature distribution are discussed in this section.

Hydrogen Feed System

The propellant pumping arrangement must supply the pressure necessary to force the hydrogen through the fuel elements, propulsion nozzle, and other components in the system. There are two basic pumping systems which can be considered for nuclear rockets; they are the topping and the bleed systems.

The topping system is shown in figure 57. Hydrogen flows from the storage tank through the pump, the nozzle wall, the heat exchanger, a turbine that drives the pump, the reactor core, and out the propulsion nozzle. The topping system is simple and efficient because all the hydrogen passes through the nozzle to produce thrust. In this concept, the topping turbine must be located downstream from the heat exchanger because it uses the energy picked up in cooling both the nozzle walls and the water moderator to drive the pump. Although the energy in each pound (gram) of gas entering the turbine is still low, at 300° R (167° K), the turbine is capable of developing thousands of horsepower (kW) because of the large mass flow passing through it. In the topping system, the turbine pressure drop must be supplied by the pump, therefore the system pressure is higher than for a bleed system of equal nozzle chamber pressure. If there is enough energy available to drive the turbine, this feed system can be used.

The other method for pumping the propellant is the bleed system (fig. 58). It is similar to the topping system except for the source of the gas that drives the turbine. A small amount of hydrogen is bled from the main flow and heated in special fuel elements to about 1860° R (1030° K). This bleed gas flows through the turbine that drives the hydrogen pump and is then discharged through an auxiliary nozzle.

A comparison of the two systems is shown in table VI based on the same powerplant conditions of chamber pressure, temperatures, flow rate, pump efficiency, etc., that were used in the reference design. The bleed system has no upper chamber pressure limit. The topping system limit occurred around 700 pounds per square inch absolute (483 N/cm^2 abs) for the engine considered. Above this point, insufficient energy is picked up to provide the required pumping power.

For cases in which a topping system cannot supply all the required pumping power, a combination of the two systems can be used to minimize the loss in thrust due to the bleed gas. This may be done at the expense of some complexity and is shown in figure 59. This combination is called a split-feed system because the pump work is split between the topping turbine and the bleed turbine. The split system thus gets around the chamber pressure limitation of the topping system and the high bleed rate of the all-bleed system.

In the reference design, the nozzle chamber pressure was chosen low enough (600 psia (414 N/cm^2 abs)) to permit investigation of any combination of systems from all-bleed to all-topping. The split-feed system, with an arbitrary work split between the bleed and topping turbines, was chosen to study the complexities and behavior of this system.

Water-Moderator System

The closed-loop flow path of the water system is shown in figure 6. The water leaves the pump, enters the reactor vessel, and passes through the core and the beryllium side reflector where it absorbs heat. The water then flows through the shell side of the heat exchanger, where it gives up this energy to the hydrogen propellant, and returns to the circulating pump to complete a cycle every 2 to 3 seconds. The water in its passage through the reactor core acts as a structural coolant and must adequately cool the aluminum in proximity to the extremely hot fuel elements.

The key to the design of the water system is to maintain a water temperature that is high enough to prevent freezing in the heat exchanger and low enough to provide adequate cooling of the aluminum. In the TWMR concept, an aluminum surface temperature of 735° R (408° K) was used as a design point with 760° R (422° K) as the allowable maximum. The operating water temperature, therefore, had to be greater than 492° R (273° K) and less than 735° R (408° K) to cool the aluminum. Obviously, a satisfactory design could be achieved if an unlimited water flow rate was used, but this would require excessive pumping power and much larger pumping equipment.

In order to determine a reasonable combination of temperature and flow rate, the amount of heat transferred to the water in the core had to be known. There are several sources of heat: (1) neutron and gamma radiation absorbed in the water, (2) gamma and

neutron radiation absorbed in the aluminum and transferred to the water, (3) heat transferred from the hot fuel assembly by conduction and radiation through the aluminum pressure tube and into the water, and (4) heat generated in other components (such as reflectors, pumps, etc.) and transferred to the water.

The heat from these sources is not generated uniformly in the core. The radial distribution is shown in figure 60 where the heat load per fuel element is plotted against reactor radius. The ratio of the average heat load to the heat load at the center of the reactor is 74 percent. Orificing the water flow to match this distribution reduced the water flow requirement by 26 percent.

Further cooling efficiency was obtained by placing a flow divider concentrically around each pressure tube, as shown in figure 61. The water is divided by flow restrictions into two flow regions: a high velocity region of 12 feet per second (3.66 m/sec) inside the flow divider, where cooling is critical, and a slower moving stream of 5 feet per second (1.52 m/sec) outside the divider.

Figure 62 shows the water flow rate and temperature level requirements for cooling the aluminum structure. From the figure, it is obvious that if the flow were increased beyond 1150 pounds per second (522 kg/sec) only a nominal increase in the allowable operating temperature would result. At flow rates below 750 pounds per second (340 kg/sec), a small change in flow rate requires a large decrease in water temperature to maintain design aluminum temperature. As a result, the water in the heat exchanger would be more subject to freezing.

Because of the complex nature of the flow paths within the reactor, the calculation of pressure losses and the orifice requirements necessary to obtain the proper flow distribution is quite uncertain. To check these uncertainties, a full-scale water flow test was performed to study the characteristics of the system (fig. 63). In the flow test, provisions were made for readily changing the orifices at the entrance to the annular passages formed by the pressure tubes and the flow dividers (fig. 61). The number of holes in the exit support plate could also be varied to control the flow in the low-velocity region.

Figure 64 is a plot of water flow in the divider region per fuel assembly as a function of reactor radius. Although the radial flow pattern is markedly improved between the first test with no orificing and the final test, it falls short of the desired distribution.

Operation above the desired distribution represents overcooling the structure due to an excess of flow. The final test required 11 percent more flow than that of the desired distribution and was used in the reference design. These tests indicate that at least 10 to 15 percent excess flow must be allowed in a complex flow system to take into account maldistribution and calculational uncertainties.

Water-hydrogen heat exchanger. - After the water leaves the reactor with a temperature rise of about 50 R^{o} (28 K^{o}), it flows through the heat exchanger, which serves as a

cooler for the water and as a preheater for the incoming hydrogen gas.

Figure 65 shows heat-transfer behavior of the TWMR heat exchanger. As the hydrogen flow is increased at a constant water flow, the value of the heat-transfer coefficient moves along one of the lines shown toward the ice region. An icing condition is defined as one in which any local temperature of the heat-exchanger tubes drops below the freezing point of water. To the left of the line labeled ice line, no such condition can occur. To the right of this line, ice should begin to form. When the ice on two adjacent tubes reaches a thickness that is equal to one-half the tube clearance, complete blockage of the water flow passage is assumed. Once ice is predicted, the analysis takes into account its effect on heat transfer. The insulating effect of the ice causes the overall heat-transfer coefficient to remain virtually constant after the icing is reached despite the increase in film coefficient resulting from locally increased water velocity. The design point for the TWMR is considerably to the left of the ice line; there is a 65 R^{O} (36 K^{O}) margin from freezing at this point.

A portion of the reference-design heat exchanger was tested to determine how well the heat-transfer characteristics could be predicted analytically. Some typical results of that test are shown in figure 66. Perfect agreement of predicted and measured heat-transfer coefficients is represented by the solid curve. The open circles indicate no ice, while the solid circles indicate points where icing was predicted analytically. A ±10-percent error band is also shown.

The agreement between predicted and measured values of heat-transfer coefficient was excellent when no ice was predicted. When ice formation was predicted analytically, the measured values tended to be higher than the predicted values. Because of this additional uncertainty, the criterion established for the TWMR was that no icing was permitted under steady-state operation. This criterion was not extended to transient conditions since some icing was assumed to occur under a likely startup sequence (fig. 67).

With the water circulating at some low flow and with no hydrogen flow, the reactor is brought to a low power level. The water temperature is then increased to near the operating point by radiant exchange between the fuel elements and pressure tube. At time zero, the flow of hydrogen is initiated.

As the cold hydrogen passes through the heat exchanger, it cools the water and, because of the negative water temperature coefficient, the reactor power begins to increase. During this time, the hydrogen and water flow are increasing. As reactor power increases, more energy is deposited in the water and its temperature begins to increase. As design operating conditions are reached, the increased water temperature terminates the power rise.

Figure 68 shows the heat-transfer characteristics of the heat exchanger during a typical 30-second startup. The solid line is the overall heat-transfer coefficient, while the broken line defines the start of icing under the flow conditions that exist during the

transient. Whenever the actual heat-transfer coefficient is above the icing line, ice formation is possible. The shaded area therefore represents the time during which icing of the heat exchanger can occur during this particular transient. The time constant for transient ice formation is short compared with the time in which icing conditions exist in this particular startup. A reasonable estimate of the ice thickness can be made by using a point by point steady-state analysis of the conditions existing during the transient. Figure 69 shows the result of such a study. The maximum ice thickness predicted during this particular transient was 0.014 inch (0.36 mm), much less than 0.050 inch (1.27 mm) required to cause complete blockage of the water flow. No problems should result by permitting transient ice conditions of this magnitude.

Transient experiments on a 19-tube heat exchanger have been performed to verify the assumption that the heat exchanger can pass through an icing condition without damage during a startup similar to the one described. No problems were encountered with ice blockage under conditions for which the predicted ice thickness was as high as 0.013 inch (0.33 mm).

Another problem in the heat exchanger is the sensitivity to changes in operating conditions. For a given heat exchanger, the operating range is limited, as shown in figure 70, to variations in heat load of only 6 percent greater and 16 percent less than the value for which the heat exchanger was originally sized. One method of overcoming this limit is by the use of a hydrogen bypass around the heat exchanger. The advantages of controlling the heat-exchanger characteristics by the use of a bypass is discussed in the section ENGINE DYNAMICS AND CONTROL STUDIES.

HEAT TRANSFER

The performance objectives of a nuclear rocket are high specific impulse and small size, which dictate high outlet gas temperature and efficient heat transfer from the fuel. The maximum specific impulse and smallest core would result if the maximum allowable operating temperature could be maintained over the entire fuel-element surface. The method of predicting the heat-transfer characteristics and the accuracy of the predictions along with the methods available for tailoring the temperature distributions are discussed herein.

Fuel-Element Heat-Transfer Analysis

The convective heat-transfer characteristics of hydrogen under the conditions in a nuclear rocket reactor must be accurately known. Much experimental work has been done on gaseous heat transfer; however, with a nuclear rocket reactor, a new problem

arises because of the extremely high metal temperature and extremely low gas temperature that exist in the inlet region of the reactor. For this condition, local heat-transfer coefficients are not accurately predicted by conventional heat-transfer correlations. Figure 71 shows results of some experimental heat-transfer work performed at Lewis in which the hydrogen properties were evaluated at film conditions. The 20 to 30 percent uncertainty in convective heat transfer for conditions similar to those in the reactor inlet region requires an extremely conservative approach to axial power optimization.

The experimental data were therefore reexamined and a new correlation was evolved, as shown in figure 72. A considerable reduction in scatter was achieved with this correlation. Bulk gas properties are used in this modified correlation and correction factors for surface- to gas-temperature ratio and for length to diameter ratio are included to obtain local heat-transfer coefficients.

Because of the complex geometry of the TWMR fuel assemblies, the heat-transfer and fluid-flow analysis was made by using two digital computer programs to calculate temperature and flow distributions within the reactor, and to determine pressure losses and orificing requirements. The first program was specifically designed for the annular fuel geometry but was later modified to allow for connecting ligaments between the fuel plates. This program calculated the performance of one fuel assembly at a time, including the heat transfer to the water, and permitted stage to stage variations in power but did not account for circumferential variation in power about the fuel assembly.

The second program is applicable to any fuel-passage geometry and allows for circumferential as well as stage to stage power variations. It uses a variable thermal conductivity in computing internal fuel-element temperatures. This program can also be used to analyze the gross flow distribution between the fuel assemblies and to determine the orificing requirements necessary to obtain the proper flow split based on the radial power distribution. It cannot, however, account for the heat transfer to the water nor conduction of heat between adjacent flow passages which, by virtue of small differences in heat-generation rates or equivalent hydraulic diameters, could operate at slightly different temperatures.

Both programs use essentially the same iterating technique to obtain a solution, adjusting gas flow between parallel passages until the pressure drop across the stages and across the fuel assemblies is balanced. Neither program accounts for axial heat conduction, which is considered to be negligible particularly because of the physical separation associated with the stage construction. These two digital codes were used together to supplement the deficiencies of each other and permitted a rather detailed analysis of a variety of fuel-element configurations, operating conditions and reactor control concepts including the use of push-pull control rods, rotating drums, and uniform poison.

Temperature Distribution

In nuclear reactors, the axial power naturally tends to be distributed according to some cosine function. Figure 73 shows the fuel-element and gas-temperature variation associated with a cosine power distribution. The maximum surface temperature is about 4960° R (2755° K) and a reactor length of about 37 inches (94 cm) is required to achieve an outlet gas temperature of 4460° R (2480° K). To approach the more desirable condition of uniform surface temperature along the entire length of the reactor, the shape of the power distribution must be altered. The desired power distribution that would result in a constant surface temperature is shown in figure 74; the maximum heat flux is approximately 10 Btu per second per square inch (1640 J/(sec)(cm^2)). The peak power occurs a short distance from the inlet as a result of the combined effect of an increasing heat-transfer coefficient and a decreasing temperature difference, the product of which determines allowable heat flux.

Figure 75 shows the gas temperature variation along the reactor length for this power distribution. With a uniform surface temperature of 4960° R (2755° K), the required length of the reactor to achieve an exit gas temperature of 4460° R (2480° K) would be about 25 inches (63.5 cm), or a 33-percent decrease in length over the cosine distribution. Figure 76 compares this desired distribution to the reference-design distribution, which was obtained by axially zoning the isotopic tungsten mixture in the fuel stages and by using end reflectors as discussed in the section NEUTRONICS. The deviation shown between the two curves would require an increase in core length of 2.5 inches (6.35 cm).

The radial power distribution across the reactor tends to produce nonuniform behavior between fuel elements; however, this irregular behavior can be compensated for by controlling the flow of propellant to each element. Figure 77 shows the gross radial power distribution of the TWMR. If the gas flow across the reactor were constant, the gas temperature in the outer elements would not be as high as the temperature of the gas emerging from the center elements. However, a uniform exit gas temperature can be obtained by orificing the flow in each of the elements to obtain the same ratio of power to flow.

Calculational Uncertainties

Uncertainties in (1) axial and radial spatial power distribution, (2) fuel loading, (3) flow passage dimensional variations, (4) flow distribution, (5) temperature sensing and reactor power adjustment, and (6) previously mentioned convective heat-transfer coefficients affect the ability to predict the fuel-element temperature during reactor operation.

In the TWMR, the cumulative effect of all uncertainties is based on a statistical combination of the increase in fuel-element temperature resulting from each uncertainty. The concept of a "hot channel" or "hot spot" factor was used to account for these effects. This combined hot-channel factor establishes a probability for the occurrence of any given fuel-element overtemperature. In this study, an allowable overtemperature of 500 R^{O} (278 K^{O}) was assumed. Once this maximum tolerable temperature has been established, the probability of exceeding it can be related to incremental changes in reactor length or exit gas temperature, as shown in figures 78 and 79.

The design core length was established at 39 inches (99 cm) to allow for all the calculational uncertainties. At this length, the probability of exceeding the allowable overtemperature limit is 4×10^{-5}. Expressing this limit in another way, one fuel stage out of 25 000 will exceed the allowable hot-spot temperature of 5460^{O} R (3030^{O} K). Since there are 26 stages per fuel element and 121 elements per reactor, one stage in eight reactor cores experiences excessive temperature. A tenfold decrease in probability (one stage in 80 cores) can be achieved by increasing the core length by about 3 inches (7.62 cm, fig. 78) or by decreasing exit gas temperature by about 80 R^{O} (44 K^{O}, fig. 79). These two examples illustrate the sacrifice in performance resulting from uncertainties in one case in the form of increased core length and in the other in the form of decreased specific impulse.

ENGINE DYNAMICS AND CONTROL STUDIES

Static and dynamic stability and the control aspects of the TWMR were also investigated in the study program. The results of these studies are presented in reference 6. Figure 80 shows the steady-state operating envelope for the TWMR. The reactor power is given as a function of total hydrogen flow rate with the design point shown at 100 percent power and flow. The system can operate at steady state anywhere within the shaded envelope. This envelope was obtained by using analog and digital simulation of the entire system; the boundaries are physical limits that exist in various parts of the system.

The upper limits that define this envelope are the maximum pump speed limit on the first-stage pump, the fuel-element temperature limit, and below about 70 percent power and flow, the bleed gas temperature limit. This limit is reached when the temperature of the bleed gas exceeds the maximum assumed turbine materials limit. At a low flow rate, there is a pump stall limit. Below this limit, operation of the pumps is undesirable.

The lower boundaries of the operating envelope are the aluminum pressure tube temperature and the topping turbine power limit. In this region, insufficient energy exists in the gas to drive the topping turbine. In obtaining this operating envelope, a hydrogen heat-exchanger bypass was used. If this bypass is not used, the lower boundary moves

up to the boundary shown by the dashed line. This line represents heat-exchanger icing.

Obviously, the heat-exchanger bypass dramatically increases the size of the system operating envelope. This increase in size is important because of the two basic operational requirements for the system. First, the system must be capable of stable operation at the design point, and second, it must be capable of performing satisfactorily during startup and shutdown. These requirements denote that the system must go from low flow and power to the design point, operate for a period of time, and then return to the low power and flow condition.

While the transient limits may be less stringent than the steady-state limits shown in this figure (fig. 80), the size of the operating envelope indicates the ease with which the limits can be avoided during startup, operation, and shutdown. For example, in the description of the heat-exchanger problems, it was seen that a startup without a bypass would probably result in some heat-exchanger ice formation. Using the heat-exchanger bypass to eliminate this boundary makes possible going from the startup condition to the design point without encountering heat-exchanger icing.

Figure 81 shows the open-loop power-flow relation during a typical startup transient using the heat-exchanger bypass. Power and flow are shown as a function of time.

The transient starts from a motoring condition, that is, a condition where hydrogen flow is produced only by tank pressure. The hydrogen flow is then ramped to the 100-percent design point just as in the startup discussed previously. The bypass is also ramped to its 100-percent design value.

The total transient takes about 25 seconds. During the early part of the startup transient, the hydrogen flow increases more rapidly than the power; that is, the system responds quicker to a flow change. The area between the two curves represents overcooling of the fuel elements due to an excess of hydrogen flow. Conversely, during shutdown, a fuel overtemperature could be expected since the power would tend to lag the flow. Therefore, care must be exercised during a shutdown sequence to ensure a reduction in reactor power before flow is reduced to prevent fuel-element overtemperature. This can be done by either increasing the poison concentration or the heat-exchanger bypass before the hydrogen flow is decreased.

It appears then that the reference design is capable of starting up from a low power condition with only the hydrogen flow and the heat-exchanger bypass being controlled. A shutdown, however, may require an initial poison insertion.

The inherent stability of the reactor at the operating point was explained in the section NEUTRONICS; however, if an adjustment in power is required, two modes of control are available. The poison concentration in the tubes can be changed and the heat-exchanger bypass can be varied. In the latter case, the core water temperature responds to bypass variation, and the water temperature coefficient causes the core reactivity to vary.

Figures 82 and 83 show some results of analog studies made to explore the basic characteristics of each of these control methods. Figure 82 shows the response of the system to a step increase in poison concentration. Figure 83 is the response to a step change in heat-exchanger bypass flow. In both cases, no other control devices were manipulated after the initial perturbation. This open-loop response is not typical of the response expected during normal reactor operation but is used in control studies to obtain information that is useful in determining the behavior, stability, and requirements of the control system.

If the two figures are examined carefully, the system response to the poison insertion is seen to be entirely different from that of the perturbation in heat-exchanger bypass flow. In figure 82, the initial reaction of the system to poison insertion is a sharp dip in reactor power. This power reduction at constant hydrogen flow causes a decrease in the fuel temperature, which has a negative temperature coefficient of reactivity.

The response of the fuel-temperature change is practically instantaneous, and the reactor power is decreased sharply to a value that is below the initial power level. This reduced power level causes the water temperature to start dropping slowly. Since the water-temperature coefficient is also negative, power increases until a new steady-state power level is reached.

During this relatively slow portion of the power recovery, the reactor could be held at any desired power level by stabilizing the water temperature. For example, the hydrogen flow rate could be decreased; however, in this particular study no such action was taken, and the power returned to about 98 percent of the initial value. The fuel and water temperature at the new steady-state condition is slightly lower than the original level to compensate for the increased poison concentration.

Figure 82 also shows that, although the inherent tendency of the core to return to design conditions gives rise to initial oscillations, they are very quickly damped out.

In contrast to this type of behavior, the characteristic of the system that uses the hydrogen bypass around the heat exchanger for control is slower. Also, the tendency for the system to oscillate is eliminated because the primary effect of a step increase in bypass flow is a resultant direct increase in water temperature, and this increase, in turn, affects the reactivity of the reactor. Because of the relatively large mass of water in the system and the transport time around the loop, this method of control is much slower than a corresponding insertion of poison directly into the core region. With two such widely different power level controls available, the design of a control system to meet any specific control requirement would appear feasible.

In addition to the poison and bypass controls just discussed, the power can be changed by changing the total hydrogen flow rate. This control method makes use of the negative temperature coefficient of the fuel element. Figure 84 shows the response of the system to an increase in hydrogen flow with poison and bypass held constant. Shown,

as before, are power, exit gas temperature, and reactivity change as a function of time. The sharp response is similar to a change in poison concentration; however, in this case, a change in fuel-plate temperature is caused by the increased hydrogen flow. The final power rise, as in the other cases, still depends on how fast the water temperature changes.

In generating the steady-state performance map, the poison concentration was fixed; only the total hydrogen flow rate and bypass were varied to obtain the complete operating envelope. Studies have shown that no other system parameters require control. The only controls required on the TWMR split-feed system appear to be those on the poison, the heat-exchanger bypass, and the total hydrogen flow rate. It does not appear that the control problems of the all-topping system would be much different from the split-feed system. Basically, the same three control parameters would also be required for an all-topping cycle.

SYSTEM SIZE AND WEIGHT

An important factor in mission studies is propulsion system size and weight. Table VII shows a weight breakdown of the reference 1500-megawatt system. The weight of all shielding that might be required has been omitted. Engine thrust structures, gimbals, and thrust vector system are not included in this weight breakdown.

The choice of the 1500-megawatt power level for the reference design was somewhat arbitrary. As already discussed, a range of reactor sizes with the same general configuration was investigated. Using the same system operating limits, chamber pressure, fuel loading, etc., as were established for the reference design permitted changing the power of the reactor by increasing or decreasing the diameter of the core while keeping the length constant. The sizes of other system components were changed to accommodate the new flow rates.

The fine-geometry fuel elements eliminate the allowable dynamic head limit of 12.5 pounds per square inch (8.62 N/cm^2) used in the reference design. Therefore, the power output of a given reactor can be increased by increasing the flow and thus improving the heat transfer. The limiting condition for this upgraded system would be the pressure drop associated with the higher flow rate. A core pressure drop limit of 250 pounds per square inch (172 N/cm^2) is felt to be reasonable at this time.

Figure 85 shows thrust to weight ratios for systems up to about 10 000 megawatts. The lower curve is for a system with the reference dynamic head limit of 12.5 pounds per square inch (8.62 N/cm^2) and includes the reference-design point at 1500 megawatts. The upper curve is for a case in which a reactor core pressure drop of 250 pounds per square inch (172 N/cm^2) was imposed. The resulting power output of each fuel element for this case is approximately 1.5 times that of the lower curve.

The reactivity limit for small size reactors that use uranium 235 fuel is also shown in figure 85. Using uranium 233 instead of uranium 235 below this level allows the limiting power to be reduced until the reactivity limit of the uranium 233 is reached. This size is the smallest feasible size for reactors using the reference parameters. The thrust to weight ratio varies from about 5 to 8.5 (lb/lb (49 to 83 N/kg)) for the cases shown.

Figure 86 shows the pressure vessel diameter as a function of reactor power level. The results for the case of a dynamic head of 12.5 pounds per square inch (8.62 N/cm^2) and the case of a reactor core pressure drop of 250 pounds per square inch (172 N/cm^2) are shown, along with the reactivity limits for uranium 235 and uranium 233 fuel. The pressure vessel diameter varies from 31 to 109 inches (79 to 277 cm) for the power range shown.

It should be emphasized that all the systems represented by figures 85 and 86 were obtained by using the same parameters as in the reference design. By changing parameters such as the chamber pressure, the fuel element size, the fuel loading, or the percent of enriched tungsten, the TWMR could be optimized to the requirements for a specific mission.

CONCLUDING REMARKS

A tungsten water-moderated reactor concept has been proposed. It consists of a thermal spectrum reactor that uses light water as a moderator and coolant, uranium dioxide as fuel, and tungsten enriched in the 184-isotope as the fuel-element structural material. As a result of detailed feasibility studies, it is concluded that

1. The tungsten water-moderated reactor concept could be developed with a reasonable degree of confidence into a nuclear rocket propulsion system that has good reliability, high specific impulse, low weight, small size, excellent growth potential, ease of development, long running time, and multirestart capability.

2. Tungsten provides a material with good thermal shock resistance, good tensile and compressive strength, good thermal conductivity, and resistance to corrosion by the propellant. These properties permit the fabrication of cermet fuel elements with very thin webs, which reduce thermal stress and increase the heat-transfer surface area in the cores.

3. Water provides an efficient moderator and a good coolant for the pressure vessel and structural members.

4. A heterogeneous core can be used in which the fuel-element assemblies are structurally independent of each other. This permits independent development of these assemblies.

The reactor neutronic studies on the TWMR concept have shown by analysis and experiment that

5. The required margins of excess reactivity can be obtained.

6. The negative water temperature reactivity coefficient required for self-stabilization in reactor startup and at operating power can be achieved.

7. Overall radial and axial power distributions in the core can be adjusted to provide maximum heat transfer by the use of natural tungsten as a parasitic absorber in selected fuel stages and support tubes.

8. The use of tungsten, enriched in tungsten 184 to reduce neutron absorption, as a fuel-element structural material is feasible and has been demonstrated. It can be produced in sufficient quantities and at reasonable unit costs.

9. The finely distributed in-core poison control system provides adequate control and response, minimum power distortion, and a method of reactor control independent of core size.

10. The neutronic aspects of the reactor are well understood.

The fuel-element studies for the TWMR concept have shown that

11. Tungsten - uranium dioxide composites are capable of operating under constant heating conditions at 4960° R (2755° K) for 10 hours or more with less than 1 percent fuel weight loss, if the exposed surfaces are clad with a thin layer of unfueled tungsten. The use of tungsten-coated uranium dioxide particles to form the composite also helps reduce fuel losses.

12. Thermal cycling aggravates the fuel-retention problem; however, the fuel loss can be limited to less than 1 weight percent by the use of small amounts of yttrium or cerium oxides in solid solution with the uranium dioxide.

13. Tungsten - uranium dioxide composites containing up to 35-volume-percent uranium dioxide have sufficient high-temperature strength and ductility to be used as self-supporting components in fuel elements.

14. The problems of fabricating tungsten - uranium dioxide into fuel-element shapes have been largely solved. Techniques have advanced from the fabrication of flat plates to the consolidation of complex configurations such as honeycombs with variable fuel loading within the stage.

15. Concentric-cylinder fuel-element configurations require many edge supports at high dynamic head conditions. High performance systems require a fine grid, such as the honeycomb element. Methods of supporting fuel assemblies against axial and lateral loads have been developed.

Engine system studies on the tungsten water-moderated reactor concept have shown that

16. The engine system has three independent methods of control: the poison control system, the heat-exchanger bypass, and the total hydrogen flow rate. These methods

can be used individually or in combination to obtain the desired system response. Analog simulation has demonstrated that the system can be started, controlled at the operating point, and shut down.

17. The heat load in the moderator water can be transferred to the incoming hydrogen propellant by a water-to-hydrogen heat exchanger. Water temperature and flow conditions can be controlled to provide adequate cooling of the core aluminum structure without freezing in the heat exchanger.

18. Reactors within the power range from about 400 to over 10 000 megawatts can be achieved by the addition of more fuel-element assemblies and an increase in the size of the auxiliary components.

Lewis Research Center,
National Aeronautics and Space Administration,
Cleveland, Ohio, April 20, 1967,
122-28-02-04-22.

REFERENCES

1. Saunders, Neal T.; Gluyas, Richard E.; and Watson, Gordon K.: Feasibility Study of a Tungsten Water-Moderated Nuclear Rocket. II. Fueled Materials, NASA TM X-1421, estimated publication, approximately, Sept. 1967.

2. Lietzke, A. F.; Slaby, Jack G.; Gedeon, Louis; Smith, Roger L.; Siegel, Byron L.; Mattson, William F.; Kacher, Henry F.; and Maag, William L.: Feasibility Study of a Tungsten Water-Moderated Nuclear Rocket. III. Fuel Elements, NASA TM X-1422, estimated publication, approximately, Oct. 1967.

3. Klann, Paul J.; Mayo, Wendell; Lantz, Edward; and Paulson, Walter A.: Feasibility Study of Tungsten Water-Moderated Nuclear Rocket. IV. Neutronics. NASA TM X-1423, estimated publication, approximately, Sept. 1967.

4. Krasner, Morton H.: Feasibility Study of a Tungsten Water-Moderated Nuclear Rocket. V. Engine System, NASA TM X-1424, estimated publication, approximately, Oct. 1967.

5. Ribble, Guy H., Jr.: Feasibility Study of a Tungsten Water-Moderated Nuclear Rocket. VI. Feed System and Rotating Machinery, NASA TM X-1425, estimated publication, approximately, Oct. 1967.

6. Mihaloew, James R.: Feasibility Study of a Tungsten Water-Moderated Nuclear Rocket. VII. System Dynamics and Control Analysis. NASA TM X-1426, estimated publication, approximately, Nov. 1967.

7. Joanou, G. D.; and Dudek, J. S.: GAM II - A B_3 Code for the Calculation of Fast-Neutron Spectra and Associated Multigroup Constants. Rep. No. GA-4265, General Atomic Division, General Dynamics, Sept. 16, 1963.

8. Joanou, G. D.; Smith, C. V.; and Vieweg, H. A.: Gather II - An IBM-7090 FORTRAN-II Program for the Computation of Thermal-Neutron Spectra and Associated Multigroup Cross Sections. Rep. No. GA-4132, General Atomic Division, General Dynamics, July 8, 1963.

9. Spielberg, D.: ATHENA - A System of Fortran Programs for Radiation Transport and Heating Calculations in Complex Reactor Geometries. Rep. No. UNC-5148 (NASA CR-54905), United Nuclear Corp., May 1966.

10. Martin, Allan E.; and Edwards, Russell K.: The Uranium - Uranium Dioxide Phase Diagram at High Temperatures. J. Phys. Chem., vol. 69, no. 5, May 1965, p. 1788.

TABLE I. - PRECISION OF FUEL-ELEMENT SIMULATION

Material	Core	
	Reference	Simulated
Absorptions per source neutron		
Hydrogen	0.071	0.069
Oxygen	.002	.002
Aluminum	.001	.014
Uranium 235	.617	.616
Tungsten	0.146	0.095
Uranium 238	.004	.058
Total tungsten and uranium 238	0.150	0.153
Total	0.851	0.854
Core	Thermal utilization	Age, cm^2
Reference	0.7857	95.16
Simulated	.7820	90.56

TABLE II. - COMPARISON OF ISOTOPIC COMPOSITION OF REFERENCE AND SPECIAL FUEL STAGES

Fuel stage	Tungsten isotope			
	182	183	184	186
	Weight in fuel stage, g			
Reference	6.18	38.82	339.61	5.52
Special:				
5 Ring	6.15	38.91	162.16	5.63
8 Ring	7.90	40.28	244.26	7.82
11 Ring	9.78	41.75	332.02	10.15

TABLE III. - REACTIVITY REQUIREMENTS

Requirement	Reactivity, Δk/k, percent
Reactivity for power tailoring	-7.4
Temperature defect	-2.5
10 Hours of operation in 1-hour cycles	-1.7
Transient xenon override	-6.0
Design and manufacturing tolerance	±1.5
Propellant hydrogen reactivity	0
Total	-19.1

TABLE IV. - REACTIVITY AND INSERTION RATE FOR CONTROL

Operational requirement	Reactivity, Δk/k, percent	Insertion rate, (Δk/k)/sec, percent
Cold shutdown to hot critical	4.5	±0.057
Temperature control (10-hr operation)	1.7	±.0035
Shutdown reactivity insertion	---	-.057
Transient xenon override	6.0	±.014
Total	12.2	------
Emergency shutdown	15.0	-5.7

TABLE V. - CHARACTERISTICS OF SMALL CORES

[20-volume-percent uranium dioxide.]

Fuel	Number of fuel elements	Core diameter, in. (cm)	Beryllium thickness, in. (cm)	Multiplication factor, k_{eff}	Maximum to average radial power
Uranium 235	37	21.0 (53.4)	4.0 (10.2)	1.11	1.19
Uranium 233	19	15.2 (38.6)	3.4 (8.6)	1.16	1.16

TABLE VI. - COMPARISON OF BLEED AND

TOPPING SYSTEM PARAMETERS

[Nozzle chamber pressure, 600 psia (414 N/cm^2 abs); flow rate, 92.7 lb/sec (42.1 kg/sec).]

Parameter	Bleed	Topping
Nozzle chamber pressure upper limit, psia; N/cm^2 abs	None	≈700; 483
Bleed rate, percent	5.1	0
Engine specific impulse, sec	819	839
Hydrogen pump discharge pressure, psia; N/cm^2 abs	945; 652	1490; 1030
Hydrogen pump horsepower; MW	7200; 5.37	11 700; 8.73

TABLE VII. - WEIGHT OF REFERENCE TUNGSTEN

WATER-MODERATED REACTOR ENGINE SYSTEM

Component	Weight, lb (kg)
Reactor components (no shield):	
Uranium dioxide fuel	200 (91)
Tungsten	3 000 (1362)
Water moderator	1 840 (835)
Reflectors	1 330 (604)
Structure and controls	2 640 (1200)
Total weight of reactor components	9 010 (4092)
Nonreactor components:	
Nozzle (area ratio, 40)	1 280 (581)
Pumps	900 (408)
Piping	1 600 (726)
Fluids	950 (431)
Total weight of nonreactor components	4 730 (2146)
Total weight of system	13 740 (6238)

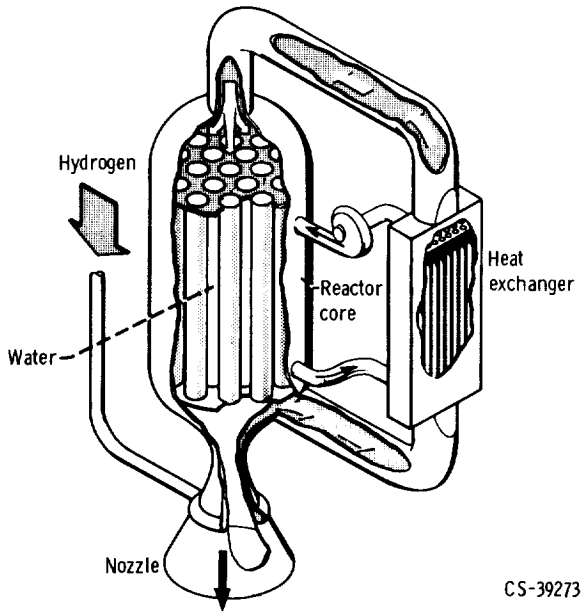

Figure 1. - Tungsten water-moderated reactor concept.

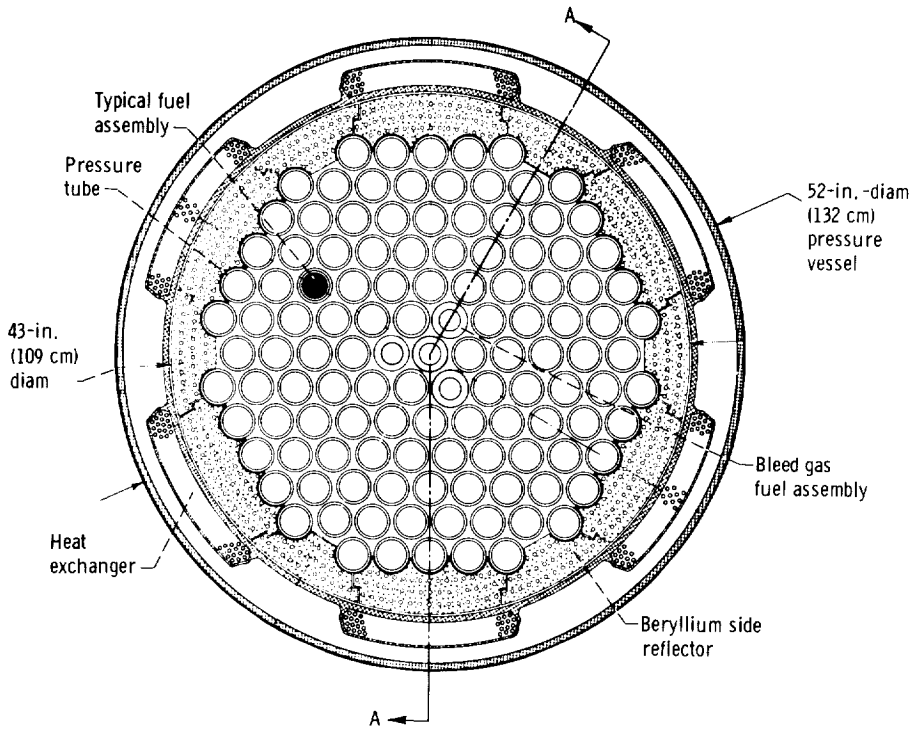

(a) Cross section.

Figure 2. - Reactor assembly.

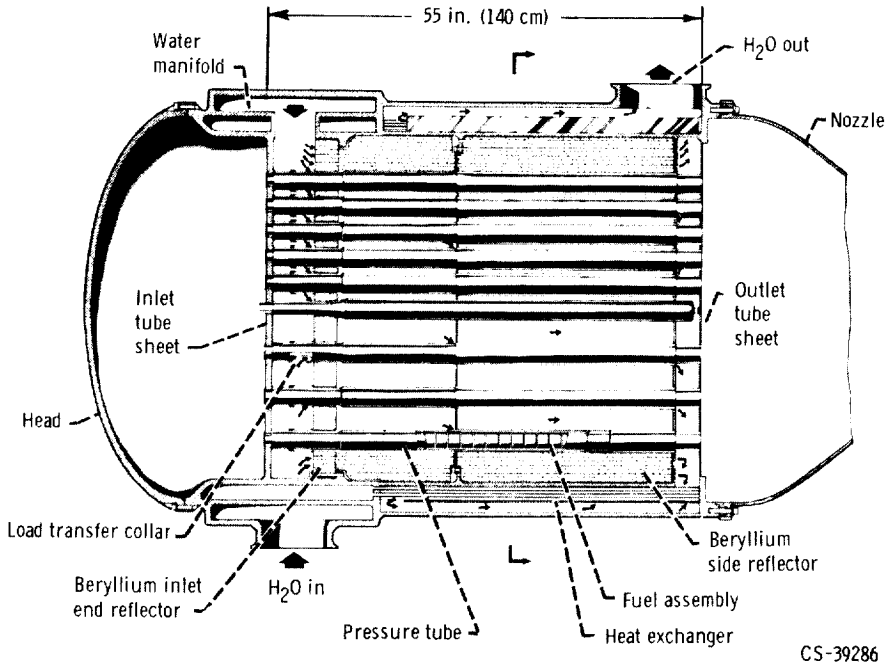

(b) Water flow in axial section AA.

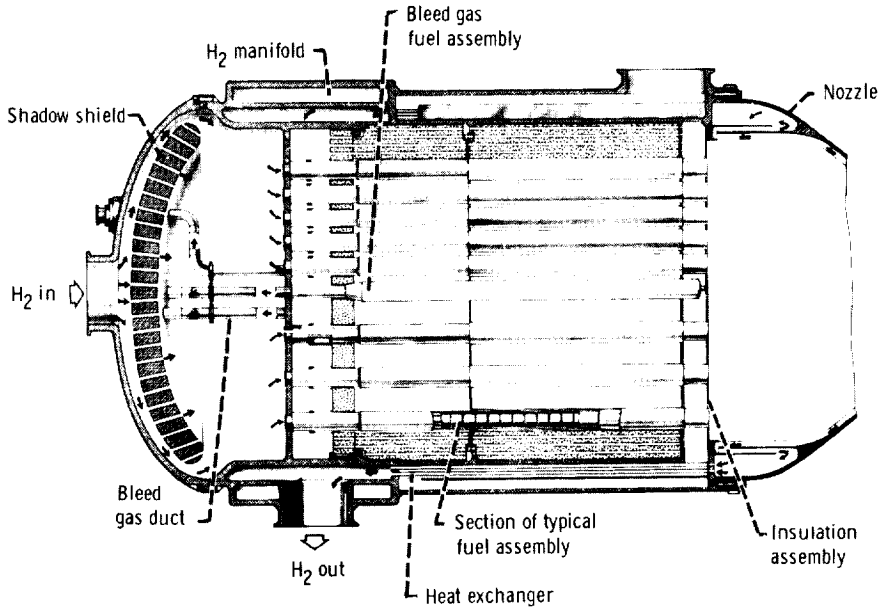

(c) Hydrogen flow in axial section AA.

Figure 2. - Continued.

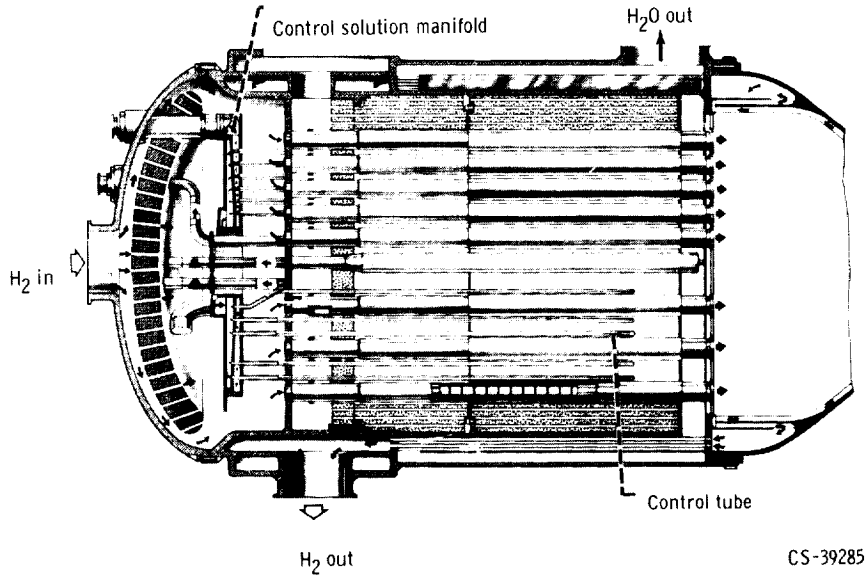

(d) Axial section AA showing control system.

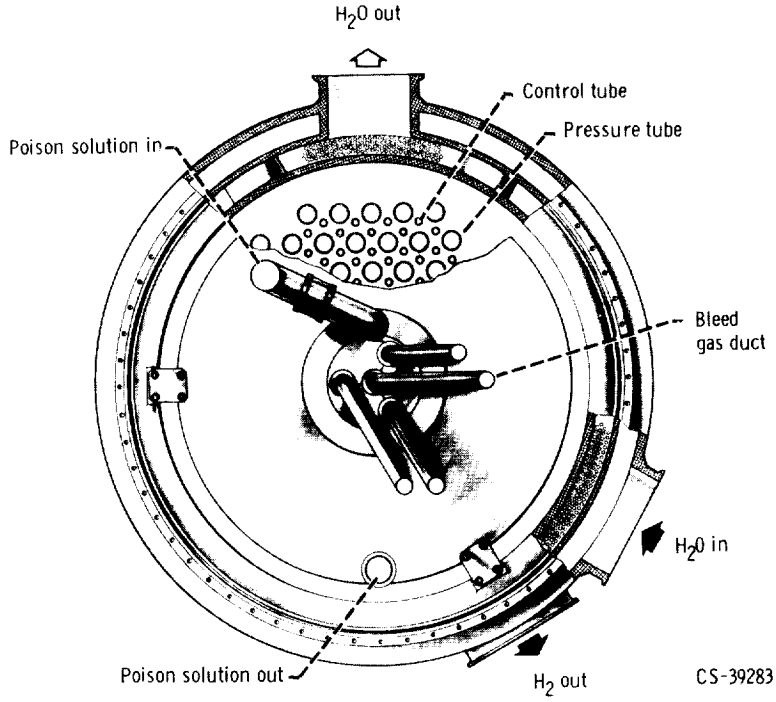

(e) End view.

Figure 2. - Concluded.

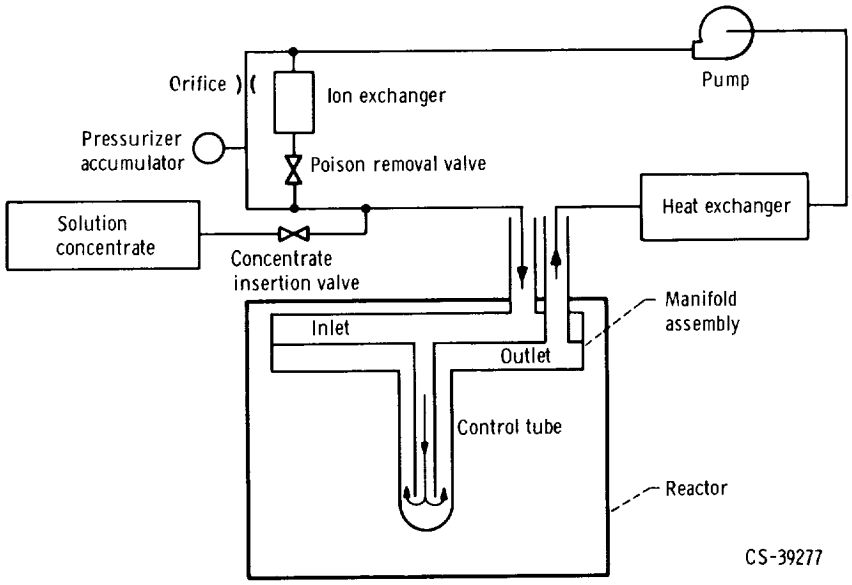

Figure 3. - Schematic diagram of reactivity control solution system.

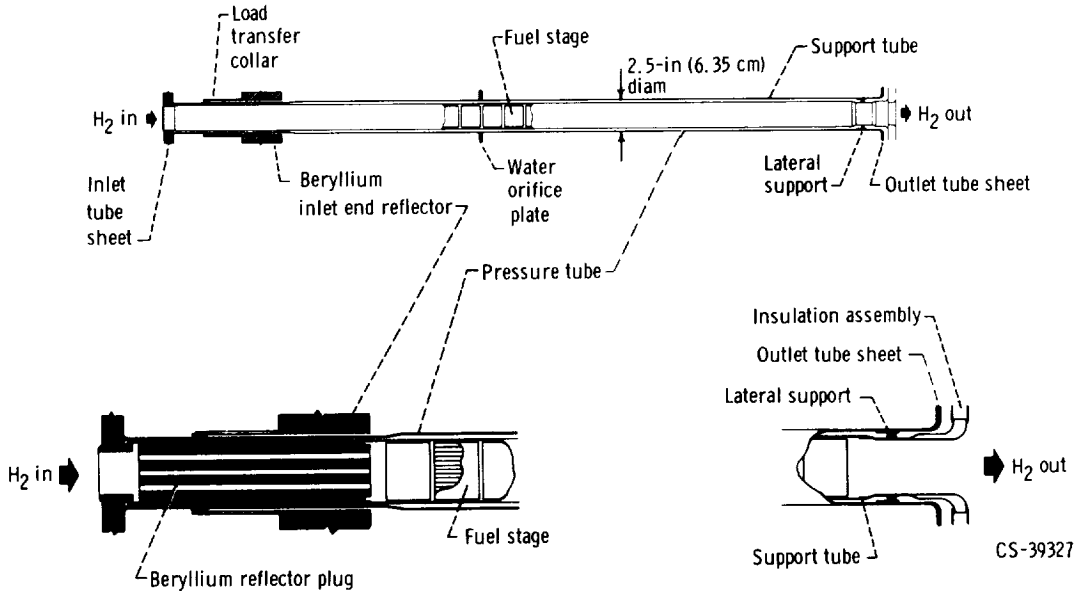

Figure 4. - Fuel-element assembly.

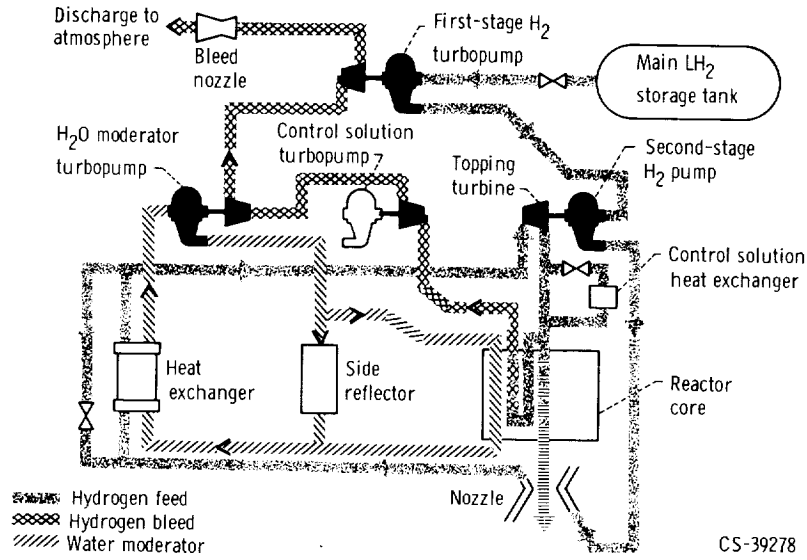

Figure 5. - Schematic diagram of overall system.

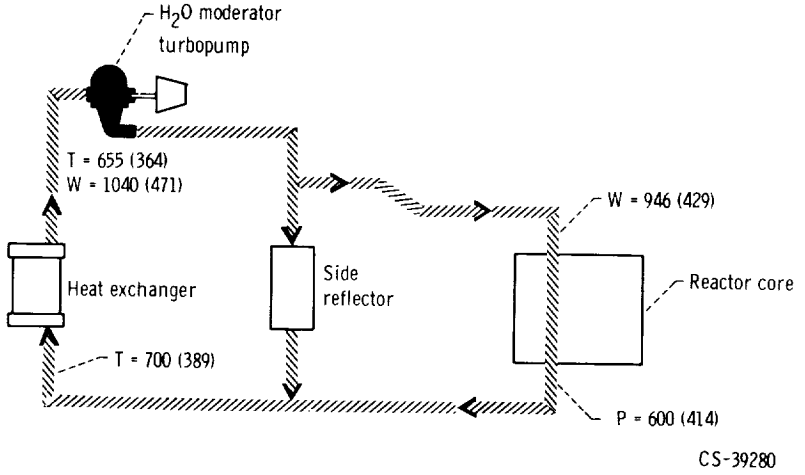

Figure 6. - Schematic diagram of water system. Pressure, P, psia (N/cm^2 abs); temperature, T, °R (°K); weight flow, W, pounds per second (kg/sec).

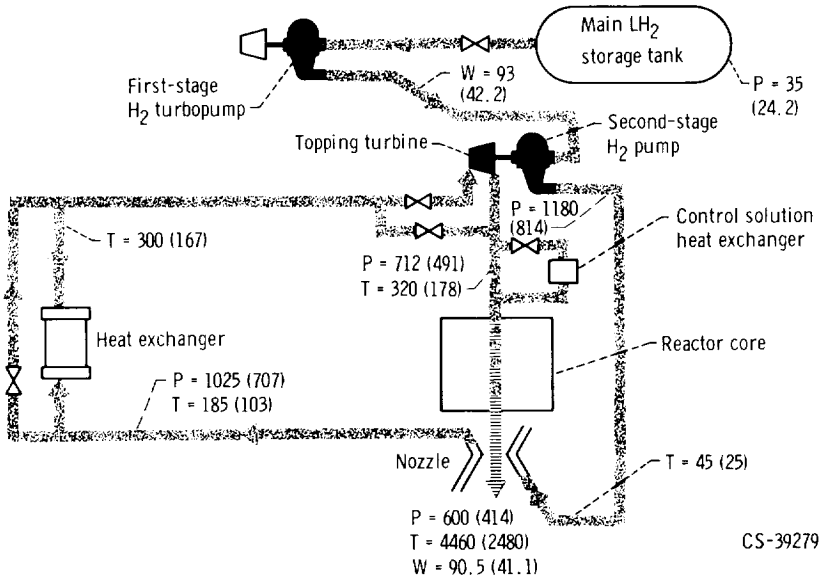

Figure 7. - Schematic diagram of hydrogen propellant system. Pressure, P, psia (N/cm^2 abs); temperature, T, °R (°K); weight flow, W, pounds per second (kg/sec).

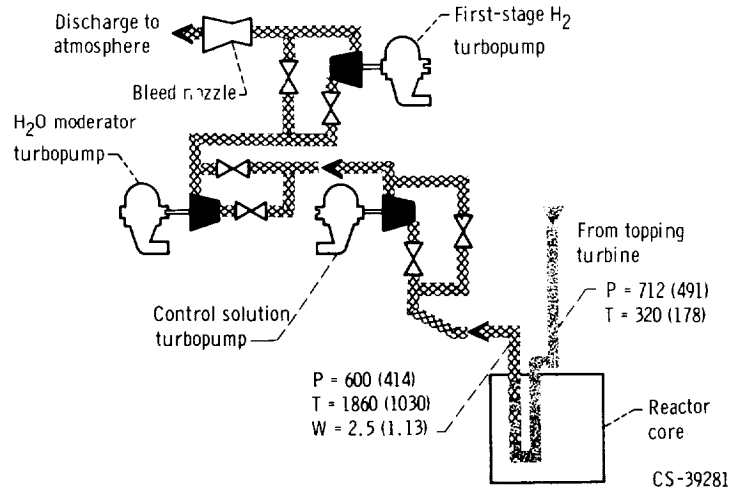

Figure 8. - Schematic diagram of hydrogen bleed system. Pressure, P, psia (N/cm^2 abs); temperature, T, °R (°K); weight flow, W, pounds per second (kg/sec).

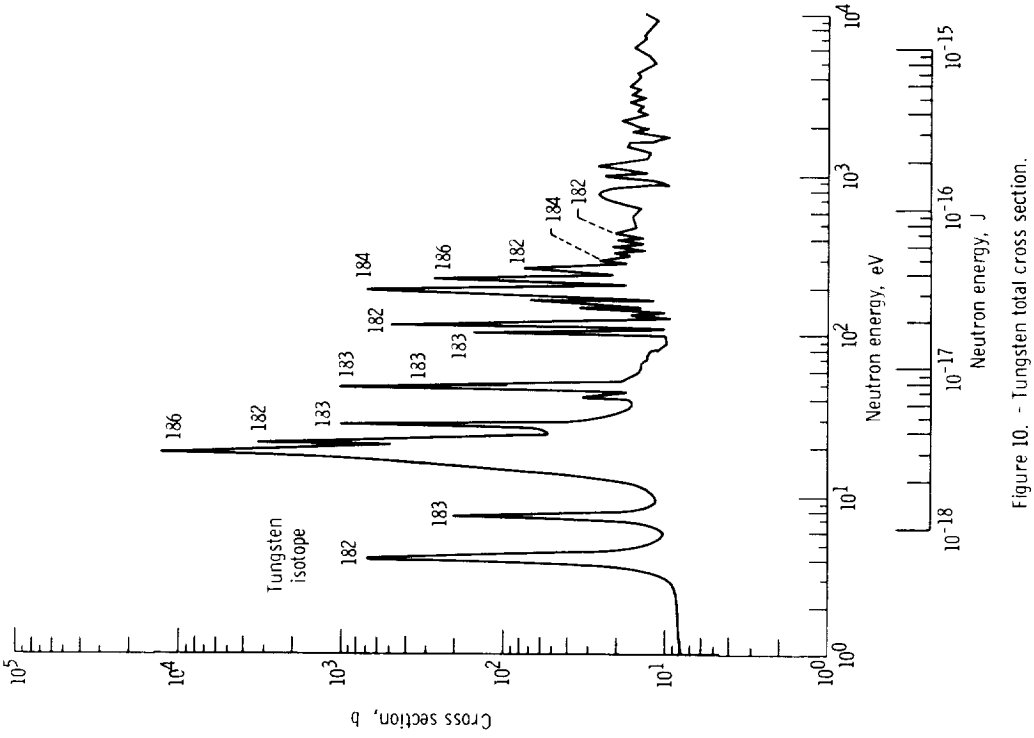

Figure 10. - Tungsten total cross section.

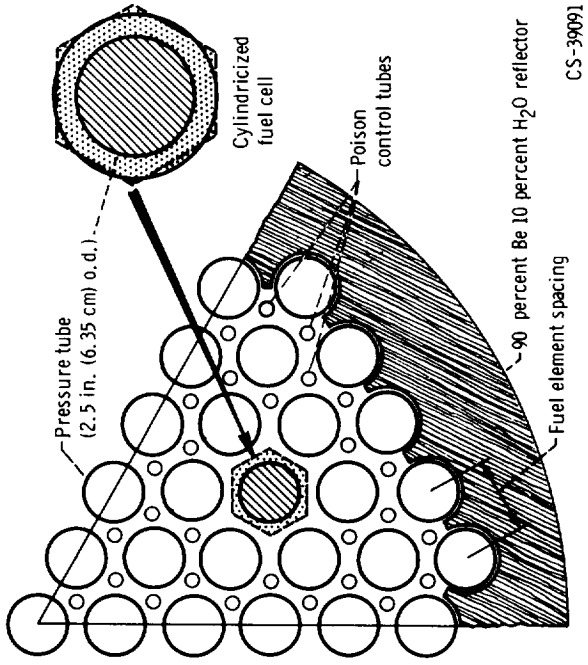

Figure 9. - Radial section of reference-design reactor.

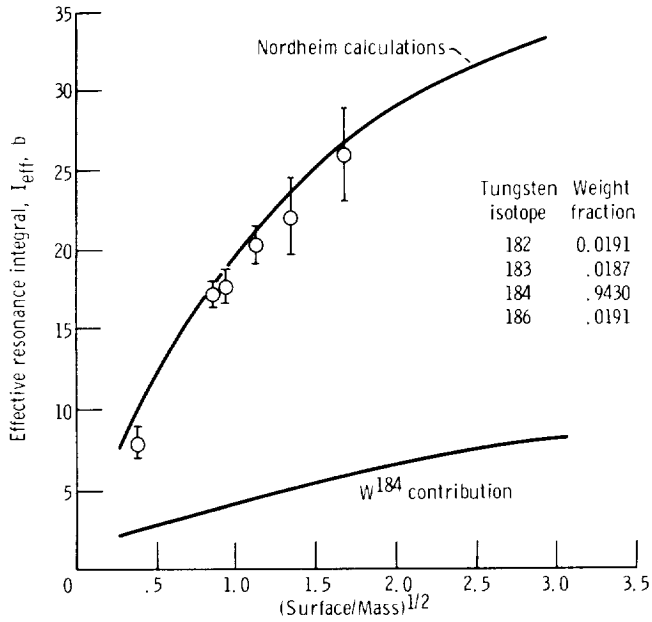

Figure 11. - Effective resonance integrals for tungsten mixtures.

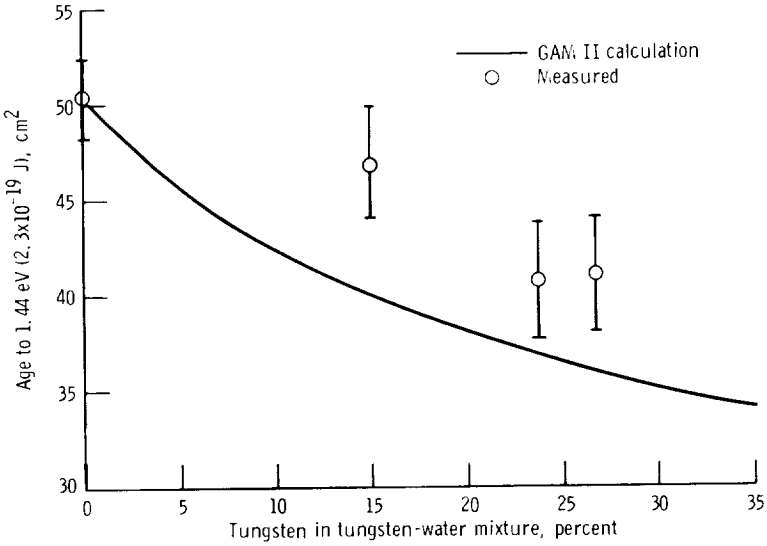

Figure 12. - Fermi age in tungsten-water mixtures for plutonium-beryllium source neutrons.

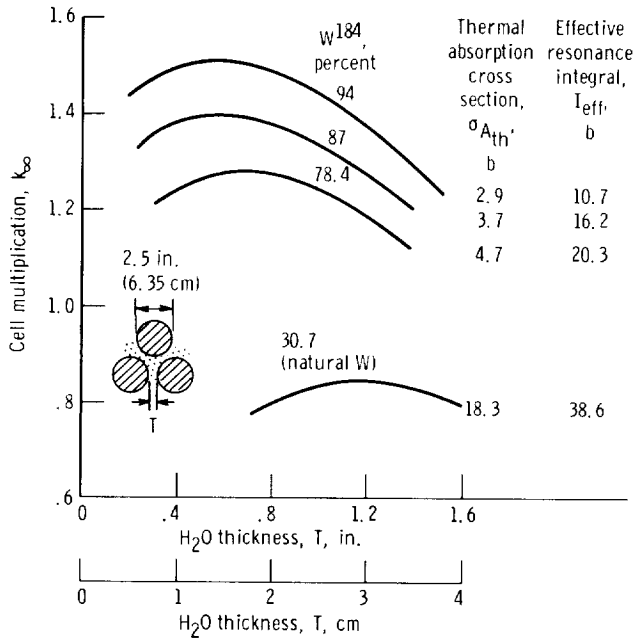

Figure 13. - Cell multiplication for tungsten - 20-volume-percent uranium dioxide fuel.

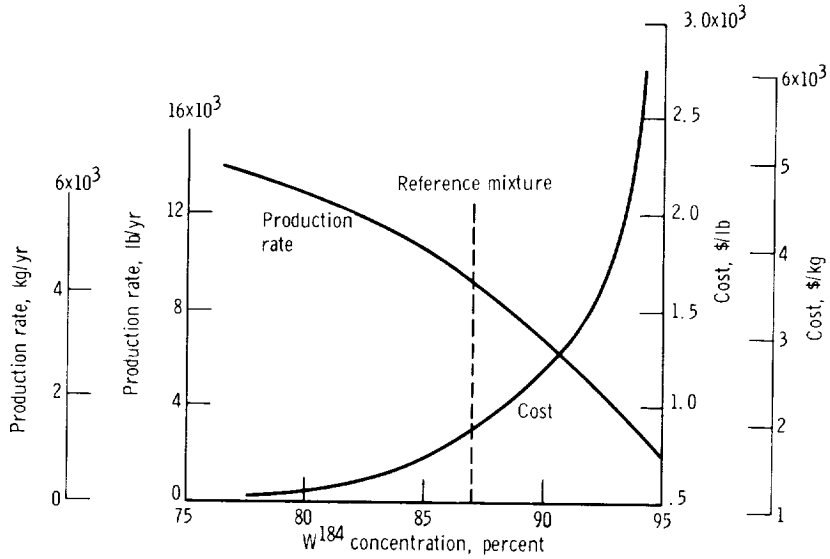

Figure 14. - Separated tungsten 184 production.

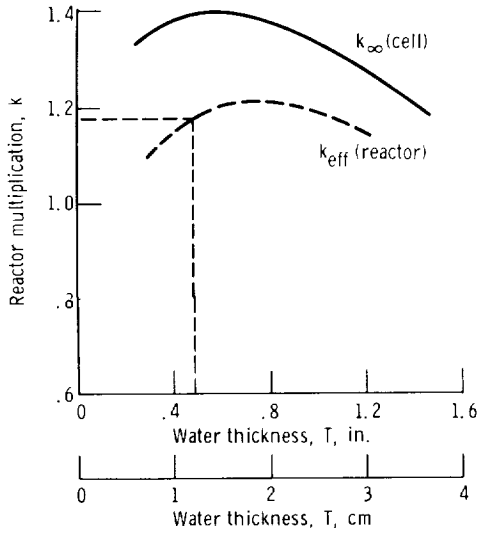

Figure 15. - Reactor multiplication for various water thicknesses for unzoned, unpoisoned reference design using 87 percent tungsten 184.

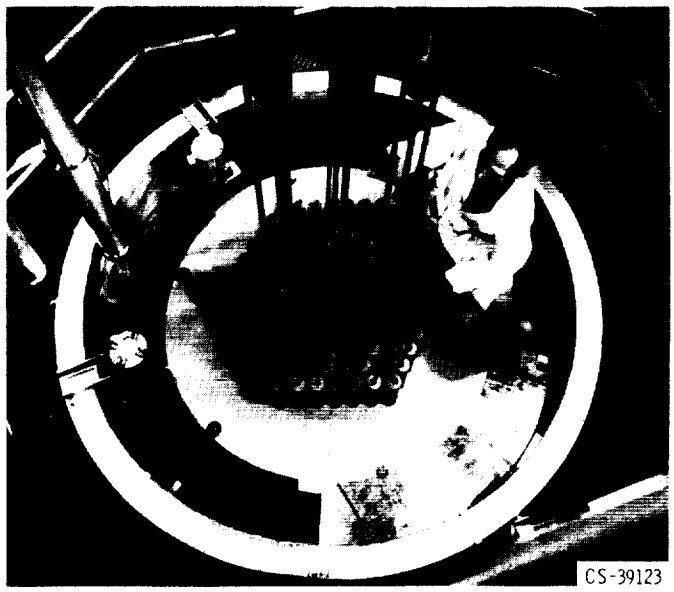

(a) Critical assembly.

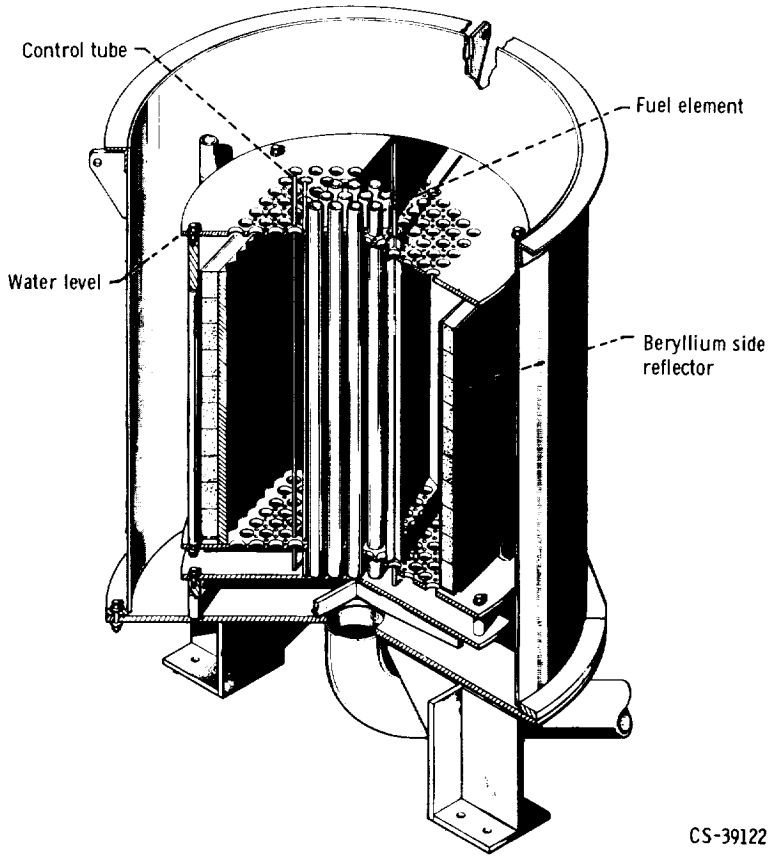

(b) Cutaway view.

Figure 16. - Reference reactor critical experiment.

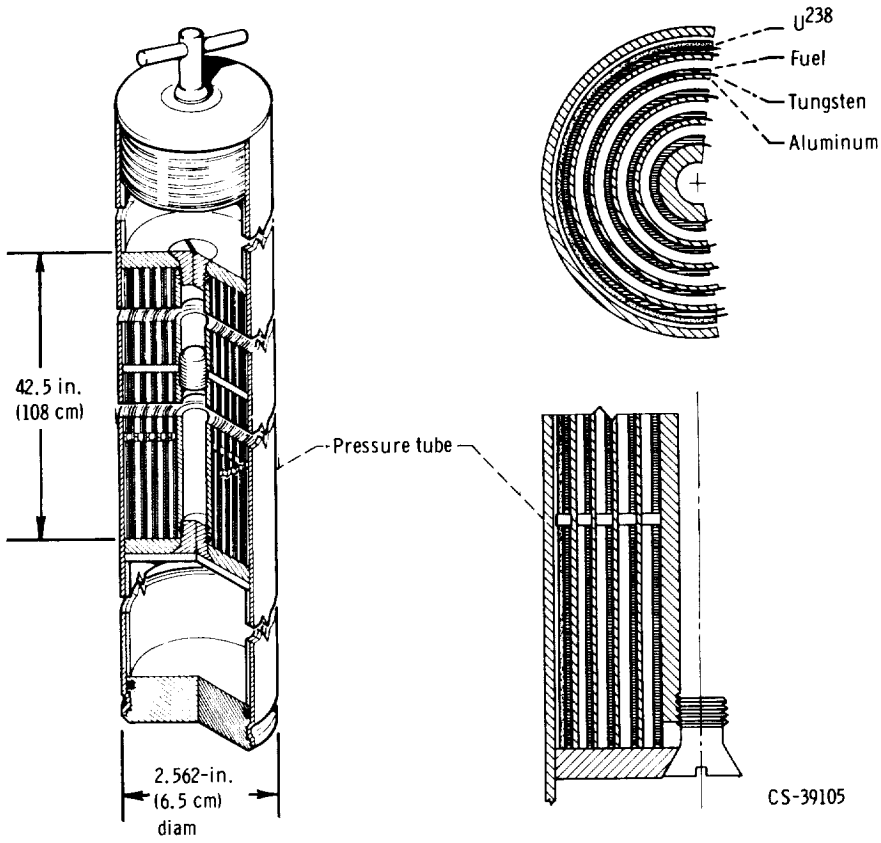

Figure 17. - Simulated fuel element.

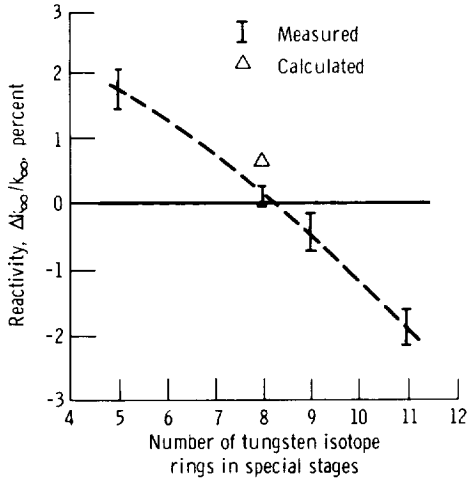

Figure 18. - Experimental check of simulation.

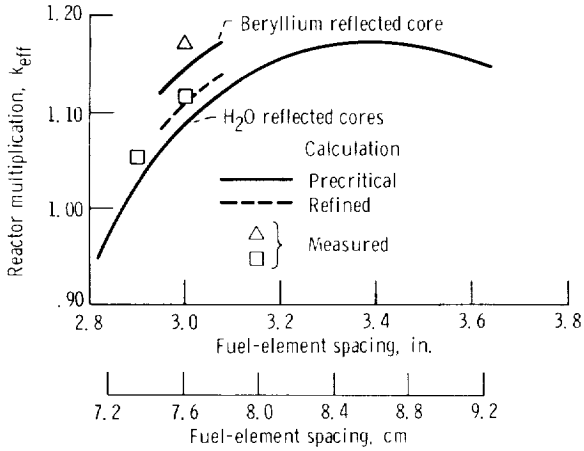

Figure 19. - Results of critical experiments.

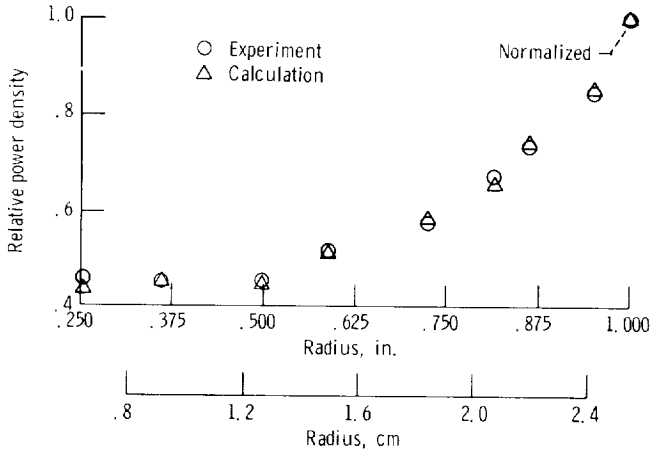

Figure 20. - Radial power density in simulated fuel element.

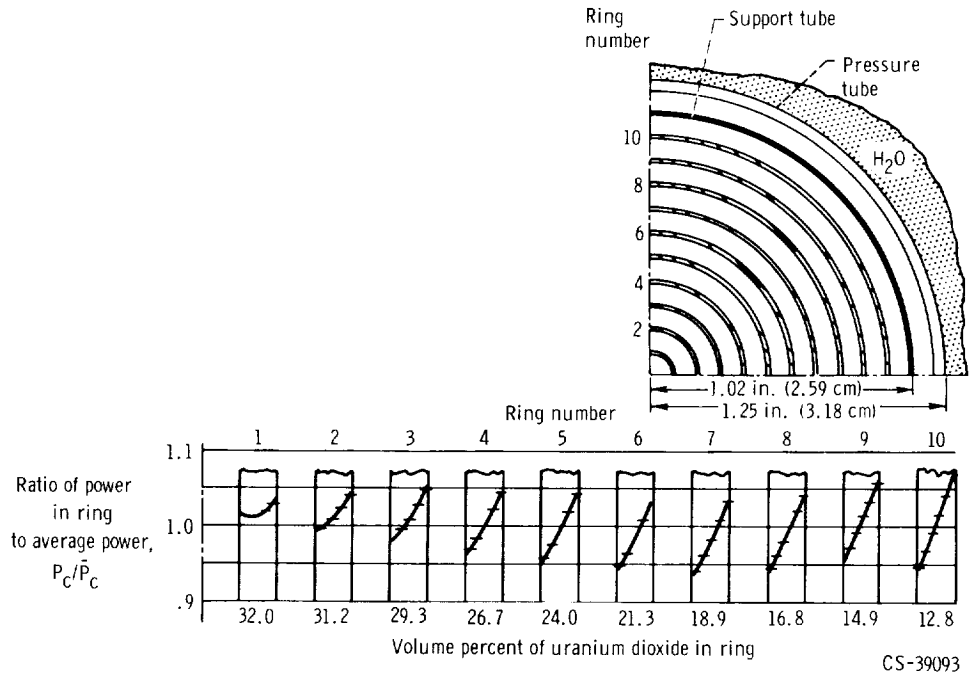

Figure 21. - Fuel-element zoning for uniform radial power density.

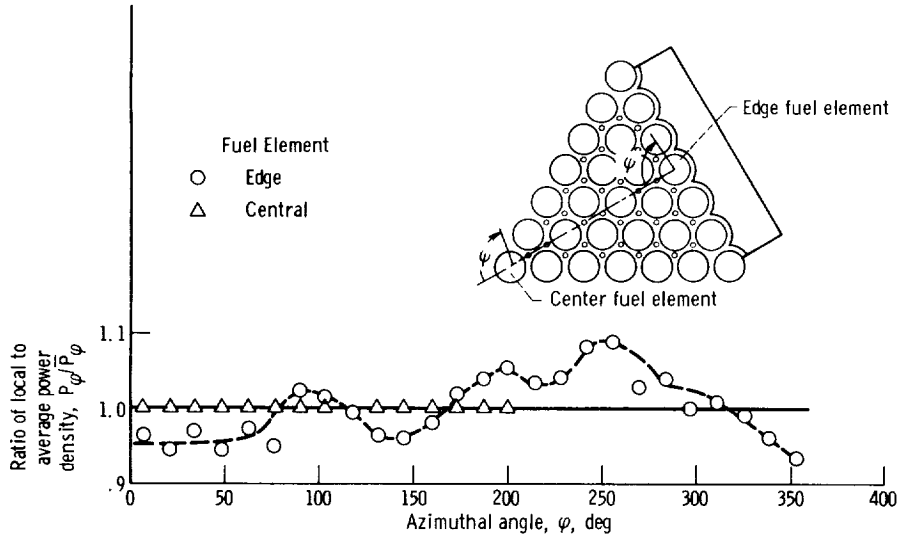

Figure 22. - Circumferential power density ratio as function of azimuthal angle.

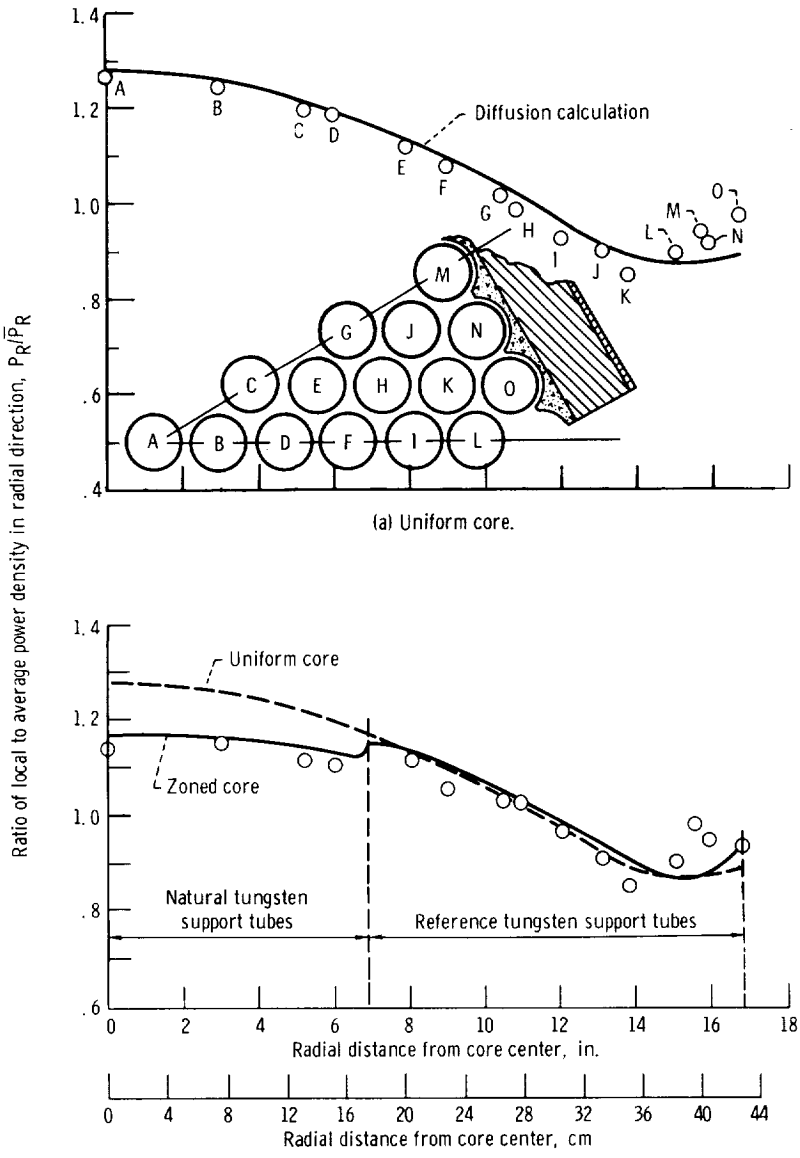

(a) Uniform core.

(b) Zoned core.

Figure 23. - Radial power density ratio.

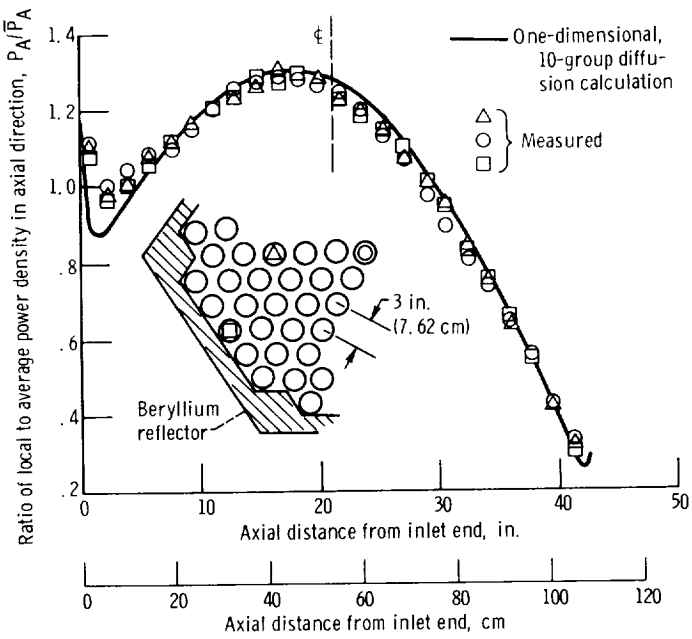

(a) Uniform core (4-in. (10.2 cm) beryllium inlet reflector).

Figure 24. - Axial power ratio.

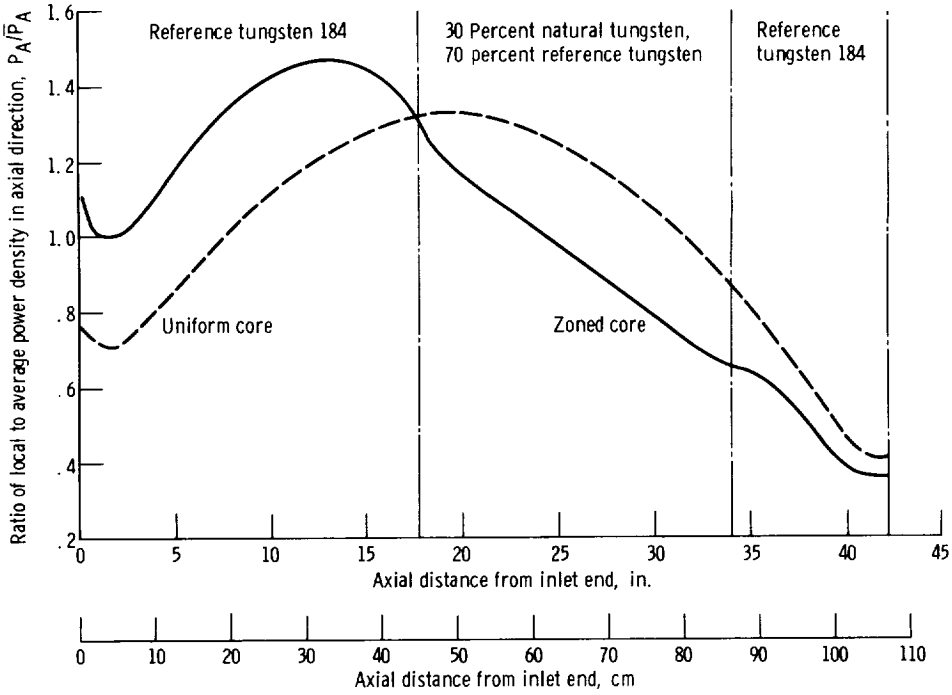

(b) Comparison of unzoned and zoned cores (3-in. (7.62 cm) beryllium inlet reflector).

Figure 24. - Concluded.

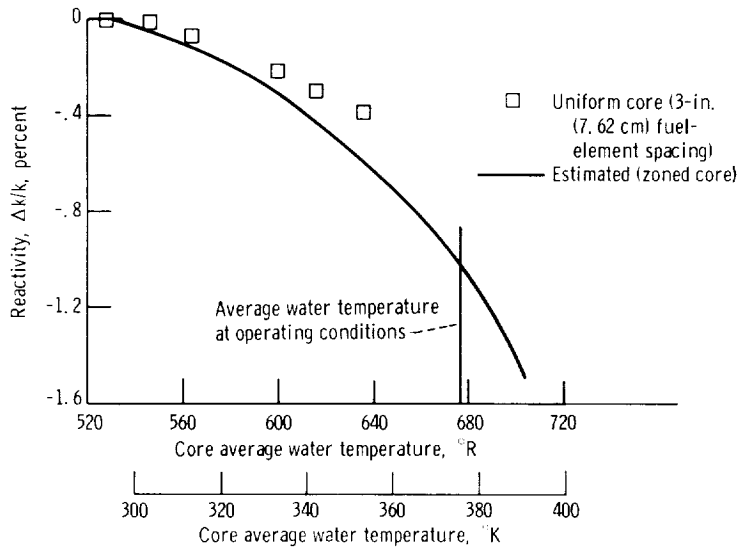

(a) Effect of water temperature.

Figure 25 - Variation of reactivity with temperature.

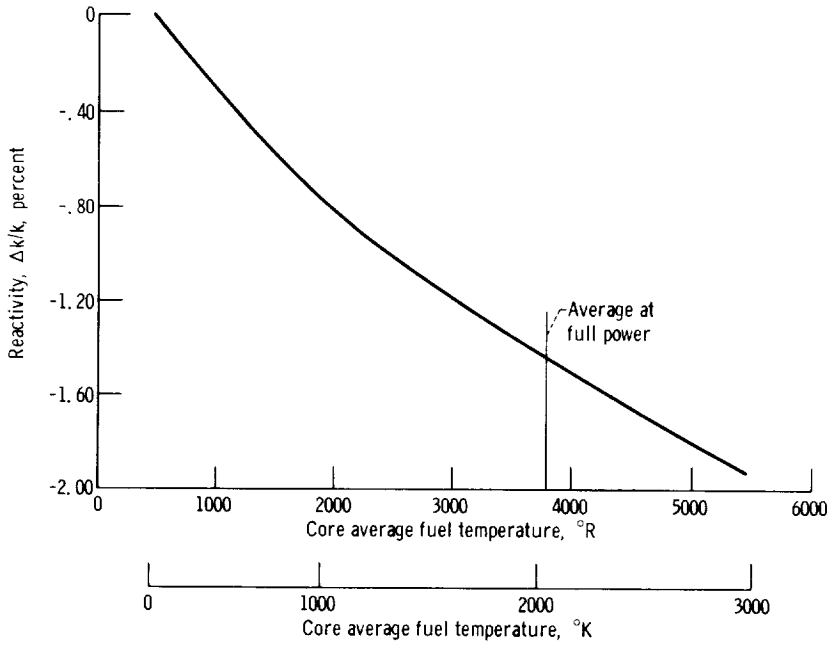

(b) Effect of fuel temperature.

Figure 25. - Concluded.

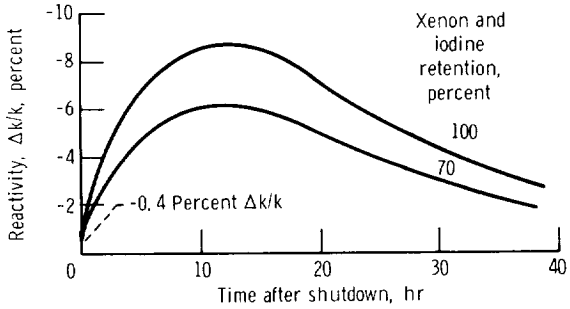

Figure 26. - Xenon generation for 1-hour full-power run after shutdown.

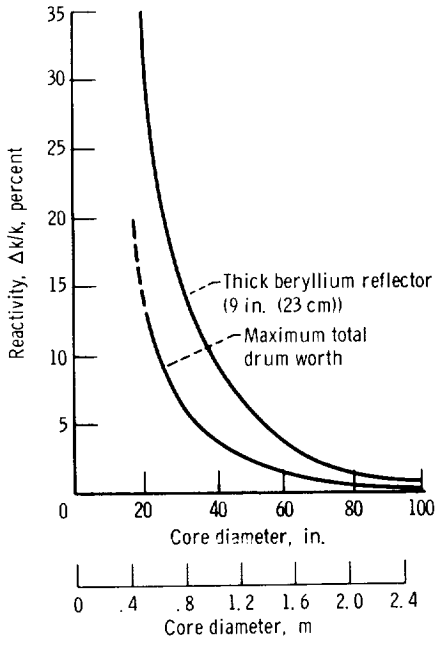

Figure 27. - Reflector reactivity.

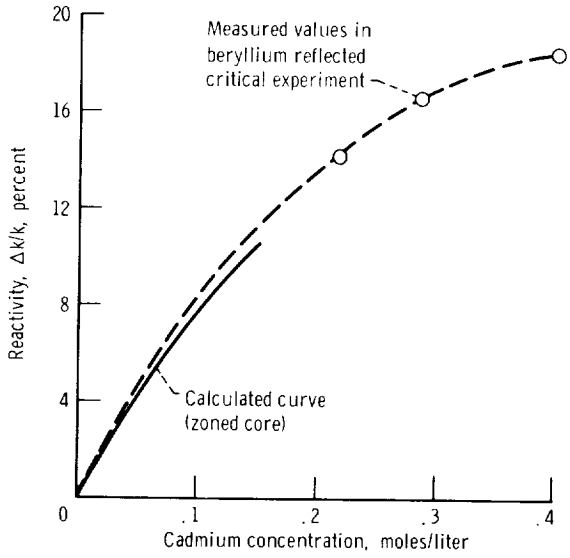

Figure 28. - Reactivity of cadmium.

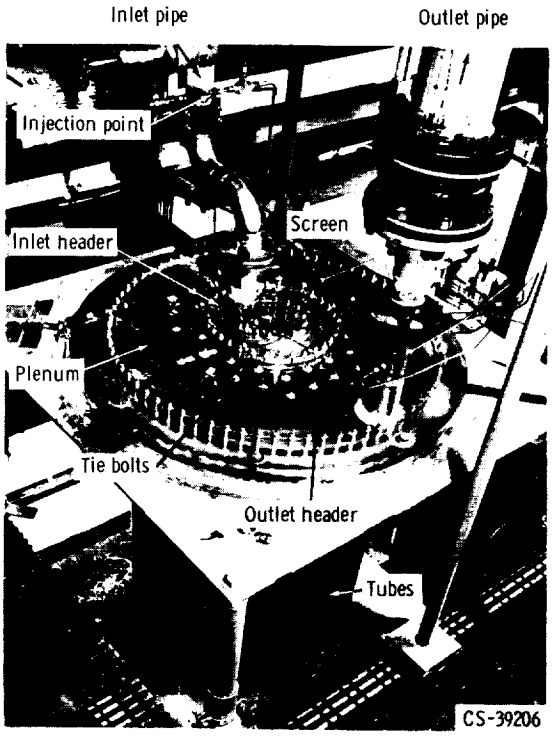

Figure 29. - Poison tube assembly flow test facility.

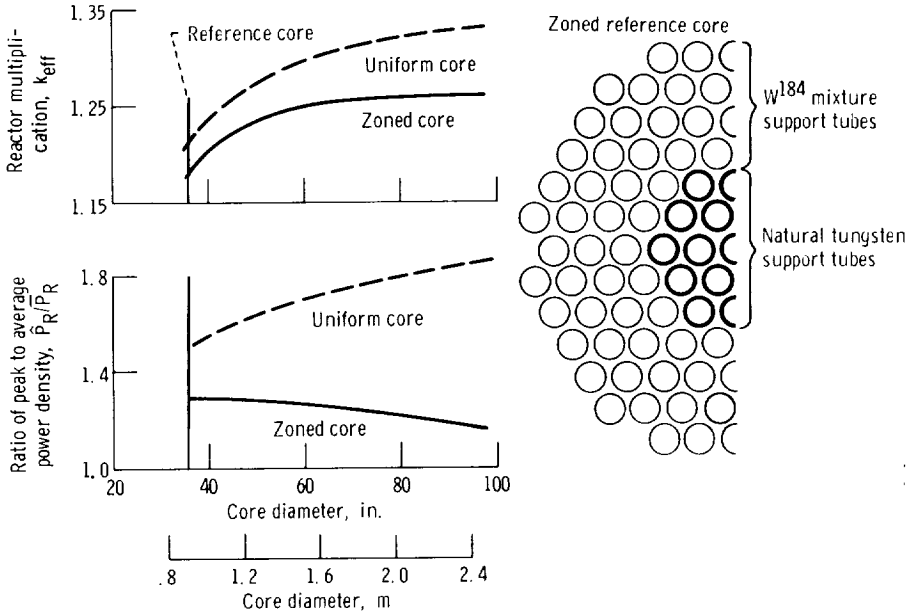

Figure 30. - Characteristics of larger cores with tungsten - 20-volume-percent uranium dioxide fuel.

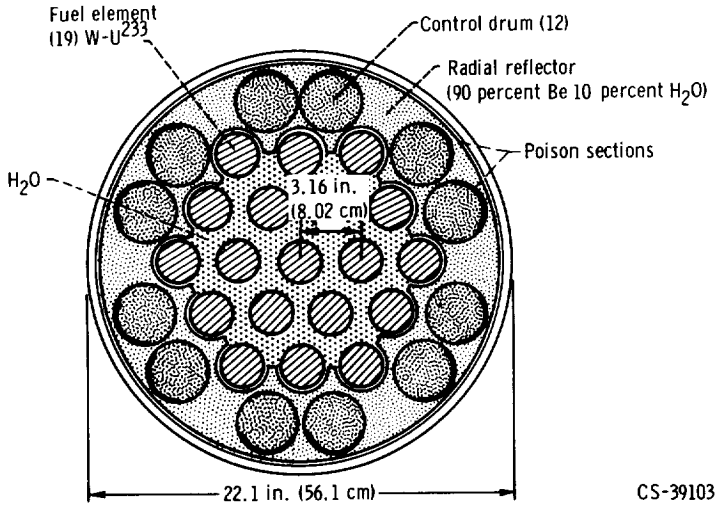

Figure 31. - Cross section of small tungsten reactor.

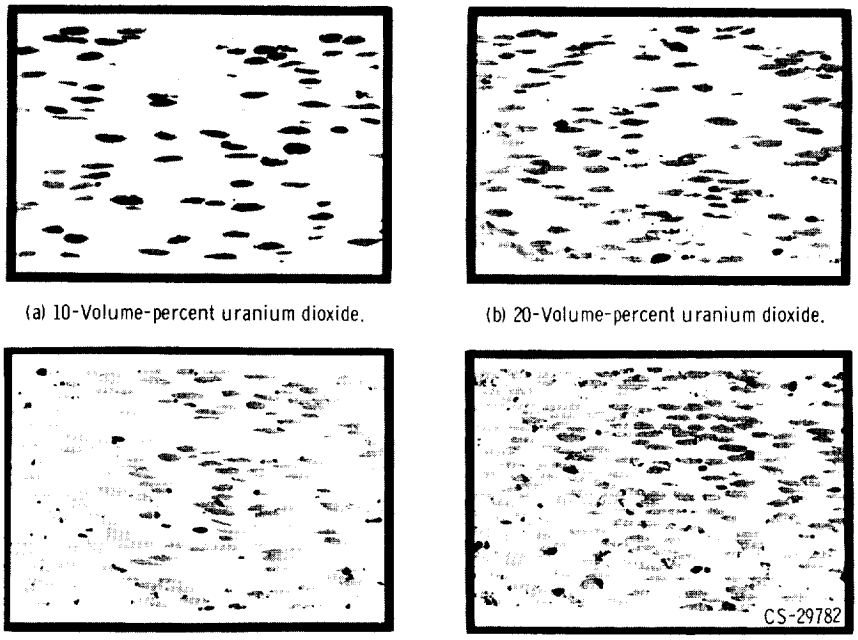

(a) 10-Volume-percent uranium dioxide.

(b) 20-Volume-percent uranium dioxide.

(c) 30-Volume-percent uranium dioxide.

(d) 40-Volume-percent uranium dioxide.

Figure 32. - Tungsten - uranium dioxide plates of various fuel loading. (Sections are parallel to rolling direction.)

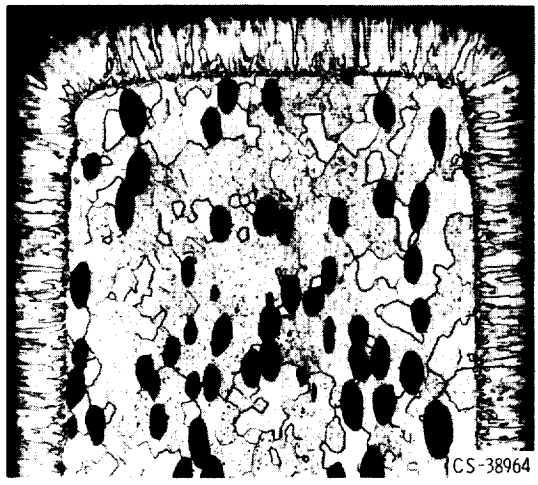

Figure 33. - Tungsten - uranium dioxide composite surface clad by vapor deposition.

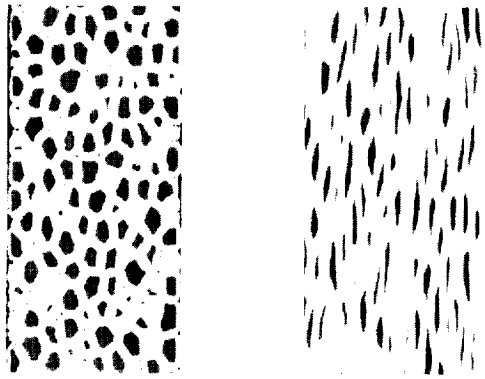

Figure 34. - Tungsten - uranium dioxide plates compacted from coated particles.

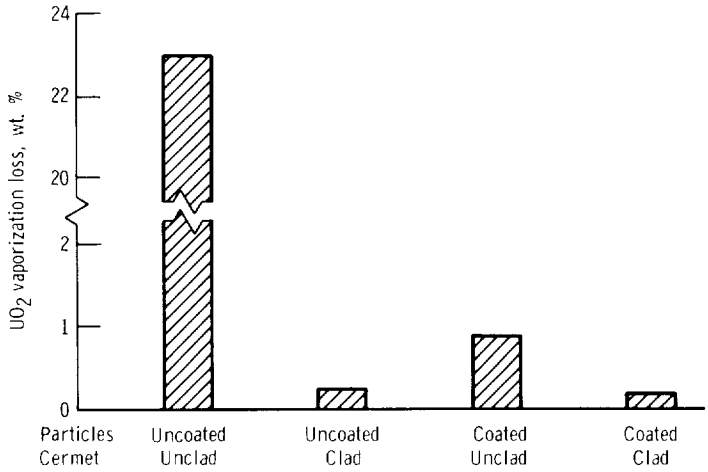

Figure 35. - Vaporization fuel loss from tungsten - uranium dioxide composites for 2-hour test at 4960° R (2755° K) in purified hydrogen at 15 pounds per square inch absolute (10.3 N/cm^2 abs).

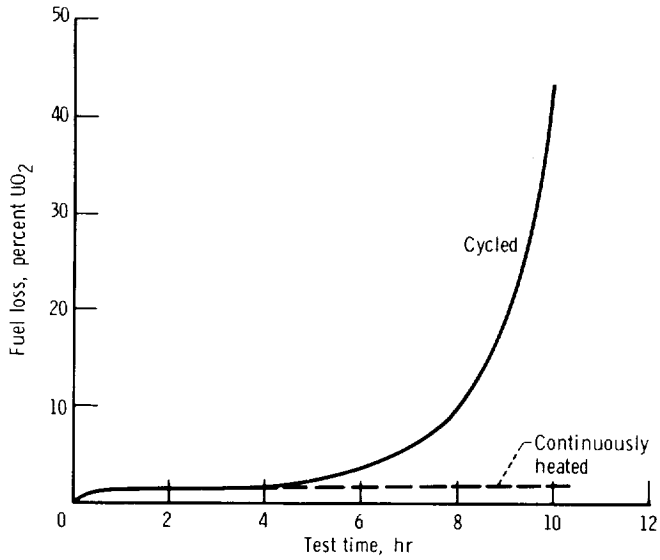

Figure 36. - Effect of 2-hour thermal cycles on fuel loss at 4960° R (2755° K) in purified hydrogen at 15 pounds per square inch absolute (10.3 N/cm^2 abs).

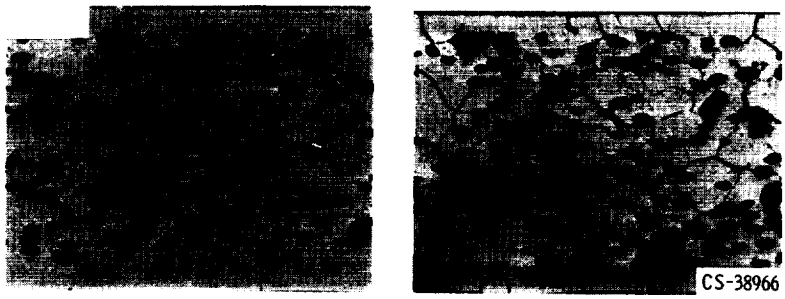

One 10-hr cycle

Five 2-hr cycles

Figure 37. - Effect of thermal cycling at 4960° R (2755° K) on tungsten - uranium dioxide composites.

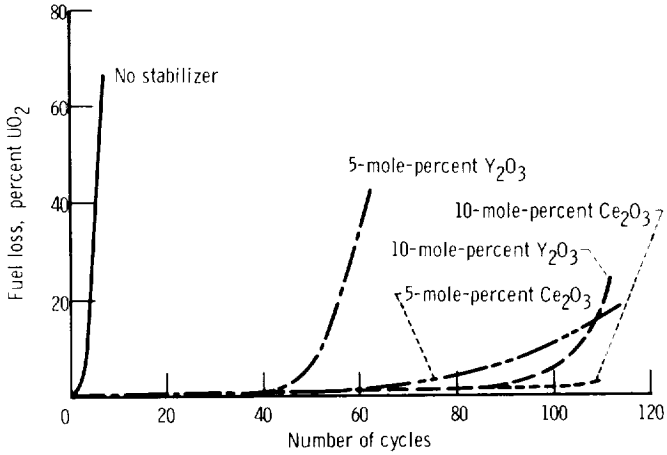

Figure 38. - Effect of cerium oxide and of yttrium oxide as stabilizers of uranium dioxide in tungsten - uranium dioxide composites. Time at 4960° R (2755° K) per cycle, 10 minutes; pure hydrogen environment at 15 pounds per square inch absolute (10.3 N/cm^2 abs).

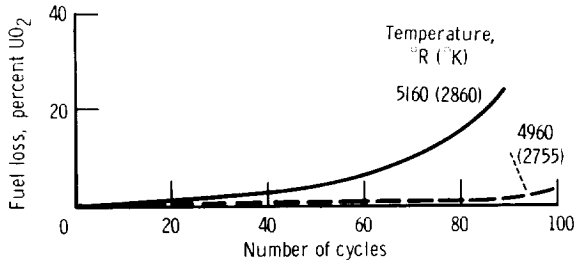

Figure 39. - Effect of temperature on tungsten - uranium dioxide composites stabilized with cerium oxide. Time at temperature per cycle, 10 minutes; pure hydrogen environment at 15 pounds per square inch absolute (10.3 N/cm^2 abs).

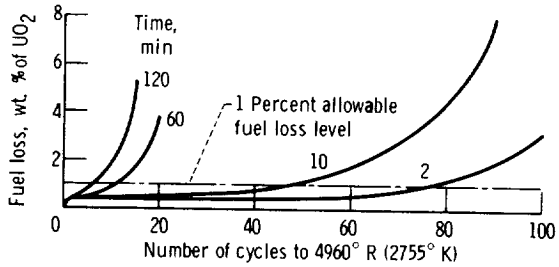

Figure 40. - Effect of time at temperature on tungsten - uranium dioxide composites stabilized with cerium oxide. Purified hydrogen environment at 15 pounds per square inch (10.3 N/cm^2).

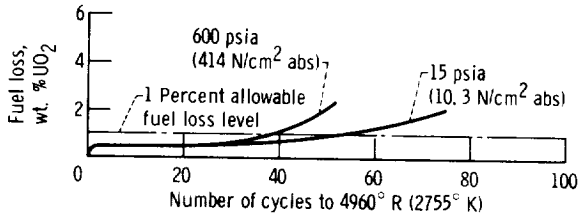

Figure 41. - Effect of hydrogen pressure on tungsten - uranium dioxide composites stabilized with cerium oxide. 10-Minute cycles in purified hydrogen.

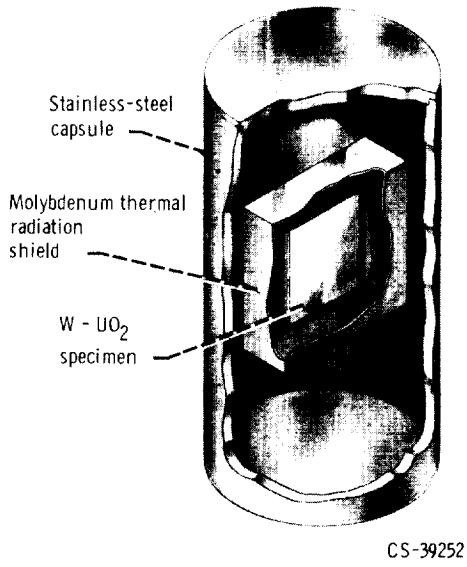

Figure 42. - In-pile capsule.

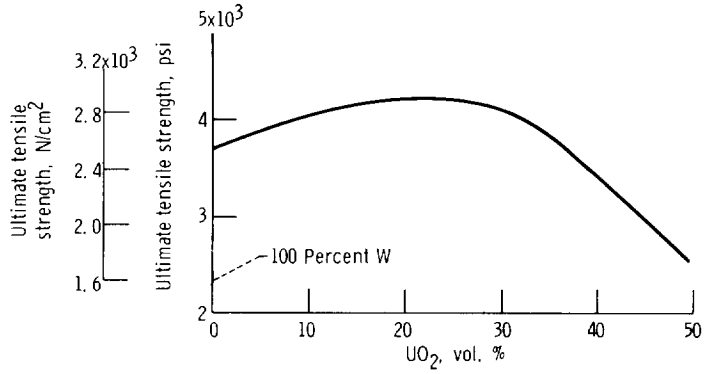

Figure 43. - Effect of uranium dioxide additions to strength of tungsten - uranium dioxide composites at 4960° R (2755° K).

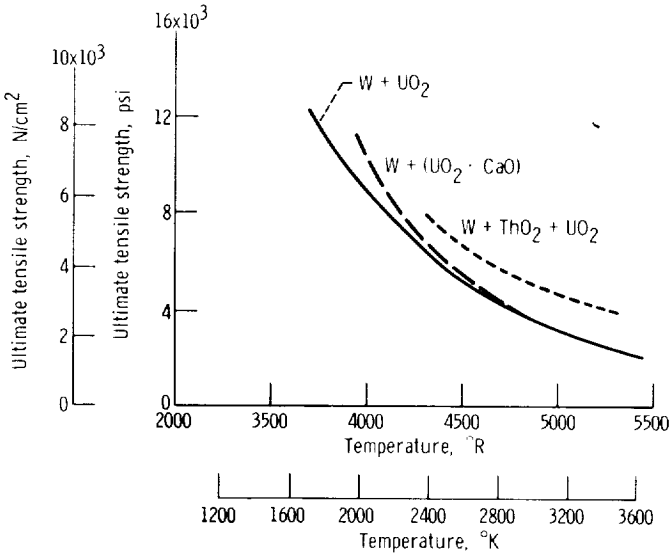

Figure 44. - Effect of core material changes on strength of tungsten - uranium dioxide composites.

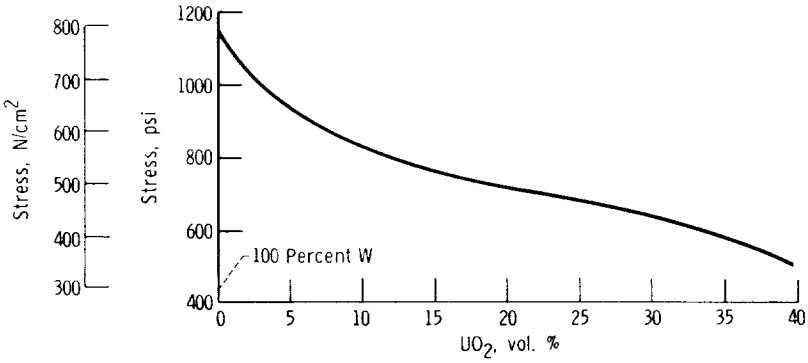

Figure 45. - Rupture stress for 10-hour life for tungsten - uranium dioxide composites at 4960° R (2755° K).

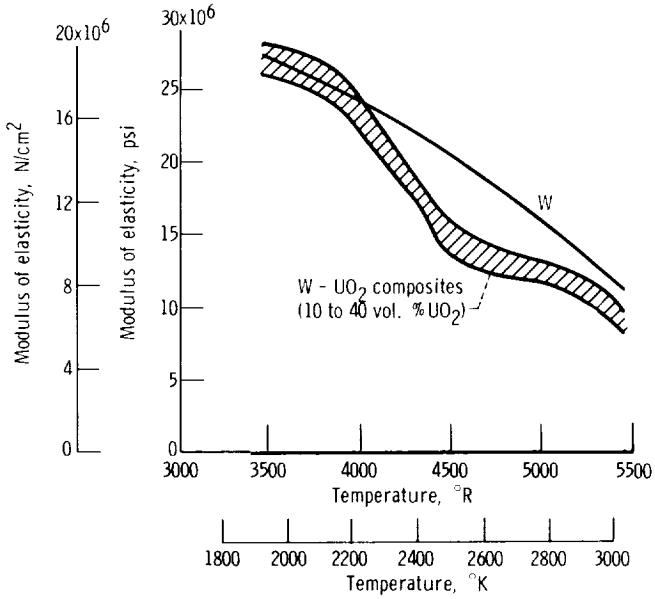

Figure 46. - Average Young's moduli as function of temperature for tungsten and tungsten - uranium dioxide composites.

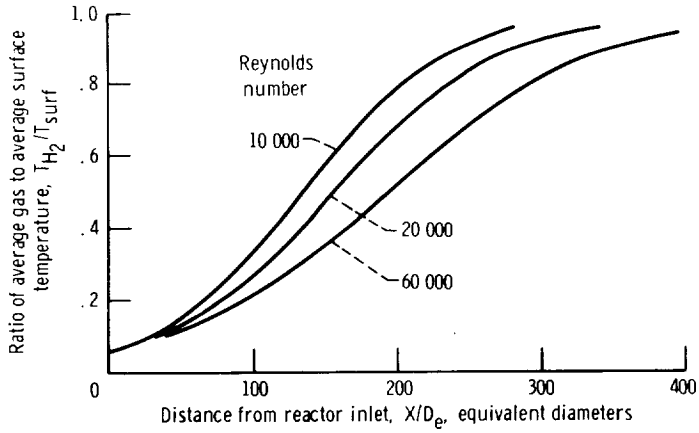

Figure 47. - Axial variation of propellant temperature relative to uniform surface temperature.

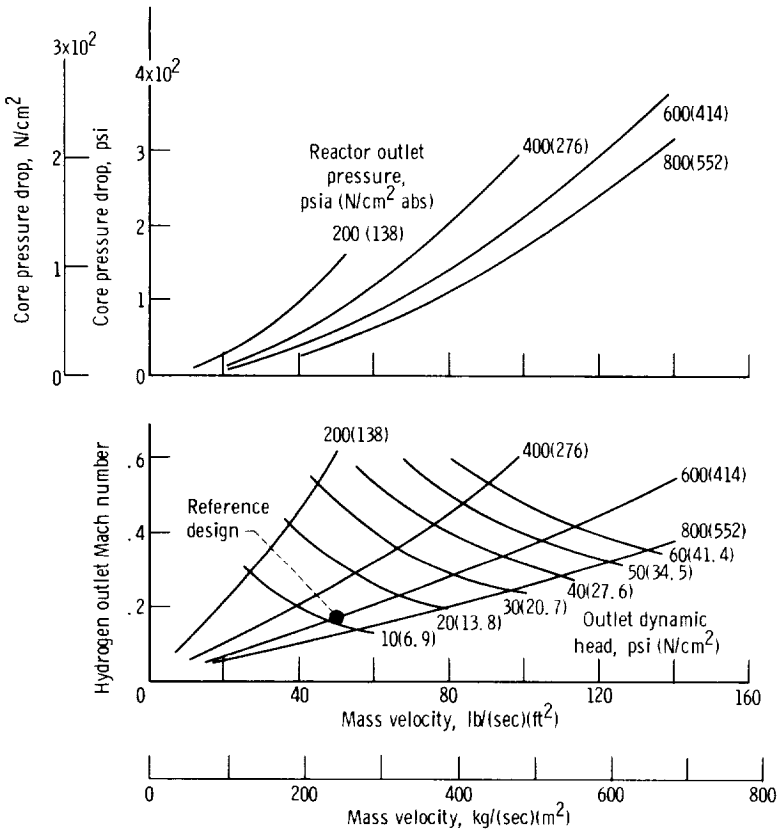

Figure 48. - Interrelation of operating parameters. Uniform surface temperature, 4960° R (2755° K); outlet gas temperature, 4460° R (2480° K); inlet gas temperature, 300° R (167° K).

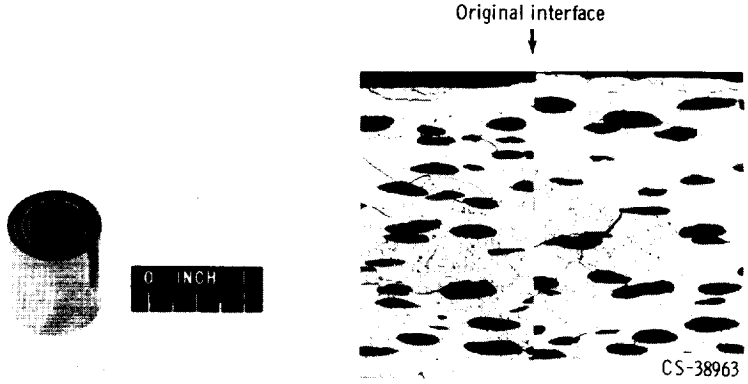

(a) Cylinders formed from W - UO_2 plates. (b) Joint obtained by gas-pressure bonding.

Figure 49. - Forming and joining of tungsten - uranium dioxide plates.

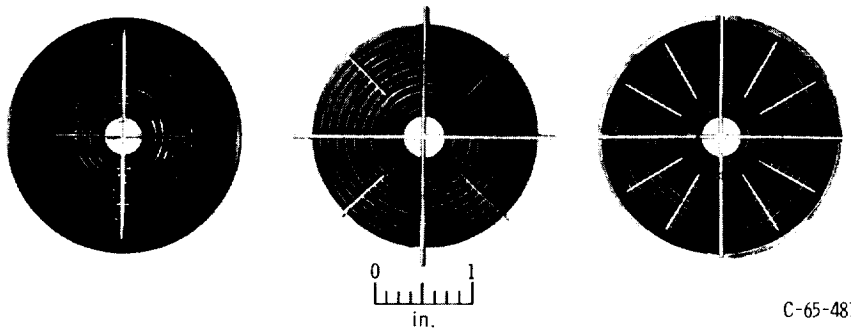

(a) Dynamic head at failure, 12.6 pounds per square inch (8.7 N/cm^2).

(b) Dynamic head at failure, 26 pounds per square inch (17.9 N/cm^2).

(c) Dynamic head at failure, 30 pounds per square inch (20.7 N/cm^2).

Figure 50. - Typical lead-antimony simulated fuel stages with leading edge supports used in cold flow tests.

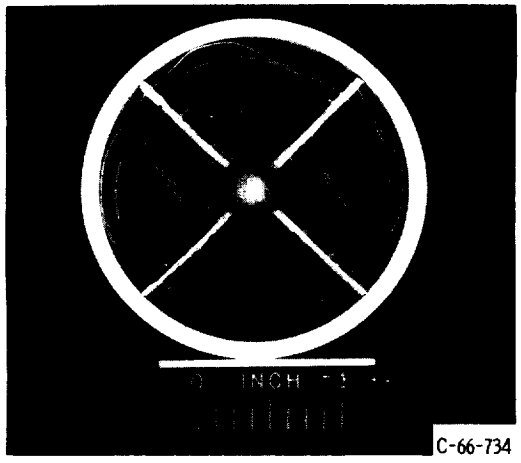

Figure 51. - Failed lead-antimony fuel stage.

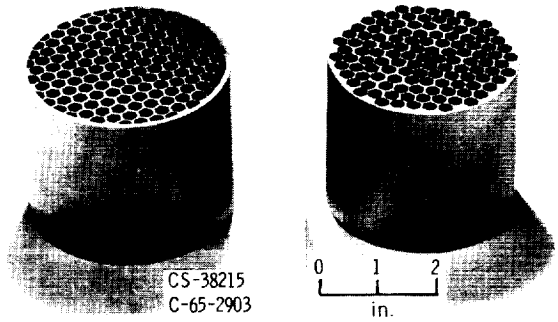

(a) Hot isostatic compacted. (b) Hot pneumatic impacted.

Figure 52. - Tungsten - uranium dioxide honeycomb structures.

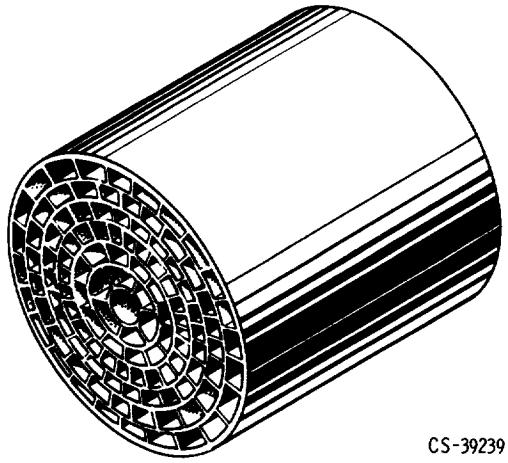

Figure 53. - Cylinder and ligament configuration.

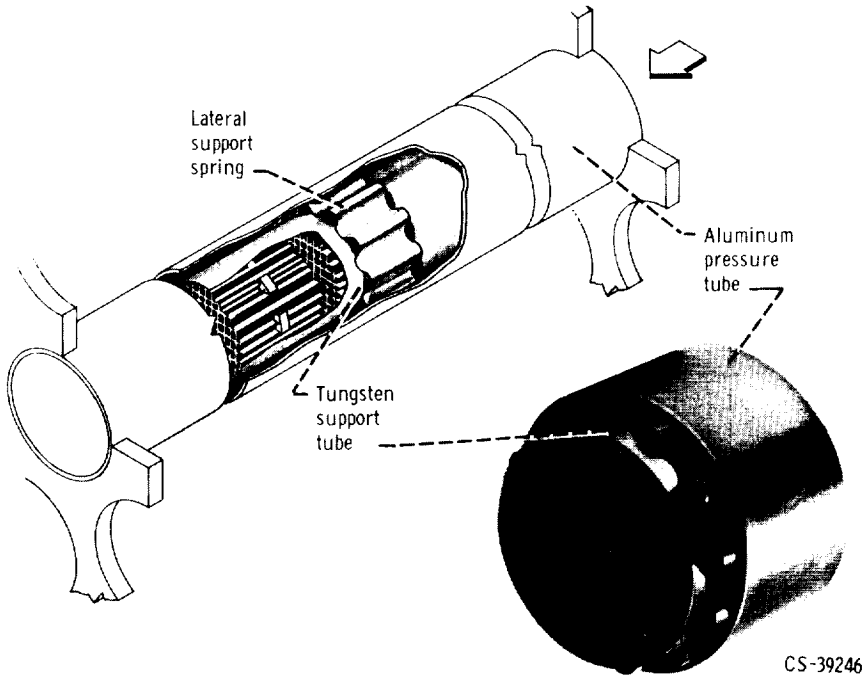

Figure 54. - Fuel assembly arrangement.

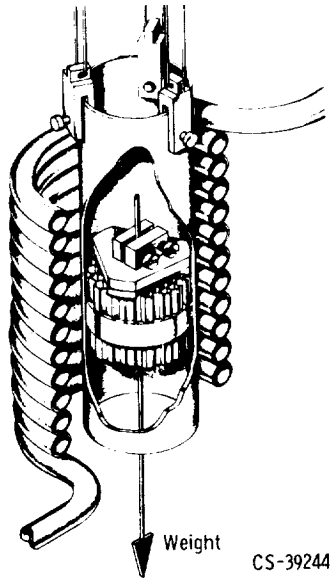

Figure 55. - Fuel stage axial support test.

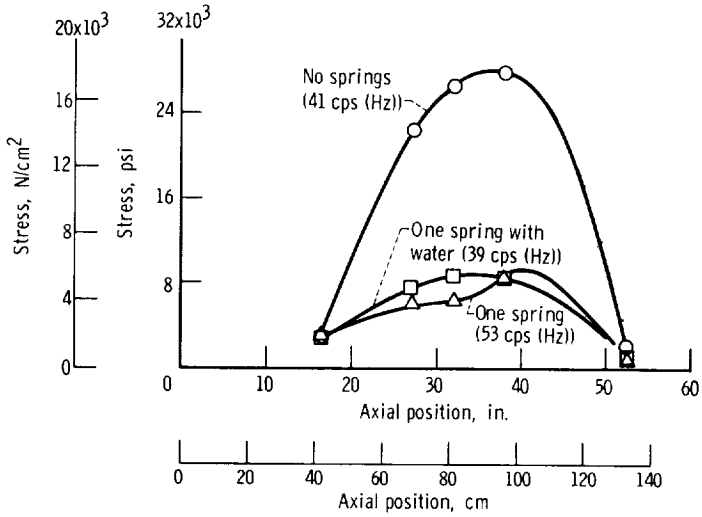

Figure 56. - Support tube bending stress under 1-g load.

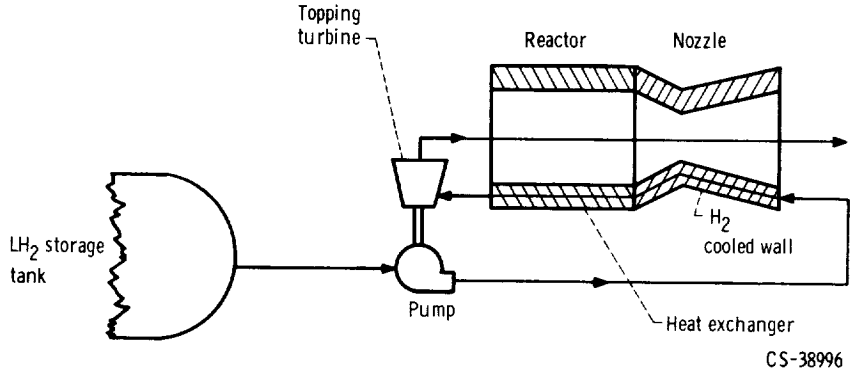

Figure 57. - Topping system.

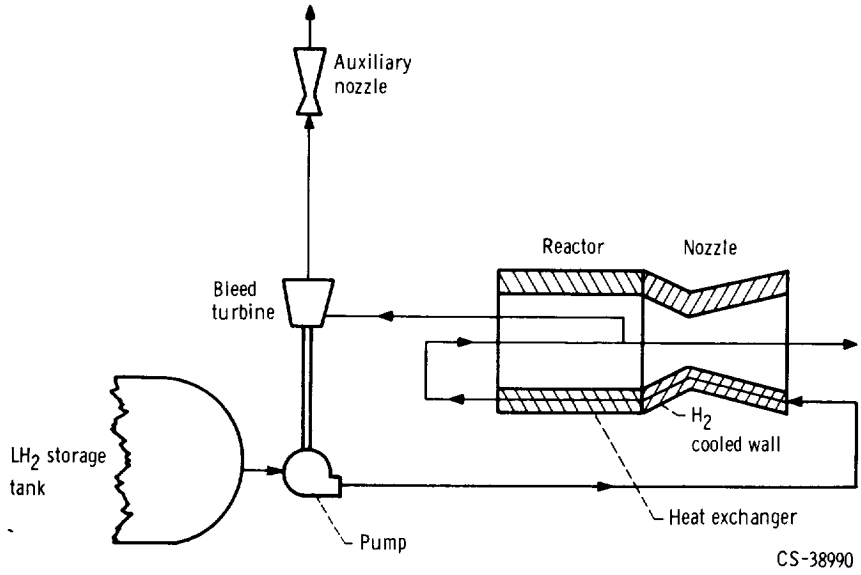

Figure 58. - Bleed system.

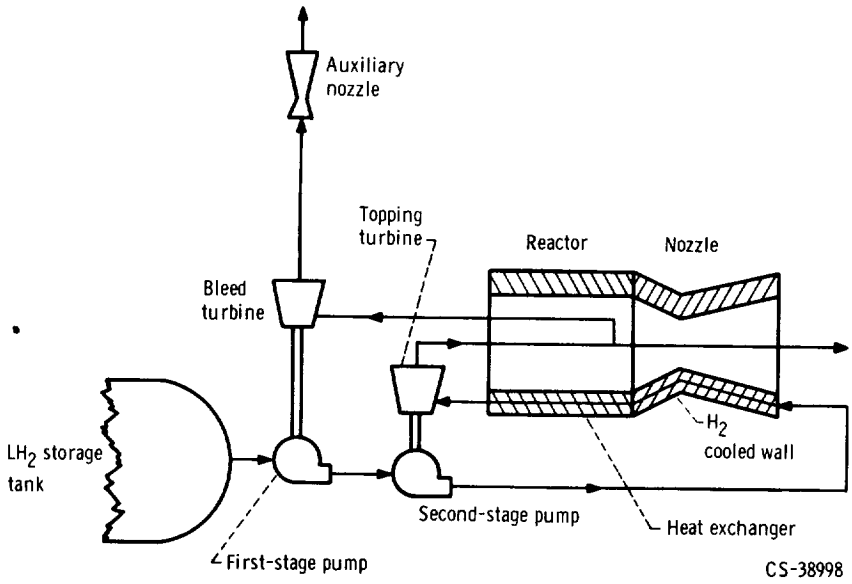

Figure 59. - Split-feed system.

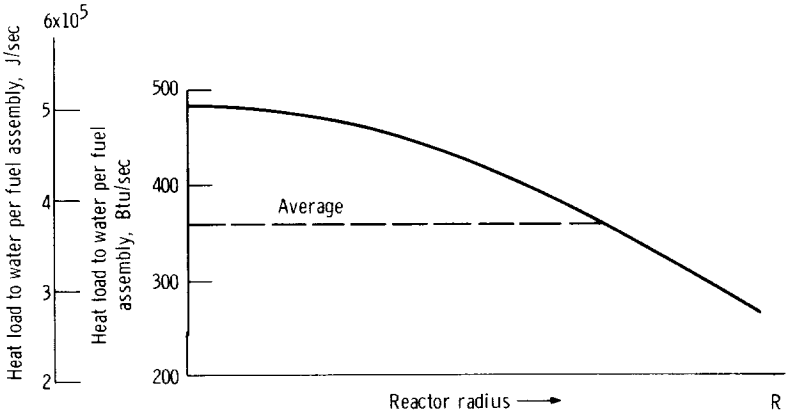

Figure 60. - Variation of heat load to water with reactor radius.

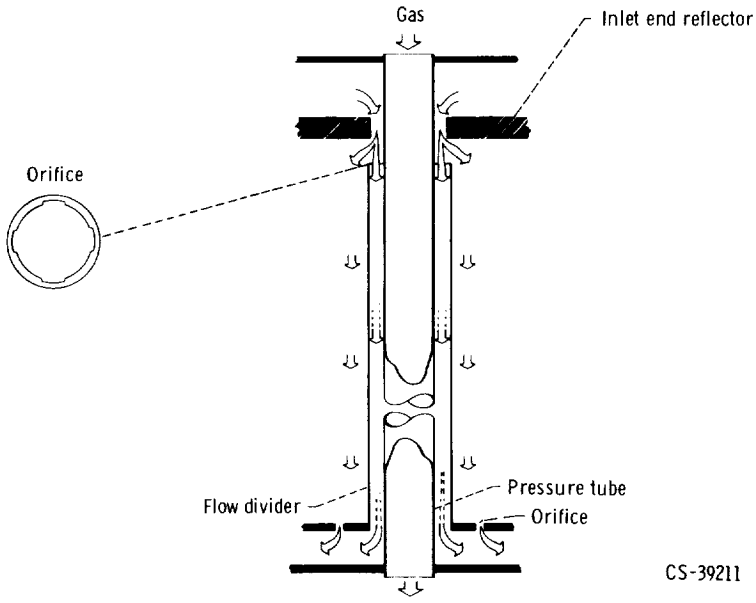

Figure 61. - Water flow around pressure tube.

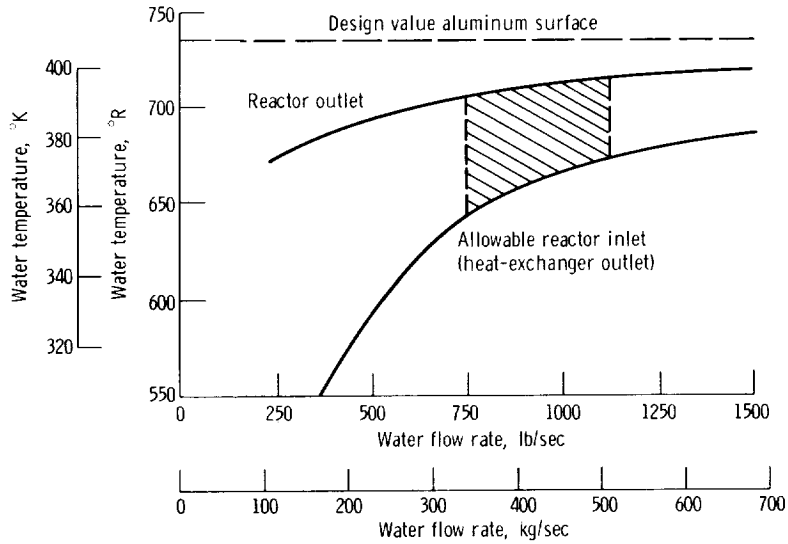

Figure 62. - Cooling requirement of aluminum structure.

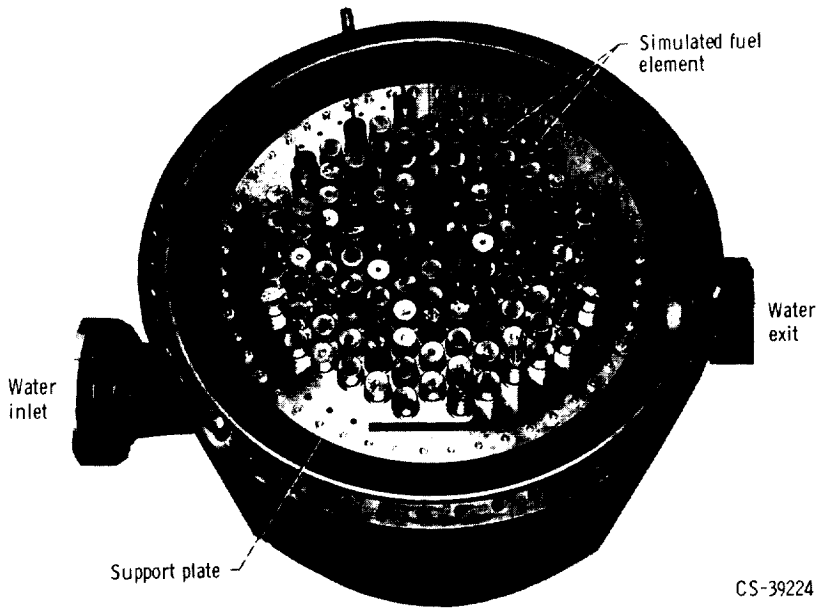

Figure 63. - TWMR water flow test facility.

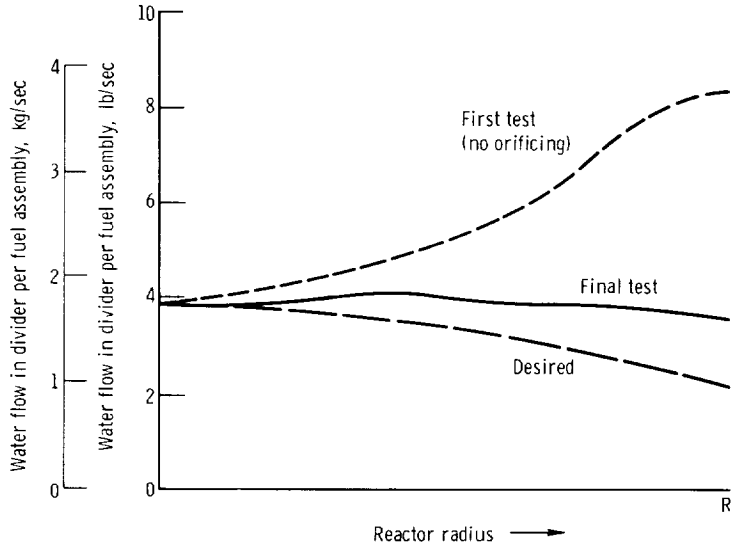

Figure 64. - Results of water flow test.

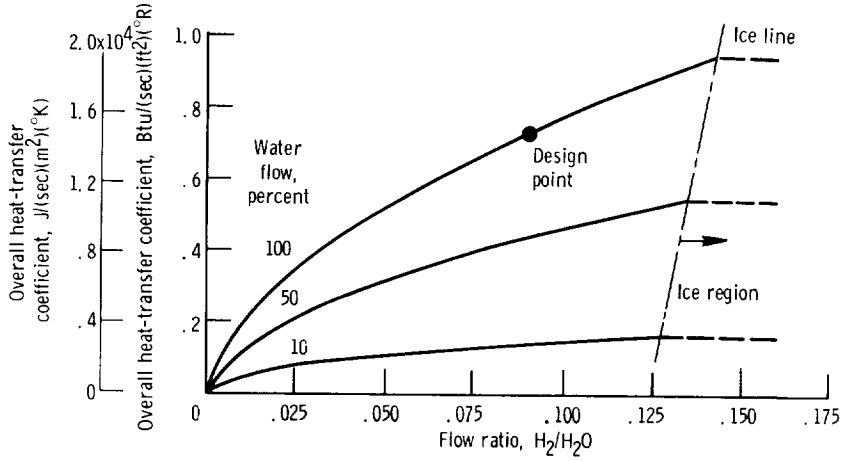

Figure 65. - Overall heat-transfer coefficient of water-hydrogen heat exchanger. Inlet temperature: water, 700° R (389° K); hydrogen, 170° R (94.5° K).

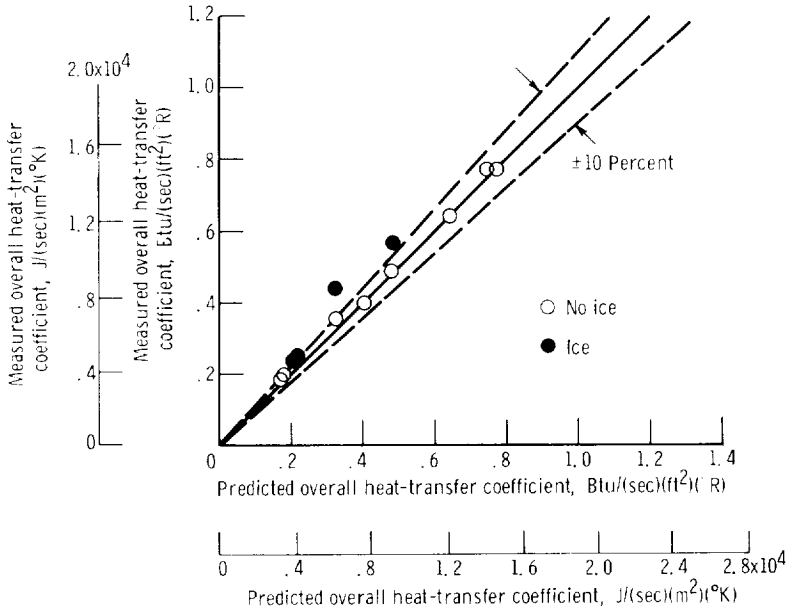

Figure 66. - Steady-state heat exchanger tests.

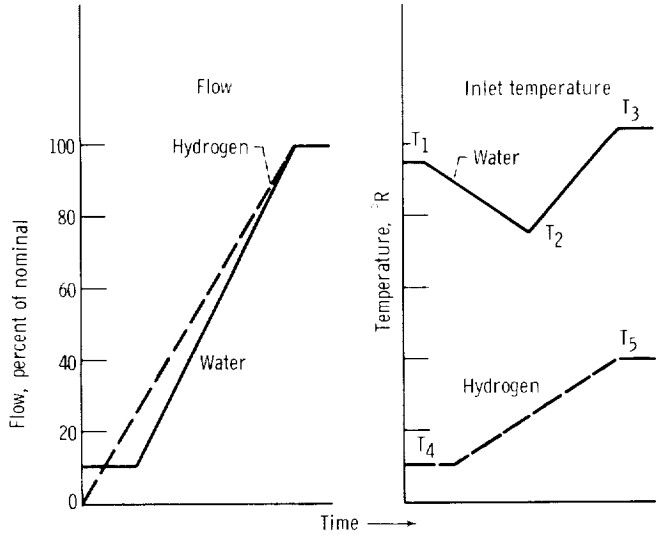

Figure 67. - Generalized startup transient in heat exchanger.

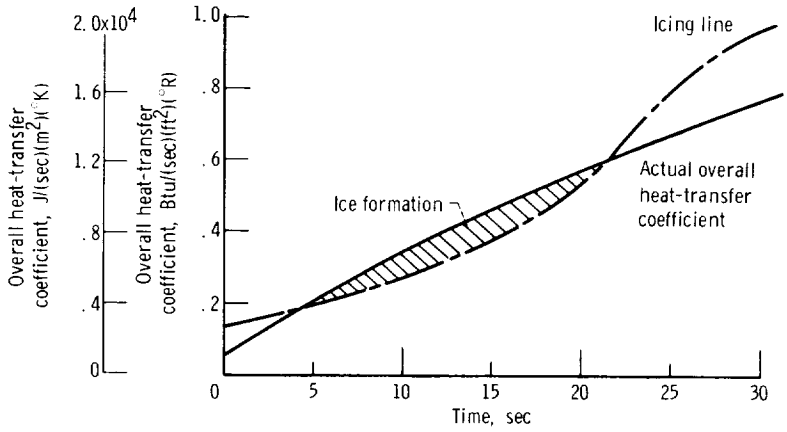

Figure 68. - Variation in heat-exchanger heat transfer during typical startup. T_1 = 680° R (378° K); T_2 = 650° R (361° K); T_3 = 700° R (389° K); T_4 = 50° R (28° K); T_5 = 180° R (100° K).

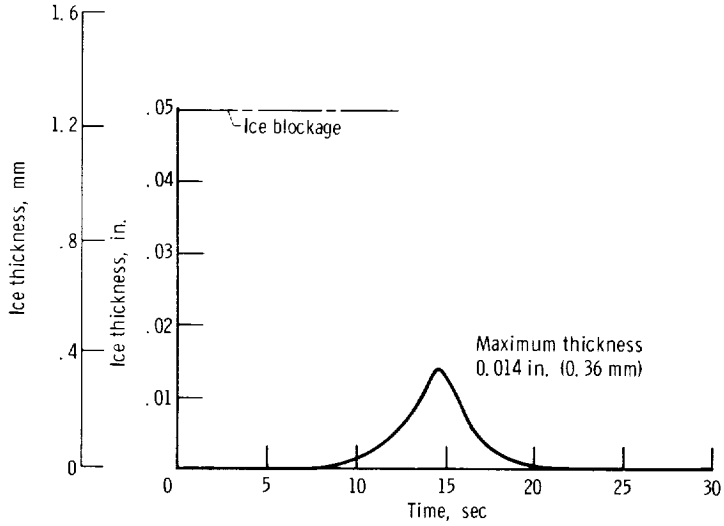

Figure 69. - Ice thickness variation during 30-second startup using pointwest steady-state analysis.

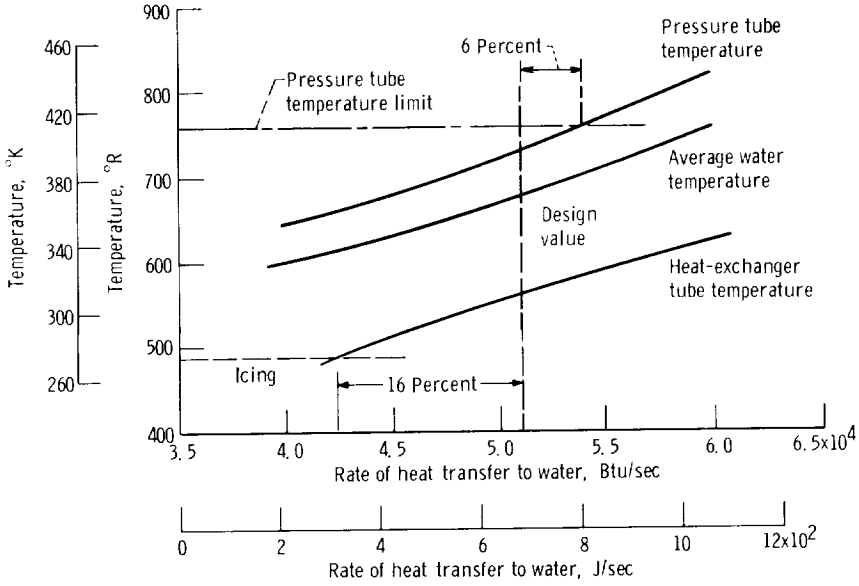

Figure 70. - Effect of heat-transfer rate on heat-exchanger performance.

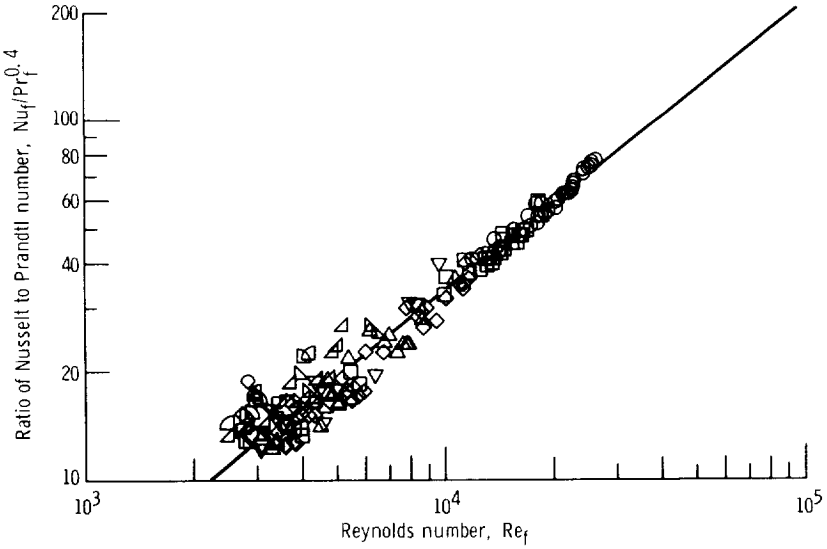

Figure 71. - Film correlation of local heat-transfer coefficients for hydrogen. $Nu_f = 0.021\ Re_f^{0.8} Pr_f^{0.4}$.

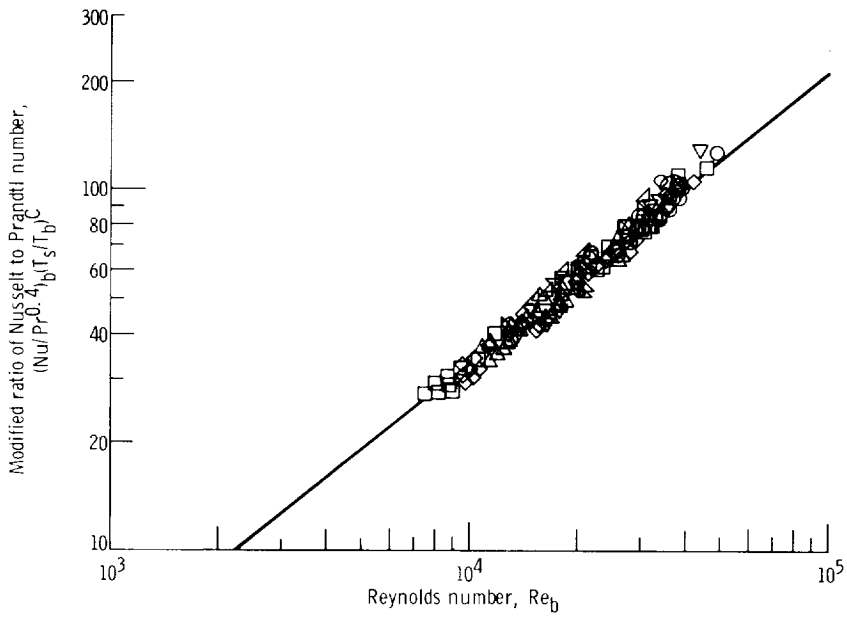

Figure 72. - Modified correlation of local heat-transfer coefficients for hydrogen. $Nu_b = 0.021\ Re_b^{0.8} Pr_b^{0.4} (T_b/T_s)^C$, where $C = 0.29 + 0.0019\ X/D_e$, T_s is surface temperature, and T_b the bulk fluid temperature.

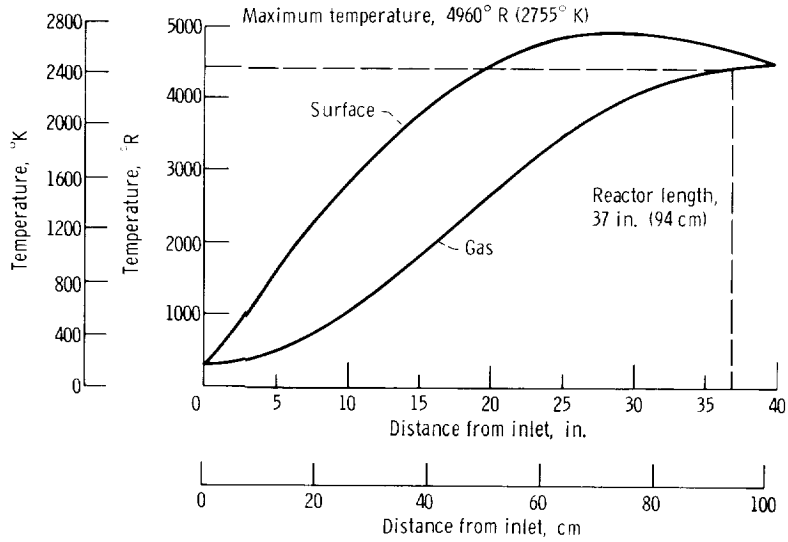

Figure 73 - Axial temperature variation with cosine power distribution. Inlet temperature, 320° R (178° K).

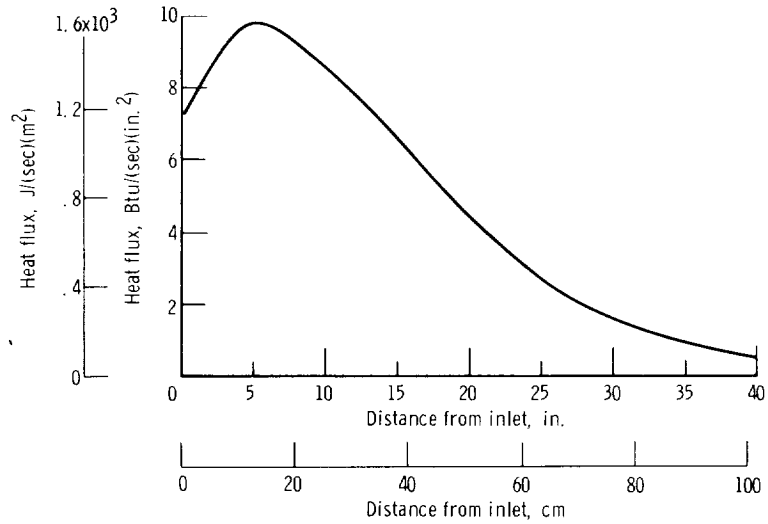

Figure 74. - Desired axial power distribution for constant surface temperature of 4960° R (2755° K). Inlet temperature, 320° R (178° K).

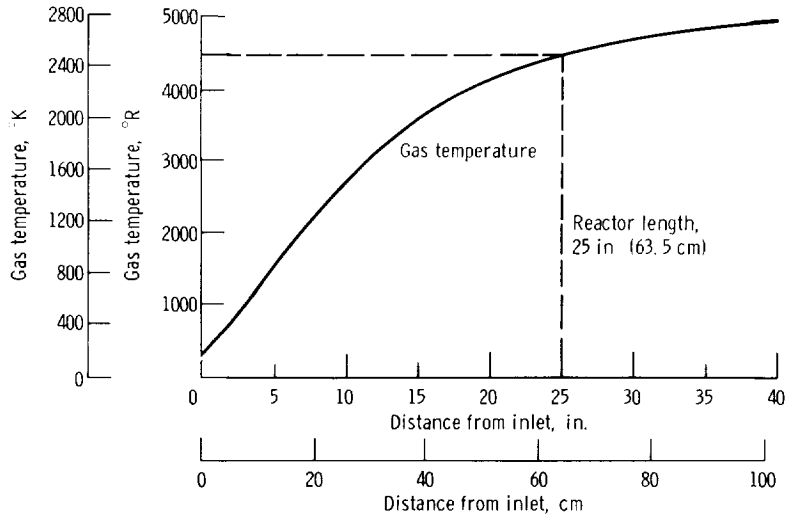

Figure 75. - Axial gas temperature variation for constant surface temperature of 4960° R (2755° K).

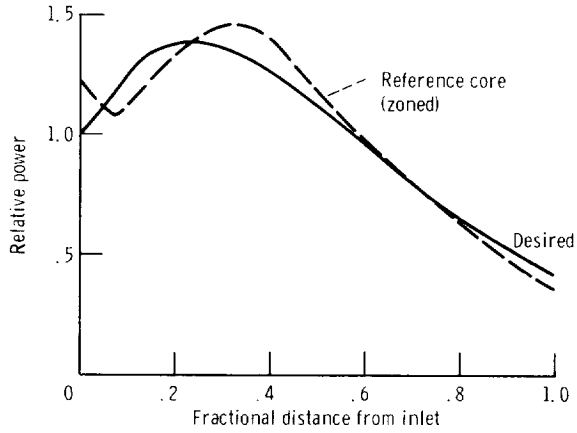

Figure 76. - Comparison between desired and reference power distribution.

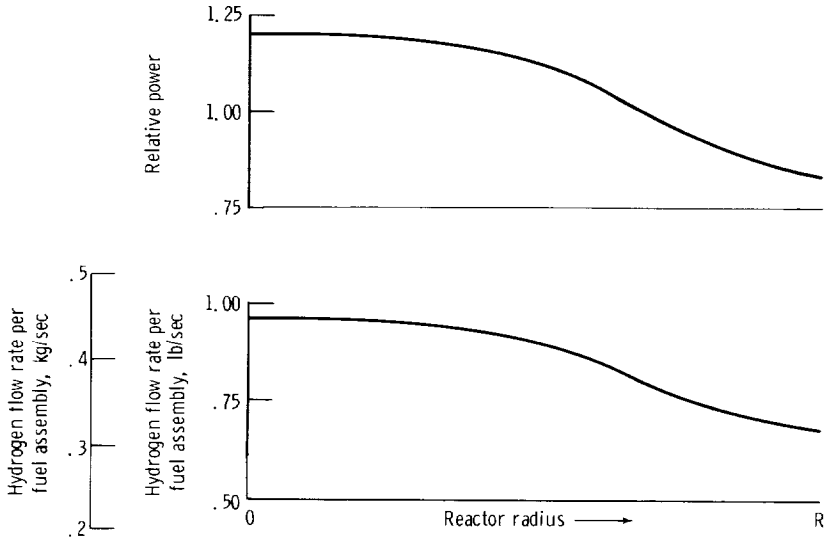

Figure 77. - Radial power and flow distribution for constant gas outlet temperature. Total flow, 92.7 pounds per second (42.1 kg/sec).

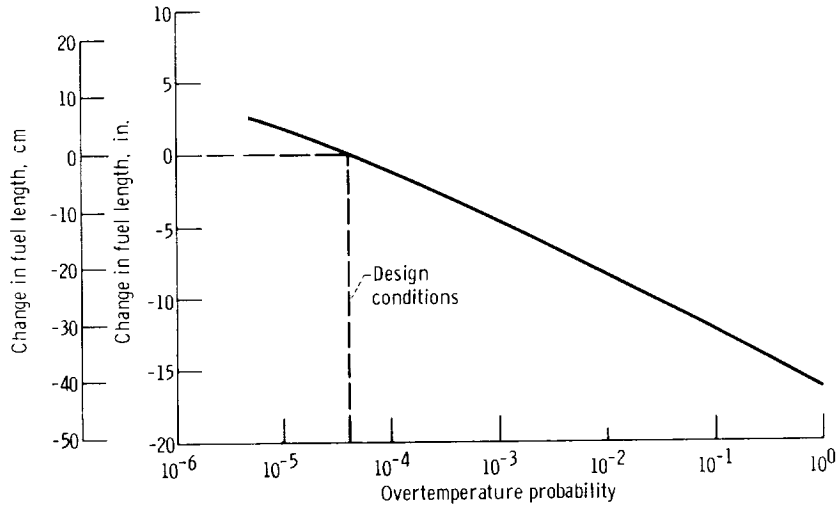

Figure 78. - Probability of 500 R° (278 K°) overtemperature as function of change in fuel length. Nominal conditions: exit gas temperature, 4460° R (2480° K); reactor length, 39 inches (99 cm); reactor power, 1500 megawatts; fuel temperature, 4960° R (2755° K).

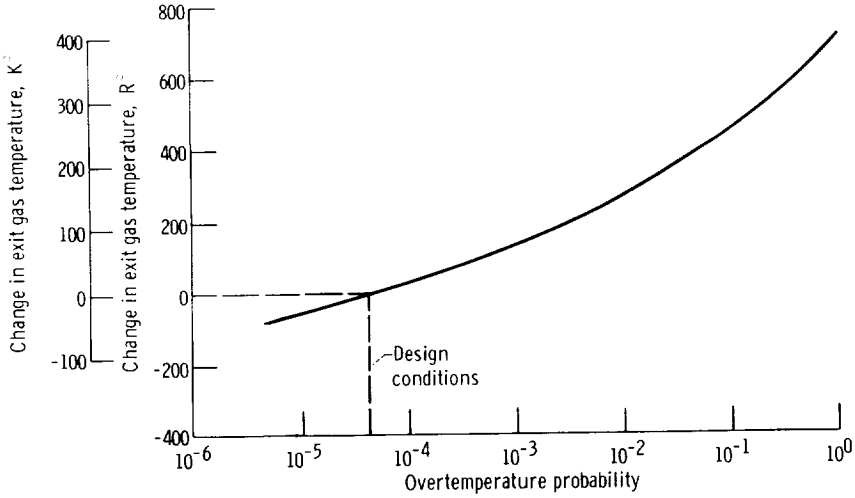

Figure 79. - Probability of 500 R° (278 K°) fuel overtemperature as function of change in exit gas temperature. Nominal conditions: exit gas temperature, 4460° R (2480° K); reactor length, 39 inches (99 cm); reactor power, 1500 megawatts; fuel temperature, 4960° R (2755° K).

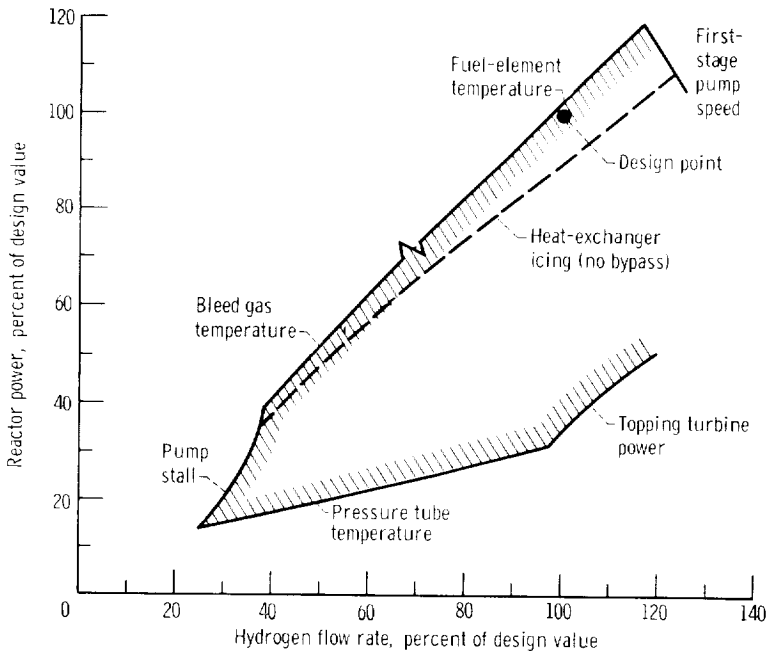

Figure 80. - Steady-state operating envelope for TWMR.

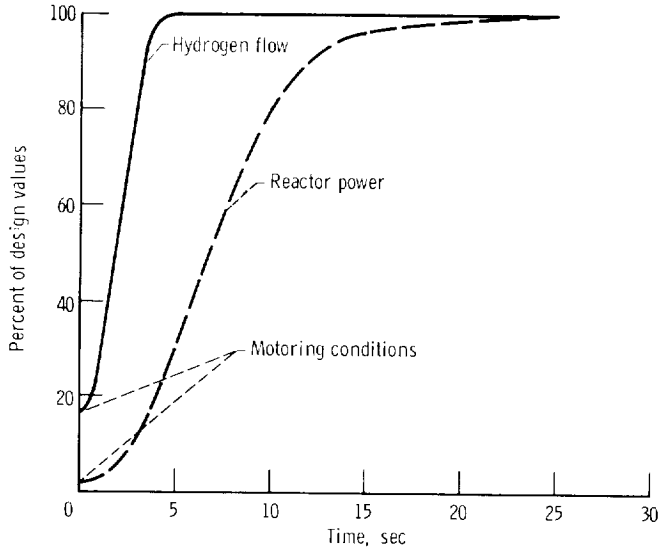

Figure 81. - Open-loop startup transient.

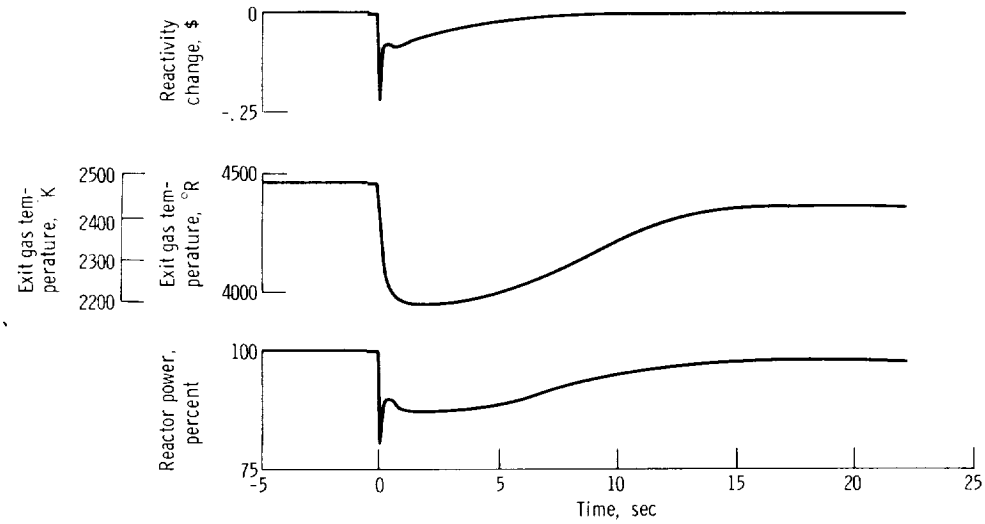

Figure 82. - Open-loop response to step increase in poison concentration.

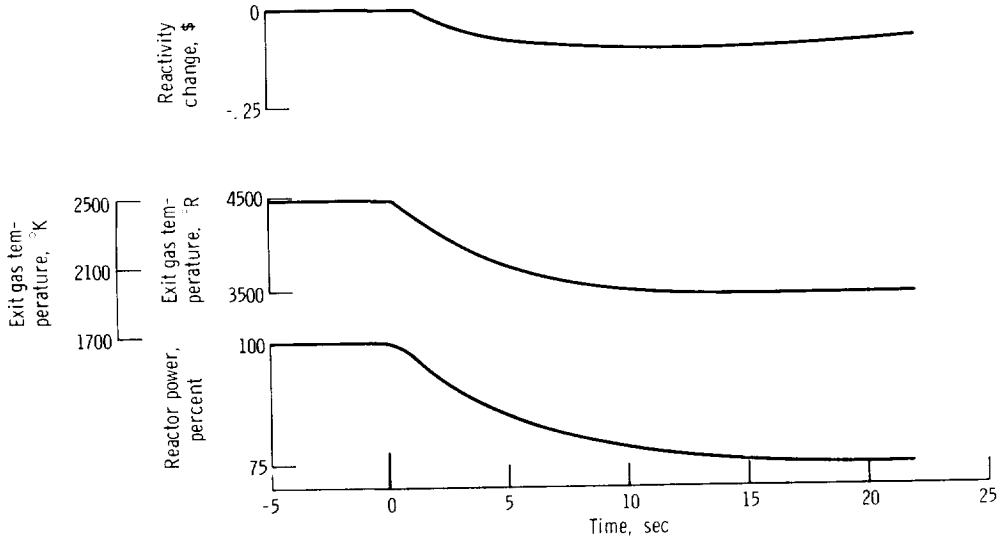

Figure 83. - Open-loop response to step increase in heat-exchanger-bypass hydrogen flow.

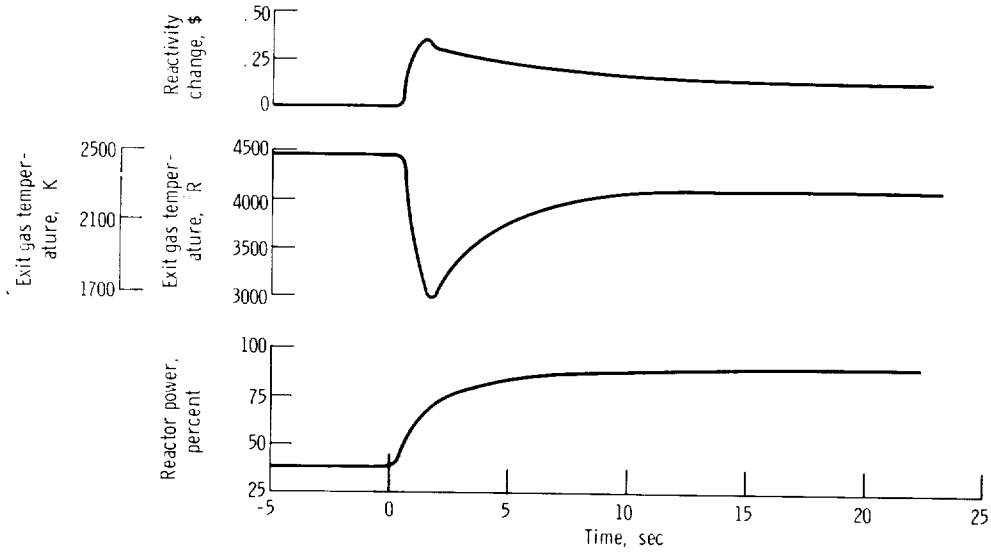

Figure 84. - Open-loop response to step increase in hydrogen flow rate.

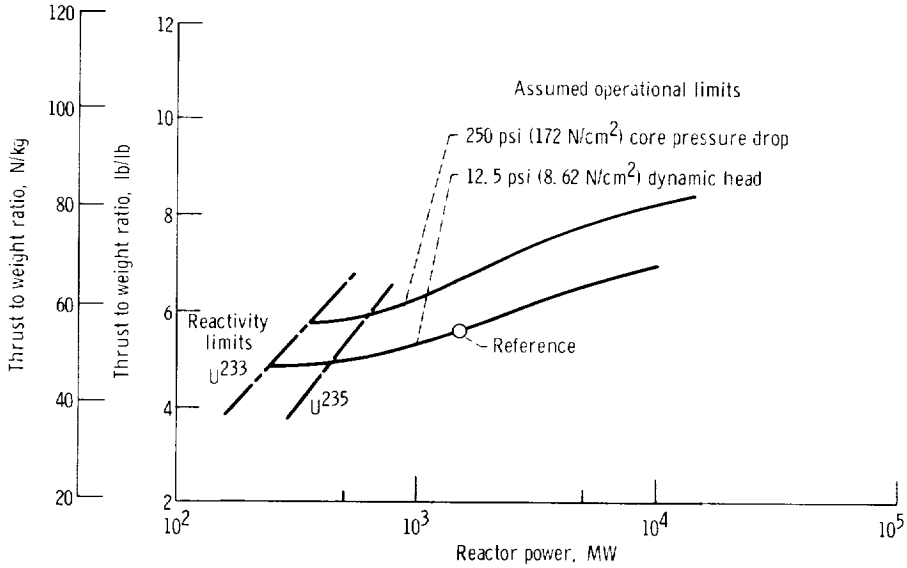

Figure 85. - Effect of power level and operational limits on TWMR thrust to engine weight ratios.

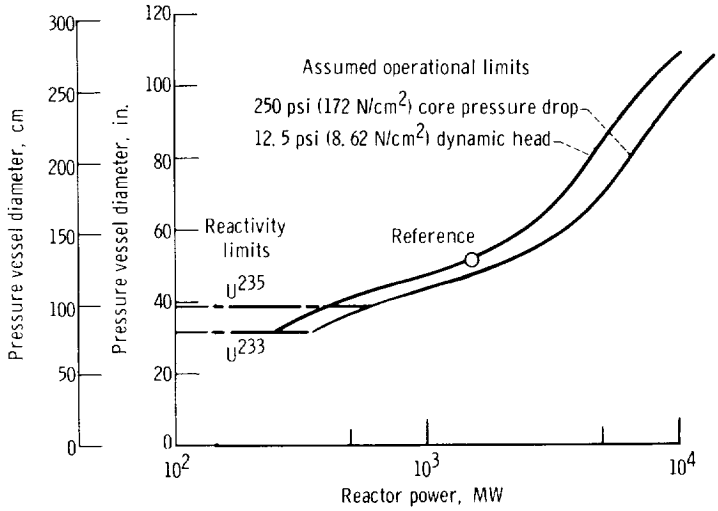

Figure 86. - Effect of power level and operational limits on vessel diameter.